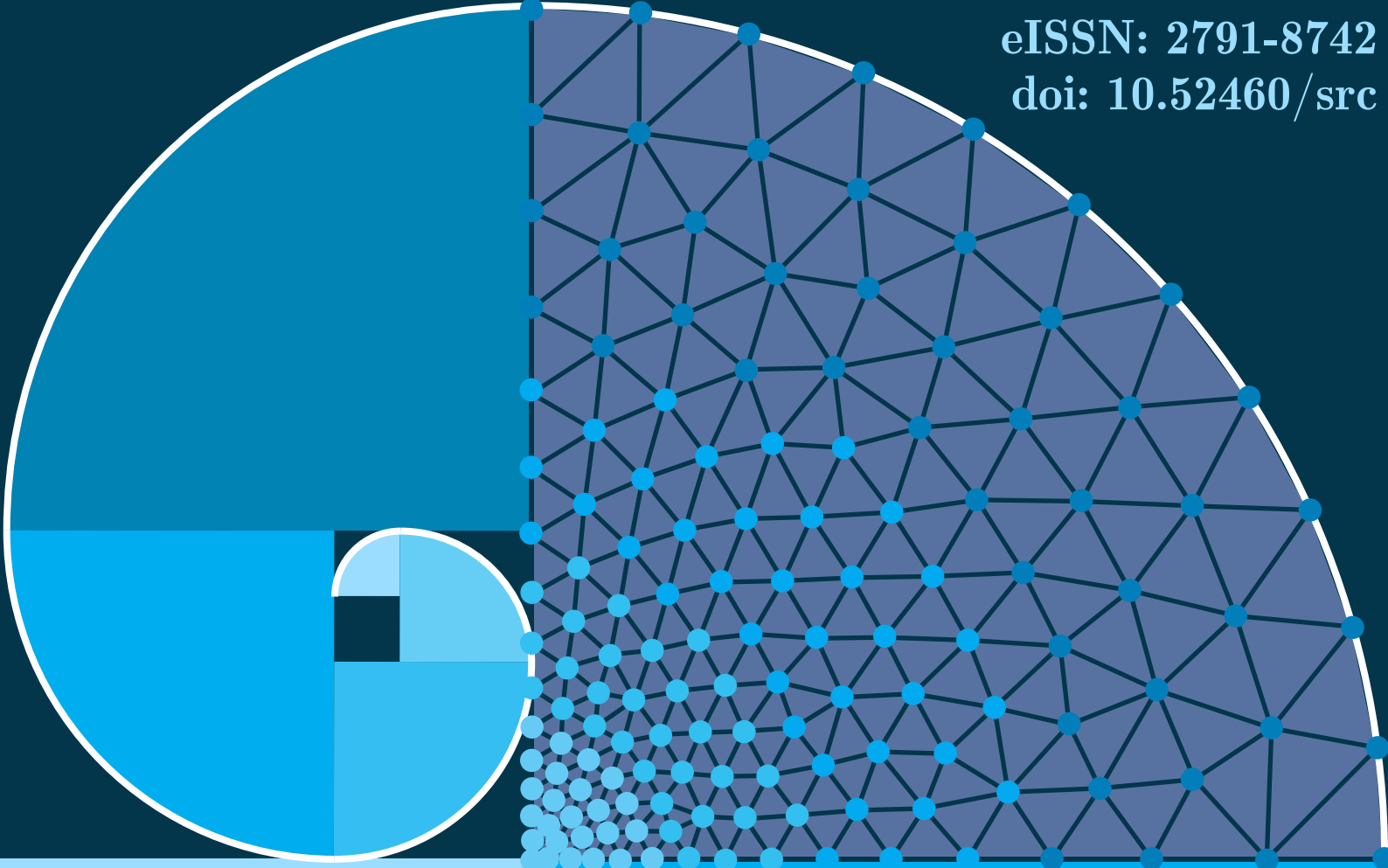
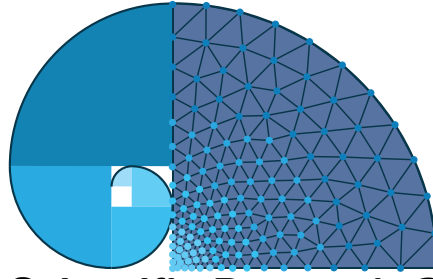


eISSN: 2791-8742  
doi: 10.52460/src



Scientific  
Research  
Communications

Volume 5  
Issue 2  
July 2025



# Scientific Research Communications

Volume 5, Issue 2, 2025

---

## Editorial

### Editor-in-Chief

Mehmet ÇEVİK

### Associate Editors

Ahmet AYKAÇ

Aydın AKAN

Ayşe KALAYCI ÖNAÇ

Faruk ÖZGER

Fatih Erdoğan SEVİLGİN

Gökçen BOMBAR

Sedat YALÇINKAYA

Sercan ACARER

Umut CEYHAN

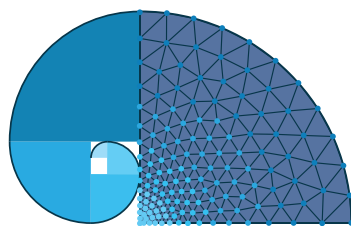
### Office

Furkan EMREM

Zehra BÜYÜKER

### Publisher

İzmir International Student Association



# Scientific Research Communications

Volume 5, Issue 2, 2025

---

## Contents

### Research Articles

**Evaluation of Autonomous Robot Alternatives for Warehouse Optimization Using the Analytic Hierarchy Process**, pp.67-76

H. Akpınar

**Renewable Energy Adoption and Economic Resilience in Africa: A Case Study of Morocco**, pp.77-93

O. A. Oyebamiji and M. A. Muhammad and K. T. Abdullahi

**Finite Element Analysis of the Transition from Multi-Station Machines to Double-Stroke Machines in the Forming Process of Ring Welded Bolts**, pp.94-103

B. Akyıldız and Ö. Özcan and İ. Özçetin

**GIS-Based Assessment of Wastewater Pollution in Afghanistan's Major Cities**, pp.104-117

H. Himat

**Efficacy of Biofumigants for Controlling Root-Knot Nematodes (Meloidogyne) in Tomato Cultivation**, pp.118-139

P. Niazi and A. B. Hejran and K. Saken



# Evaluation of Autonomous Robot Alternatives for Warehouse Optimization Using the Analytic Hierarchy Process

Huriye Akpınar \* 

Independent Researcher, İzmir, Türkiye

## Research Article

\*Correspondence:  
huriyeakpinar@gmail.com

Received: 9 November 2024  
Accepted: 10 July 2025  
Published: 30 July 2025

## Keywords

Multi-criteria decision making  
Analytic hierarchy process  
Robot selection

This is an open access article  
under the CC BY NC license.



## Abstract

In today's world, the optimization of storage and logistics processes is of great importance for efficiency and cost-effectiveness. In this context, the use of autonomous robots emerges as a potential solution to improve storage operations. However, selecting among different autonomous robot alternatives is a complex process that requires consideration of multiple criteria. This study examines the use of the analytic hierarchy process method, a multi-criteria decision-making technique, for evaluating autonomous robot alternatives in warehouse optimization. These techniques allow decision-makers to evaluate alternatives systematically and objectively based on defined criteria. The method used in the study assesses the hierarchical structure between criteria and sub-criteria, using pairwise comparison matrices to determine the relative importance of each criterion. The evaluation was based on five main criteria: carrying capacity, speed, maneuverability, battery life, and investment cost. This approach facilitates a clear articulation of priorities among the criteria by decision-makers. The study aims to select the most suitable one among three different robot alternatives for a warehouse. As a result of the study, the most suitable robotic alternative was identified, and the findings were analyzed and interpreted.

## 1. Introduction

In today's rapidly evolving industrial landscape, the optimization of storage and logistics processes has become increasingly critical for ensuring operational efficiency and cost-effectiveness. With the rise of e-commerce and the demand for faster delivery times, warehouses are under constant pressure to enhance their operational capabilities. Autonomous robots present a promising solution for improving these processes by automating tasks that were traditionally performed manually. However, the challenge lies in selecting the most suitable autonomous robot for a specific warehouse environment, given the wide variety of available options and the complex requirements of modern warehousing operations (Peng et al., 2014).

Selecting the right autonomous robot involves evaluating multiple factors, including cost, performance, reliability, flexibility, and sustainability. Each of these criteria plays a significant

**How to cite this paper:** Akpınar, H. (2025). Evaluation of autonomous robot alternatives for warehouse optimization using the analytic hierarchy process. *Scientific Research Communications*, 5(2), 67-76. <https://doi.org/10.52460/src.2025.006>



role in determining the overall effectiveness of the robot within the warehouse setting. Cost considerations encompass both the initial investment and the ongoing operational expenses, while performance metrics include the robot's speed, accuracy, and ability to handle various tasks (Bensalem et al., 2009). Reliability is crucial for minimizing downtime and ensuring consistent operations, whereas flexibility refers to the robot's adaptability to different tasks and environments. Sustainability, increasingly important in today's business world, addresses the environmental impact and energy efficiency of the robot (Chakraborty et al., 2018).

Given the multifaceted nature of this decision-making process, multi-criteria decision-making (MCDM) techniques offer a structured and objective approach to evaluating and comparing different autonomous robot alternatives. The Analytic Hierarchy Process (AHP) is one such MCDM technique that is particularly well-suited for this purpose. AHP helps decision-makers systematically assess the importance of various criteria and sub-criteria, providing a clear framework for comparing alternatives based on these prioritized factors. By using pairwise comparison matrices, AHP quantifies the relative importance of each criterion, enabling a detailed and nuanced evaluation of each robot option.

In this study, we apply the AHP method to evaluate three different autonomous robot alternatives for a warehouse environment. Our goal is to identify the most suitable robot that aligns with the specific needs and priorities of the warehouse, considering all relevant criteria. The structured approach provided by AHP not only facilitates a thorough comparison but also helps in making a well-informed and transparent decision. This ensures that the selected robot will enhance the overall efficiency, reliability, and sustainability of the warehouse operations.

The following sections of this paper will delve into the specifics of the criteria used for evaluation, the methodology of the AHP process, and the detailed analysis of each robot alternative. We will discuss the results of the pairwise comparisons, highlight the strengths and weaknesses of each robot option, and present our final recommendation based on the comprehensive evaluation. By thoroughly examining the selection process and outcomes, this study aims to contribute valuable insights into the application of MCDM techniques for optimizing warehouse operations through the integration of autonomous robots.

## 2. Literature Review

Markowski & Bilski (2023) discuss the evaluation of distributed frameworks using optimization routines to determine the shortest path for robots in a warehouse, comparing Dijkstra, Floyd-Warshall, and Bellman-Ford algorithms for avoiding downtime and collisions among robots. Kattepur et al. (2018) highlight the use of distributed optimization techniques in coordinating robotic units for warehouse inventory automation, emphasizing the importance of task/resource allocation among autonomous agents to maximize efficiency and scalability. Yang et al. (2021) introduces a maximin-based multi-objective evolutionary algorithm using a one-by-one update scheme, which enhances multi-robot scheduling optimization for intelligent warehouse systems and addresses real-world scheduling challenges effectively. Smit et al. (2024) proposes a multi-objective Deep Reinforcement Learning approach to learn effective allocation policies in collaborative human-robot order picking systems, aiming to maximize pick efficiency and improve workload fairness among human pickers.

Haghani et al. (2021) discusses optimizing the coordination of a fleet of robots in a warehouse to maximize net profit while respecting constraints, providing insights into vehicle routing problems with time windows. Ho et al. (2024) introduce a Federated Deep Reinforcement Learning algorithm for task scheduling in heterogeneous autonomous robotic systems, optimizing warehouse task scheduling and showing improved performance in minimizing task queue length. Gödeke & Detzner (2023) propose a simulative approach to address the

fleet sizing problem combined with decentralized Multi-Robot Task Allocation (MRTA) for Autonomous Mobile Robots (AMRs) in warehouses. Liu et al. (2024) focus on enhancing robot perception and navigation in logistics warehouses through an improved Gmapping algorithm, resulting in better obstacle detection rates and increased accuracy in travel distance. Sugiura et al. (2023) proposes a method utilizing BLPSO and MIQCPs for optimizing product assignments and in-shelf layout in warehouses to enhance picking operations efficiency through autonomous mobile robots. Kalempa et al. (2021) present a novel approach to optimize production in smart factories using autonomous robots for efficiency and flexibility in warehouse logistics through Multi-Robot Preemptive Task Scheduling with Fault Recovery (MRPF). Thammachantuek & Ketcham (2022) develop an algorithm for path planning of autonomous mobile robots that considers the shortest, smoothest, and safest paths, offering an evolutionary operator to prevent local optimum trapping.

Al Khatib et al. (2024) discusses the use of Autonomous Mobile Robots in warehouse operations to lower human error and increase efficiency, highlighting advancements in inventory management within the healthcare industry. Cognominal et al. (2021) examine the evolving field of autonomous mobile robotics, detailing recent technological advancements and a broad spectrum of applications across industries driven by innovation and interdisciplinary integration. Farinelli et al. (2017) explore advanced strategies for coordinating multiple robots in logistics settings, focusing on algorithms and architectures that enable efficient task distribution, path planning, and system scalability in dynamic environments. Taleb et al. (2025) focus on developing robust path-planning algorithms to ensure seamless navigation of autonomous mobile robots in warehouse settings, addressing challenges related to dynamic obstacles and real-time decision-making.

Zhan (2025) explores innovative applications of artificial intelligence in logistics scheduling, presenting advanced computational methods designed to optimize task allocation, resource utilization, and real-time decision-making in complex supply chain environments. Dabic-Miletic and Knezevic (2024) examine methods for selecting optimal alternatives to achieve sustainable intralogistics in automotive industry warehouse supply chains, with an emphasis on balancing operational efficiency and environmental considerations. Lee & Kim (2024) develop an adaptive path planning method based on the AHP, tailored to account for varying mobile robot driving environments, with the goal of enhancing navigation efficiency and decision-making in dynamic operational contexts.

Liu et al. (2022) propose a deep learning-based approach for accurately identifying warehouse goods, aiming to enhance the precision and efficiency of robot-assisted picking operations within automated logistics systems. Puljiz et al. (2018) explore the implementation of augmented reality technologies in autonomous warehouses, identifying key challenges and potential opportunities for enhancing human-robot collaboration, spatial awareness, and operational efficiency. Pietrantoni et al. (2024) investigate the integration of collaborative robots across manufacturing, logistics, and agriculture, presenting expert insights into technical challenges, safety considerations, and human factors influencing successful adoption.

Parikh et al. (2022) present the design and implementation of an autonomous mobile robot system tailored for inventory management in the retail industry, highlighting its potential to improve stock accuracy, operational efficiency, and real-time data tracking. Suszyński and Rogalewicz (2020) apply multi-criteria decision-making methods to support the selection of industrial robots for assembly tasks, aiming to improve decision quality by systematically evaluating key performance and operational factors. D'Andrea and Wurman (2008) discuss the future challenges associated with coordinating large fleets of autonomous vehicles within distribution facilities, emphasizing issues related to scalability, real-time decision-making, and system robustness in practical robotic applications. Finco et al. (2023) investigate various

manual picking workstation configurations within robotized and automated warehouse systems, analyzing the trade-offs between ergonomic design and productivity to inform optimal system integration and worker performance.

Keith and La (2024) provide a comprehensive review of autonomous mobile robots designed for warehouse environments, examining their capabilities, deployment challenges, and the evolving technologies that support their integration into modern logistics systems. Li et al. (2024) explore the use of machine learning techniques to enhance the performance of automated picking systems in warehouse robots, aiming to improve efficiency and accuracy in warehouse operations. Sayeed et al. (2022) explore various approaches and challenges within the Internet of Robotic Things (IoRT), focusing on the integration of robotics with IoT technologies to enable intelligent perception, communication, and autonomous decision-making in connected environments. Dabic-Miletic (2024) addresses the challenges of integrating artificial intelligence and robotics into sustainable warehouse management systems (WMS), focusing on how these technologies can enhance economic resilience within supply chains. Finally, Licardo et al. (2024) conduct a systematic review of intelligent robotics, highlighting emerging technologies and trends that are shaping the future of autonomous systems across various industrial applications.

Although a wide range of studies have focused on improving robotic coordination, navigation, and scheduling in warehouse environments, few have directly addressed the challenge of selecting the most suitable autonomous robot using a structured, criteria-based evaluation framework. Moreover, many of these studies do not explicitly incorporate expert judgment or prioritize decision criteria systematically.

To address this gap, this study applies the AHP, which is well-suited for problems involving subjective judgment and hierarchical structuring of decision factors. By integrating expert preferences and performing pairwise comparisons, AHP provides a transparent and consistent basis for evaluating autonomous robot alternatives in a warehouse setting.

### 3. Analytic Hierarchy Process

AHP is a method used to solve multi-criteria decision-making problems. AHP is used to reduce complexity in the decision-making process and helps the decision-maker to weigh different criteria and alternatives. Here are the basic steps of the AHP method (Saaty, 1980):

- Step 1: Creating a Decision Tree: The first step is to create a decision tree. This tree shows the goals, criteria, and alternatives in a hierarchical structure.
- Step 2: Creating Pairwise Comparison Matrices: For each criterion or alternative, a pairwise comparison matrix is created. In these matrices, it is indicated how much more important each pair is compared to the other. The scale usually ranges from 1 to 9, where 1 means equal importance and 9 means much more important.
- Step 3: Calculating Priorities: Using the pairwise comparison matrices, the importance of each criterion or alternative relative to others is determined. In this step, a consistency check is also performed.
- Step 4: Consistency Check: The consistency of the importance degrees for each criterion or alternative is checked using the pairwise comparison matrices. If the matrices are inconsistent, the comparisons are reviewed and redone.
- Step 5: Determining the Best Alternative: After calculating the priorities and checking consistency, the best alternative or alternatives are determined. These alternatives represent the most suitable ones in the decision-making process.

#### 4. Problem Statement

In this section, a problem related to optimizing operations in a large warehouse of a company operating in the logistics sector is addressed. The company's warehouse is where the entry and exit of hundreds of products are managed, and it is desired to modernize it by replacing manual operations with autonomous robots. The company is evaluating different autonomous robot alternatives: These alternatives are Autonomous Robot (AR)-1, AR-2 and AR-3. The logistics company used the AHP method to determine which autonomous robot is the most suitable. Criteria such as Carrying Capacity (C1), Speed (C2), Maneuverability (C3), Battery Life (C4), and Investment Cost (C5) were determined by experts. The decision matrix was first created as follows. The AHP steps are applied to Table 1 and the final weights are provided in Table 2. The hierarchy of the problem is provided in Figure 1.

To derive the pairwise comparisons required by the AHP method, expert judgments were obtained from three professionals with more than 10 years of experience in logistics and warehouse automation. The experts included a warehouse operations manager, a robotics systems engineer, and a supply chain consultant. Data were collected through structured interviews where each expert completed a Saaty scale-based comparison matrix. The geometric mean method was used to aggregate the individual judgments into a single consensus matrix for analysis.

The pairwise comparisons among the criteria were conducted through structured interviews with three logistics experts working in warehouse management. Each expert independently evaluated the relative importance of the criteria using the Saaty 1–9 scale, where 1 represents equal importance and 9 indicates extreme importance of one element over another. Their responses were aggregated using the geometric mean to form the final pairwise comparison matrix. The consistency ratio (CR) of the matrix was calculated and found to be 0.07, which is within the acceptable limit ( $CR < 0.10$ ), indicating consistent judgments.

**Table 1.** The decision matrix

Criteria	C1	C2	C3	C4	C5
C1	1	5	3	7	5
C2	1/5	1	2	5	3
C3	1/3	1/2	1	3	5
C4	1/7	1/5	1/3	1	9
C5	1/5	1/3	1/5	1/9	1

**Table 2.** Criteria weights

Rank	Criterion name	Criterion weight
1	C1	0.513
2	C2	0.261
3	C3	0.129
4	C4	0.063
5	C5	0.033

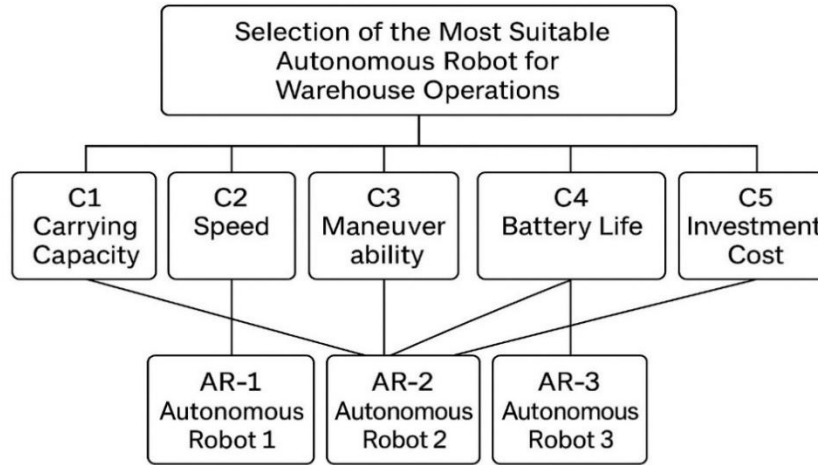


**Figure 1.** The hierarchy of the problem

As shown in Table 2, the AR selection results indicate that C1 holds the highest priority. The subsequent priorities, based on the calculated weights, are assigned to C2, C3, C4, and C5, respectively.

The evaluation of each AR is presented in Table 3, while Table 4 provides the final values for each AR. According to Table 4, AR-1 holds the highest priority, followed by AR-2 and AR-3 based on the calculated weights.

**Table 3.** AR weights

C5		
1	AR-1	0.785
2	AR-2	0.149
3	AR-3	0.066
C4		
1	AR-1	0.63
2	AR-2	0.218
3	AR-3	0.151
C3		
1	AR-1	0.709
2	AR-2	0.179
3	AR-3	0.113
C2		
1	AR-1	0.799
2	AR-2	0.105
3	AR-3	0.096
C1		
1	AR-1	0.637
2	AR-2	0.258
3	AR-3	0.105



**Table 4.** Autonomous robot results

Rank	Alternatives	Alternative Weight
1	AR-1	0.693
2	AR-2	0.201
3	AR-3	0.106

## 5. Conclusion

The logistics sector is a continuously growing and evolving industry that plays a crucial role in the transportation, storage, and distribution of goods along the supply chain. Effective and efficient logistics operations are essential for enhancing the competitiveness of businesses. In recent years, autonomous robots have emerged as a significant innovation in the logistics sector. These robots are machines that can perform tasks without the need for human intervention, and they are typically used in storage and transportation operations. The use of autonomous robots can make operations such as warehouse management and material handling faster, more efficient, and safer.

Autonomous robots, especially those used in large warehouses and distribution centers, are less prone to errors compared to manual labor and can ensure the continuity of operations. Moreover, these robots can often work in areas that are inaccessible or difficult for humans to reach, allowing for more efficient use of warehouse space. Therefore, many businesses in the logistics sector are considering integrating autonomous robots into their operations.

This study evaluates three different autonomous robot alternatives for optimizing the warehouse operations of a company in the logistics sector. The comparison criteria include Carrying Capacity, Speed, Maneuverability, Battery Life, and Investment Cost. Separate comparison matrices were created for each criterion for the three alternatives, AR-1, AR-2, and AR-3, and the importance ranking of the criteria was determined using the AHP method. The results show that Carrying Capacity is the most important criterion. Among the three autonomous robot alternatives, AR-1 was found to be the most suitable, followed by AR-2 and AR-3.

The selection of AR-1, which ranked highest in carrying capacity, speed, and maneuverability, suggests a strong operational fit for warehouses prioritizing high throughput and flexibility. However, it should be noted that AR-1 had a relatively lower performance in terms of investment cost, indicating a trade-off between performance and affordability. Organizations with budget constraints may need to reconsider the weight assigned to investment cost or conduct a cost-benefit analysis to justify the higher initial expenditure. This result underscores the importance of aligning robot selection not only with technical performance but also with the financial and strategic goals of the organization.

The findings of this study provide practical value for warehouse managers and logistics companies seeking to integrate autonomous robots into their operations. The AHP-based framework can be directly applied to assess robot procurement decisions by tailoring the criteria weights according to firm-specific needs (e.g., cost sensitivity, speed priorities). Moreover, the decision model is adaptable and can be reused in other warehouse contexts or expanded to include more alternatives and criteria over time. This makes the methodology both scalable and customizable for strategic decision-making in automation planning.

Despite its usefulness, this study has several limitations. First, the number of alternatives was limited to three, which may not reflect the full spectrum of available autonomous robot solutions in the market. Second, the weightings were based on expert judgment, which may introduce subjectivity despite consistency checks. Third, the decision criteria were assumed to be independent, whereas real-world decisions often involve interdependencies that may be better captured using methods like Analytic Network Process (ANP).

Future research can expand the model by incorporating more alternatives, additional criteria (e.g., maintenance cost, software compatibility), and dynamic criteria interrelationships using fuzzy AHP or ANP. Additionally, combining AHP with other MCDM techniques such as TOPSIS or MARCOS may enhance the robustness of decision-making. Longitudinal studies involving real-life implementation of selected robots would also help validate the practical impact of such models.

### Authorship Contribution Statement

The author is solely responsible for the conceptualization, methodology, data collection, analysis, and manuscript preparation.

### Conflict of Interest

The author declares no conflict of interest.

### References

- Al Khatib, I., Alasheh, S., & Shamayleh, A. (2024). The drivers of complexity in inventory management within the healthcare industry: A systematic review. *International Journal of Service Science, Management, Engineering, and Technology (IJSSMET)*, 15(1), 26. <https://doi.org/10.4018/IJSSMET.347332>
- Bensalem, S., Gallien, M., Ingrand, F., Kahloul, I., & Thanh-Hung, N. (2009). Designing autonomous robots. *IEEE Robotics & Automation Magazine*, 16(1), 67–77. <https://doi.org/10.1109/MRA.2008.931631>
- Chakraborty, S., Mukherjee, S., Nag, T., Biswas, B., Garang, B., & Nayak, A. (2018). A low cost autonomous multipurpose vehicle for advanced robotics. *2018 9th IEEE Annual Ubiquitous Computing, Electronics & Mobile Communication Conference (UEMCON)* (pp. 1067–1078). IEEE. <https://doi.org/10.1109/UEMCON.2018.8796543>
- Cognominal, M., Patronymic, K., & Wańkiewicz, A. (2021). Evolving field of autonomous mobile robotics: Technological advances and applications. *Fusion of Multidisciplinary Research, An International Journal*, 2(2), 189–200. <https://doi.org/10.63995/USAS3015>
- Dabić-Miletić, S., & Knežević, N. (2024). Selecting optimal alternatives for sustainable intralogistics in automotive industry warehouse supply chains. *Journal of Green Economics and Low-Carbon Development*, 3\*(4), 223–234. <https://doi.org/10.56578/jgelcd030402>
- Dabić-Miletić, S. (2024). The challenges of integrating AI and robotics in sustainable WMS to improve supply chain economic resilience. *Journal of Industrial Intelligence*, 2(2), 119–131. <https://doi.org/10.56578/jii020205>
- D'Andrea, R., & Wurman, P. (2008, November). Future challenges of coordinating hundreds of autonomous vehicles in distribution facilities. *2008 IEEE International Conference on Technologies for Practical Robot Applications* (pp. 80–83). IEEE. <https://doi.org/10.1109/TEPRA.2008.4686677>



- Farinelli, A., Boscolo, N., Zanotto, E., & Pagello, E. (2017). Advanced approaches for multi-robot coordination in logistic scenarios. *Robotics and Autonomous Systems*, 90, 34-44. <https://doi.org/10.1016/j.robot.2016.08.010>
- Finco, S., Ashta, G., Persona, A., & Zennaro, I. (2023). Investigating different manual picking workstations for robotized and automated warehouse systems: Trade-offs between ergonomics and productivity aspects. *Computers & Industrial Engineering*, 185, 109668. <https://doi.org/10.1016/j.cie.2023.109668>
- Gödeke, J., & Detzner, P. (2023, September). A simulative approach to AMR fleet sizing in decentralized multi-robot task allocation. *2023 IEEE 28th International Conference on Emerging Technologies and Factory Automation (ETFA)* (pp. 1-8). IEEE. <https://doi.org/10.1109/ETFA54631.2023.10275717>
- Haghani, N., Li, J., Koenig, S., Kunapuli, G., Contardo, C., Regan, A., & Yarkony, J. (2021). *Multi-robot routing with time windows: A column generation approach* [Preprint]. arXiv. <https://doi.org/10.48550/arXiv.2103.08835>
- Ho, T. M., Nguyen, K.-K., & Cheriet, M. (2022, December). Federated deep reinforcement learning for task scheduling in heterogeneous autonomous robotic system. *\*GLOBECOM 2022 - 2022 IEEE Global Communications Conference\** (pp. 1134-1139). IEEE. <https://doi.org/10.1109/GLOBECOM48099.2022.10000980>
- Kalempa, V. C., Piardi, L., Limeira, M., & de Oliveira, A. S. (2021). Multi-robot preemptive task scheduling with fault recovery: A novel approach to automatic logistics of smart factories. *Sensors*, 21(19), 6536. <https://doi.org/10.3390/s21196536>
- Keith, R., & La, H. M. (2024). *Review of autonomous mobile robots for the warehouse environment* [Preprint]. arXiv. <https://doi.org/10.48550/arXiv.2406.08333>
- Lee, J., & Kim, C. (2024). Development of an adaptive AHP path planning method considering the mobile robot driving environment. *IEEE Access*, 12, 95565-95575. <https://doi.org/10.1109/ACCESS.2024.3423421>
- Li, K., Wang, J., Wu, X., Peng, X., Chang, R., Deng, X., & Hong, B. (2024). *Optimizing automated picking systems in warehouse robots using machine learning* [Preprint]. arXiv. <https://arxiv.org/abs/2408.16633>
- Licardo, J. T., Domjan, M., & Orehovački, T. (2024). Intelligent robotics – A systematic review of emerging technologies and trends. *Electronics*, 13(3), 542. <https://doi.org/10.3390/electronics13030542>
- Liu, X., Gong, G., Hu, X., Shang, G., & Zhu, H. (2024). Cognitive enhancement of robot path planning and environmental perception based on Gmapping algorithm optimization. *Electronics*, 13(5), 818. <https://doi.org/10.3390/electronics13050818>
- Liu, H., Zhou, L., Zhao, J., Wang, F., Yang, J., Liang, K., & Li, Z. (2022). Deep-learning-based accurate identification of warehouse goods for robot picking operations. *Sustainability*, 14(13), 7781. <https://doi.org/10.3390/su14137781>
- Markowski, T., & Bilski, P. (2021). Optimization of autonomous agent routes in logistics warehouse. *International Journal of Electronics and Telecommunications*, 67(4), 559-564. <https://doi.org/10.24425/ijet.2021.137846>
- Parikh, H., Saijwal, I., Panchal, N., & Sharma, A. (2022). Autonomous mobile robot for inventory management in retail industry. In P. K. Singh, S. T. Wierzchoń, J. K. Chhabra, & S. Tanwar (Eds.), *Futuristic trends in networks and computing technologies* (pp. 93-110). Springer. [https://doi.org/10.1007/978-981-19-5037-7\\_7](https://doi.org/10.1007/978-981-19-5037-7_7)

- Peng, L., Liu, L., Long, T., Wang, H., & Chen, L. (2014). Sequential RBF surrogate-based efficient optimization method for engineering design problems with expensive black-box functions. *Chinese Journal of Mechanical Engineering*, 27, 1099-1111. <https://doi.org/10.3901/CJME.2014.0820.138>
- Pietrantoni, L., Favilla, M., Fraboni, F., Mazzoni, E., Morandini, S., Benvenuti, M., & De Angelis, M. (2024). Integrating collaborative robots in manufacturing, logistics, and agriculture: Expert perspectives on technical, safety, and human factors. *Frontiers in Robotics and AI*, 11, 1342130. <https://doi.org/10.3389/frobt.2024.1342130>
- Puljiz, D., Gorbachev, G., & Hein, B. (2018). *Implementation of augmented reality in autonomous warehouses: Challenges and opportunities* [Preprint]. arXiv. <https://doi.org/10.48550/arXiv.1806.00324>
- Sayeed, A., Verma, C., Kumar, N., Koul, N., & Illés, Z. (2022). Approaches and challenges in Internet of Robotic Things. *Future Internet*, 14(9), 265. <https://doi.org/10.3390/fi14090265>
- Saaty, T. L. (1980). *The analytic hierarchy process: Planning, priority setting, resource allocation*. McGraw-Hill.
- Smit, I. G., Bukhsh, Z., Pechenizkiy, M., Alogariastos, K., Hendriks, K., & Zhang, Y. (2024). *Learning efficient and fair policies for uncertainty-aware collaborative human-robot order picking* [Preprint]. arXiv. <https://doi.org/10.48550/arXiv.2404.08006>
- Suszyński, M., & Rogalewicz, M. (2020). Selection of an industrial robot for assembly jobs using multi-criteria decision making methods. *Management and Production Engineering Review*, 11(1), 62-72. <https://doi.org/10.24425/mper.2020.132944>
- Sugiura, A., Suzuki, T., Ihara, K., Sakuma, T., & Kato, S. (2023). Generating products placement in warehouse using BLP SO and MIQCPs. *Proceedings of the International Conference on Robotics and Automation*, 22(2), 345-358. <https://doi.org/10.5220/0012359600003636>
- Taleb, M. A., Korsoveczki, G., & Husi, G. (2025). Automotive navigation for mobile robots: Comprehensive review. *Results in Engineering*, 27, 105837. <https://doi.org/10.1016/j.rineng.2025.105837>
- Thammachantuek, I., & Ketcham, M. (2022). Path planning for autonomous mobile robots using multi-objective evolutionary particle swarm optimization. *PLOS ONE*, 17(8), e0271924. <https://doi.org/10.1371/journal.pone.0271924>
- Ueno, K., Kinoshita, T., Kobayashi, K., & Watanabe, K. (2015). Development of a robust path-planning algorithm using virtual obstacles for an autonomous mobile robot. *Journal of Robotics and Mechatronics*, 27(3), 286-292. <https://doi.org/10.20965/jrm.2015.p0286>
- Yang, S., Chen, W., Wang, L., Zhang, X., & Li, Y. (2021). A novel maximin-based multi-objective evolutionary algorithm using one-by-one update scheme for multi-robot scheduling optimization. *IEEE Access*, 9, 121316-121328. <https://doi.org/10.1109/ACCESS.2021.3105102>
- Zhan, Y. (2025). Innovative applications of artificial intelligence in logistics scheduling. In G. A. Tsihrintzis, M. N. Favorskaya, R. Kountcheva, & S. Patnaik (Eds.), *Advances in computational vision and robotics: ICCVR 2024* (pp. 451-465). Springer. [https://doi.org/10.1007/978-3-031-85952-6\\_45](https://doi.org/10.1007/978-3-031-85952-6_45)



# Renewable Energy Adoption and Economic Resilience in Africa: A Case Study of Morocco

Oluwaseun A. Oyebamiji<sup>1\*</sup>, Muhammad Abdulaziz Muhammad<sup>2</sup>, Kamal Tasiu Abdullahi<sup>3</sup>

<sup>1</sup>Ege University, Faculty of Agriculture, Department of Agricultural Economics, İzmir, Türkiye

<sup>2</sup>Bayero University, Department of Economics, Kano, Nigeria

<sup>3</sup>Istanbul University, Faculty of Economics, Department of Economics, İstanbul, Türkiye

## Research Article

\*Correspondence:  
seunharde@gmail.com

Received: 20 May 2025  
Accepted: 25 July 2025  
Published: 30 July 2025

## Keywords

Renewable energy  
Economic resilience  
Morocco  
Sustainable development  
Energy transition

This is an open access article  
under the CC BY NC license.



## Abstract

Morocco faces significant challenges in meeting its rapidly growing electricity demand, which is projected to increase by two to five times by 2030. In response, the country has set ambitious renewable energy targets—aiming for 42% of total installed capacity by 2020 and 52% by 2030. This study examines the relationship between renewable energy adoption and economic resilience in Morocco, in the context of increasing electricity needs and aggressive renewable targets. Employing a Structural Vector Autoregression model covering the period 1980–2024, the analysis reveals that renewable energy investments contribute positively to GDP growth, though their effects on emissions are mixed. While large-scale solar and wind projects have enhanced energy security and job creation, persistent infrastructure deficits and policy shortcomings limit their environmental impact. To ensure sustainable development, policymakers must complement renewable expansion with stricter energy efficiency standards, advanced clean technologies, and robust environmental regulations. Targeted subsidies and integrated planning will be essential to prevent economic growth from undermining environmental sustainability. Immediate action is needed to align Morocco's energy goals with its climate commitments.

## 1. Introduction

The adoption of renewable energy is seen as essential for sustainable development (United Nations, 2021; Sovacool & Dworkin, 2014). Renewable energy helps reduce climate change risks and promotes stronger economic systems. As governments worldwide confront climate change, energy security, and economic challenges, the transition to renewable energy has become even more important (IEA, 2020).

The Intergovernmental Panel on Climate Change (IPCC) stresses that reducing greenhouse gas emissions and cutting dependence on fossil fuels demands urgent action. Renewable energy, generated from natural sources like the sun, wind, water, and geothermal heat, offers a safer and more sustainable alternative (REN21, 2020). Falling technology costs, better energy

**How to cite this paper:** Oyebamiji, O. A., Muhammad, M. A., & Abdullahi, K. T. (2025). Renewable energy adoption and economic resilience in Africa: A case study of Morocco. *Scientific Research Communications*, 5(2), 77–93. <https://doi.org/10.52460/src.2025.007>

storage, and improved grid integration have made renewable options increasingly competitive (IRENA, 2021). Countries are now more aware of the need to fight climate change and unlock the economic benefits of renewable energy. As a result, many are expanding efforts to shift toward low-carbon energy systems.

Economic resilience is the ability of an economy to withstand and recover from internal and external shocks while maintaining its core functions (Cherevatskyi, 2023; Ramli & Ithnin, 2022; Hynes et al., 2022). This concept has gained traction, especially after global disruptions like the COVID-19 pandemic (Filipenko, 2022). Resilience includes the capacity to adapt to adverse conditions and avoid business failures and production declines (Radic et al., 2022). It also covers natural, technological, economic, and political factors (Steen et al., 2024).

The link between renewable energy and economic resilience is increasingly evident. Countries with a more balanced and diverse energy supply recover faster from economic crises. When renewables make up a large share of the energy mix, recovery is even quicker (Donohue et al., 2023). In developing countries, innovations in renewable energy have improved efficiency and reduced harmful emissions (Aldieri et al., 2023). However, integrating renewables into electricity markets brings new uncertainties and risks, making it necessary to evaluate financial resilience (Sharma et al., 2024). Better connections between power and gas systems, enabled by renewables, offer critical economic benefits and help manage fluctuations in power supply (Sayed et al., 2023).

In response to these trends, many countries have launched programs to promote renewable energy use. Morocco has made notable efforts but still faces challenges in securing its future energy needs, particularly for electricity. Setting ambitious renewable energy goals: 42 per cent of total electricity generation capacity by 2020 and 52 per cent by 2030 (PMV, 2022). As global demand for energy rises, Morocco is giving more attention to renewable options that are accessible, affordable, and sustainable (Belakhdar et al., 2014).

Population growth and economic development are expected to drive Morocco's electricity demand to double relative to the North Mediterranean region (Kousksou et al., 2015; Ouammi et al., 2012). Projections suggest that annual electricity demand could climb from 35 TWh in 2016 to between 80 TWh and 170 TWh by 2030. Meeting this demand would require increasing generation capacities by four times by 2030 and more than ten times by 2050.

This study investigates the impact of renewable energy on Morocco's economy through two key research objectives:

- Research Question 1: Evaluate the economic implications of renewable energy investments in Morocco.
- Research Question 2: Examine the dynamic interrelationships among renewable energy deployment, economic growth, and carbon emissions.

By addressing these questions, the study aims to bridge a critical gap in Morocco's renewable energy strategy. The resulting insights will illuminate both the potential advantages and inherent constraints of expanding renewable energy initiatives. Moreover, the findings will inform the development of more resilient and sustainable energy policies tailored to Morocco's long-term economic and environmental goals.

## 2. Theoretical Framework

### 2.1. Resilience and sustainable development theories

Sustainable development became a major global framework after the release of the Brundtland Report in 1987. The report defined it as "development that meets the needs of the present

without compromising the ability of future generations to meet their own needs" (World Commission on Environment and Development [WCED], 1987). It responded to rising concerns about environmental degradation and the limits of traditional economic models that pursued growth without accounting for social and ecological costs.

However, the integration of resilience theory with sustainable development remains an underdeveloped area in the Brundtland framework, particularly regarding systemic shocks and long-term adaptability. While the WCED (1987) report established the triple-bottom-line approach, it did not fully account for how socio-ecological systems maintain functionality during disruptions—a gap later addressed by Folke et al. (2010) in their work on resilience thinking. Their research demonstrates that sustainable development requires not just balance among economic, environmental and social factors, but also the capacity to absorb disturbances and reorganise while undergoing change (Folke et al., 2010). This evolutionary perspective is critical for energy transitions, where lock-in effects and infrastructure inertia create vulnerability to climate shocks.

The "limits to growth" thesis (Meadows et al., 1972) implicitly acknowledged resilience concepts through its emphasis on system feedback loops, but contemporary scholars have strengthened this connection. Walker and Salt (2012) argue that resilience provides the missing operational framework for sustainable development, particularly through their concept of "transformability" –the capacity to create fundamentally new systems when ecological, economic or social conditions make the existing system untenable (Walker & Salt, 2012). In Morocco's energy transition, this manifests in the need to simultaneously phase out fossil fuel dependence while building renewable energy systems that can withstand climate variability and economic fluctuations, a challenge documented by Ouedraogo et al. (2017) in African energy systems.

Recent scholarship bridges this theoretical gap by framing sustainable development as inherently dependent on resilience capacities. According to Bahadur et al. (2015), the "resilience dividend" emerges when development initiatives combine WCED's intergenerational equity with capacities to anticipate, absorb and adapt to shocks (Bahadur et al., 2015). This fusion proves particularly relevant for Morocco's solar megaprojects, where Benatia et al., (2025) and Leichenko & O'Brien (2024) demonstrate that renewable energy infrastructure must be designed not just for low emissions, but also for climate resilience and equitable access—what they term "triple-win" sustainability (Benatia et al., 2025; Leichenko & O'Brien, 2024).

What sets sustainable development apart is its insistence on linking economic, environmental, and social objectives. This integration moves beyond sectoral approaches, encouraging development models that are more resilient, equitable, and sensitive to long-term needs. The framework stresses that true progress means balancing economic growth with environmental protection and social justice, making sure benefits are distributed fairly and that resource use does not undermine future well-being.

In the energy sector, sustainable development principles have played a crucial role in driving the shift from fossil fuels to renewable sources. This transition is necessary not only to curb greenhouse gas emissions and limit climate change but also to secure reliable energy access and promote social equity. Applying sustainable development thinking enables policymakers to design energy strategies that advance growth while protecting ecosystems and reducing inequalities. Recognizing the interconnectedness of economic, environmental, and social systems is central to achieving these goals and building a truly sustainable future.



## 2.2. Empirical evidence

Renewable energy adoption shows a positive relationship with economic resilience, as documented in several studies (Oraibi et al., 2023; Ahmad et al., 2022). Successful projects provide clean, reliable energy while supporting broader sustainable development goals (Shirley & Medhin, 2022; Onuoha et al., 2023). Systemic risk analysis frameworks for electricity markets have stressed the importance of accounting for the diversity and composition of energy sources in models of economic resilience.

Evidence from empirical studies proves that renewable energy adoption strengthens resilience in developing regions. Innovations in clean energy improve system efficiency and help countries withstand energy shocks and environmental risks (Aldieri et al., 2023). Distributed energy systems (DESS) based on clean technologies present a promising strategy for sustainable development and poverty reduction in rural and remote areas. These systems can raise living standards, boost local economies, and improve environmental outcomes (Ahmad et al., 2022).

Income distribution patterns also influence renewable energy consumption. Lower income inequality tends to encourage greater adoption of clean energy sources (Mehmood et al., 2022). These findings underline the role of renewable energy in advancing economic resilience and sustainable growth in low- and middle-income countries.

Integrating renewable sources such as hydro, wind, solar, and biomass offers a reliable and cost-effective solution to persistent electricity challenges (Lawal, 2023). Such projects can create jobs and stimulate economic activities, especially in rural areas with limited grid access (Adebayo et al., 2023). Renewable energy adoption also supports climate change mitigation by reducing carbon emissions (Ebhotu & Tabakov, 2022).

However, several challenges remain. Developing sufficient technical capacity, securing adequate financing, and improving access to reliable energy data are critical (Onuoha et al., 2023). Building strong public-private partnerships and creating business models that support productive energy use can help lower costs and manage regulatory risks.

In conclusion, the empirical literature highlights the multifaceted benefits of renewable energy adoption, including enhanced economic resilience, improved environmental outcomes, and equitable development in low- and middle-income countries. However, challenges such as technical limitations, financing constraints, and data gaps underscore the need for targeted policy interventions. These findings provide a critical foundation for understanding the role of renewable energy in sustainable development and highlight gaps that the present study aims to address, particularly in the context of Morocco's unique socioeconomic and environmental landscape. This review sets the stage for an in-depth analysis of how renewable energy adoption influences Morocco's economic resilience and informs policy recommendations for overcoming identified barriers.

## 3. Methodology

### 3.1. Structural Vector Autoregression model

To address the objectives of this study, a Structural Vector Autoregression (SVAR) model was employed to analyze the dynamic relationships between renewable energy adoption, economic resilience, and carbon emissions in Morocco. The SVAR framework is well-suited for capturing the interdependencies among multiple time-series variables, as it models each variable as a function of its own lagged values and the lagged values of all other variables in the system (Khan et al., 2021). Unlike traditional VAR models, SVAR imposes structural restrictions to identify causal relationships, making it particularly effective for examining how

shocks to one variable, such as renewable energy adoption, propagate through the system to affect economic growth and environmental outcomes.

In this study, the SVAR model treats all variables—GDP, alternative energy (AENRGY), and CO<sub>2</sub> emissions—as endogenous, allowing for mutual interactions among them. This approach captures the dynamic feedback loops inherent in Morocco's energy-economic system, where renewable energy investments may influence GDP growth, which in turn affects emissions. The model's focus on stationary variables ensures robust econometric analysis, enabling the estimation of Impulse Response Functions (IRFs) and variance decompositions to assess the short- and long-term impacts of renewable energy shocks (Khan et al., 2021). By modeling these relationships, the SVAR framework provides insights into how Morocco's renewable energy policies contribute to economic resilience while addressing environmental sustainability.

Mathematically, the base of the SVAR model commences as:

$$Y_t = \beta_{10} - \beta_{12}Z_t + \gamma_{11}y_{t-1} + \gamma_{12}Z_{t-1} + \varepsilon_{yt} \quad (1)$$

$$Z_t = \beta_{20} - \beta_{21}Y_t + \gamma_{21}y_{t-1} + \gamma_{22}Z_{t-1} + \varepsilon_{zt} \quad (2)$$

Given that  $Y_t$  and  $Z_t$  are endogenous variables according to Equations (1) and (2), the contemporaneous effects of  $Z_t$  on  $Y_t$  and  $Y_t$  on  $Z_t$ , respectively, are captured by  $\beta_{12}$  and  $\beta_{21}$ . While the coefficients  $\varepsilon_{yt}$  and  $\varepsilon_{zt}$  represent structural flaws, the coefficients  $\gamma_i$  represent the lagged link between the variables.

Accordingly, Equations (3) to (10) below present the structural specification of the SVAR model:

$$\begin{aligned} \beta_0 Y_t &= \beta_1 Y_{t-1} + \beta_2 Y_{t-2} + \cdots + \beta_p Y_p + \varepsilon_t \beta_0 Y_t \\ &= \beta_1 Y_{t-1} + \beta_2 Y_{t-2} + \cdots + \beta_p Y_p + \varepsilon_t \end{aligned} \quad (3)$$

The reduced form of SVAR is specified as:

$$\begin{aligned} Y_t &= C + A_1 Y_{t-1} + A_2 Y_{t-2} + \cdots + \beta_p Y_p + \varepsilon_t Y_t \\ &= C + A_1 Y_{t-1} + A_2 Y_{t-2} + \cdots + \beta_p Y_p + \varepsilon_t \end{aligned} \quad (4)$$

Therefore,

$$\begin{aligned} \log RGDP_t &= \alpha_{10} - \alpha_{12} \log RENEW_t - \alpha_{13} \log CO2_t + \sum_{t-1}^p \beta_{11} {}^t \log RGDP_{t-1} \\ &\quad + \sum_{t-1}^p \beta_{12} {}^t \log RENEW_{t-1} + \sum_{t-1}^p \beta_{13} {}^t \log CO2_{t-1} + \mu_t^{RGDP} \end{aligned} \quad (5)$$

and

$$\begin{aligned} \beta_0 Y_t &= \beta_1 Y_{t-1} + \beta_2 Y_{t-2} + \cdots + \beta_p Y_p + \varepsilon_t \beta_0 Y_t \\ &= \beta_1 Y_{t-1} + \beta_2 Y_{t-2} + \cdots + \beta_p Y_p + \varepsilon_t \end{aligned} \quad (6)$$

The reduced form of SVAR is specified as:

$$\begin{aligned} Y_t &= C + A_1 Y_{t-1} + A_2 Y_{t-2} + \cdots + \beta_p Y_p + \varepsilon_t Y_t \\ &= C + A_1 Y_{t-1} + A_2 Y_{t-2} + \cdots + \beta_p Y_p + \varepsilon_t \end{aligned} \quad (7)$$



Therefore, for the structural form of real GDP the proxy of growth, Equation (8) represents the SVAR as:

$$\begin{aligned} \log RGDP_t = & \alpha_{10} - \alpha_{12} \log RENEW_t - \alpha_{13} \log CO2_t + \sum_{t-1}^p \beta_{11}^t \log RGDP_{t-1} \\ & + \sum_{t-1}^p \beta_{12}^t \log RENEW_{t-1} + \sum_{t-1}^p \beta_{13}^t \log CO2_{t-1} + \mu_t^{RGDP} \end{aligned} \quad (8)$$

Likewise, renewable energy (Renew) and alternative energy (AEnergy) – used interchangeably in this study – are represented as follows:

$$\begin{aligned} \log RENEW_t = & \alpha_{20} - \alpha_{22} \log RGDP_t - \alpha_{23} \log CO2_t + \sum_{t-1}^p \beta_{21}^t \log RENEW_{t-1} \\ & + \sum_{t-1}^p \beta_{22}^t \log RGDP_{t-1} + \sum_{t-1}^p \beta_{23}^t \log CO2_{t-1} + \mu_t^{GE} \end{aligned} \quad (9)$$

Finally, the emission's SVAR equation represented by CO<sub>2</sub> is expressed as:

$$\begin{aligned} \log CO2_t = & \alpha_{30} - \alpha_{32} \log RGDP_t - \alpha_{33} \log RENEW_t + \sum_{t-1}^p \beta_{31}^t \log CO2_{t-1} \\ & + \sum_{t-1}^p \beta_{32}^t \log RENEW_{t-1} + \sum_{t-1}^p \beta_{33}^t \log RGDP_{t-1} + \mu_t^{EG} \end{aligned} \quad (10)$$

The matrix form of Equations (8)–(10) is also provided below for clarity:

$$\begin{bmatrix} RGDP \\ RENEW \\ CO2 \end{bmatrix} = \begin{pmatrix} 1 & & \\ & 1 & \\ & & 1 \end{pmatrix} \begin{bmatrix} + & + & + \\ + & 1 & + \\ + & + & 1 \end{bmatrix} \begin{bmatrix} \mu_t^{RGDP} \\ \mu_t^{GE} \\ \mu_t^{EG} \end{bmatrix} \quad (11)$$

where

$$\begin{aligned} A = \begin{bmatrix} 1 & A_{12} & A_{13} \\ A_{21} & 1 & A_{23} \\ A_{31} & A_{32} & 1 \end{bmatrix}, \quad C = \begin{bmatrix} C_1 \\ C_2 \\ C_3 \end{bmatrix}, \quad Z = \begin{bmatrix} EXTRATE \\ GE \\ GDP \end{bmatrix}, \\ Z_{t-1} = \begin{bmatrix} EXTRATE_{t-1} \\ GE_{t-1} \\ GDP_{t-1} \end{bmatrix}, \quad U_t = \begin{bmatrix} \mu_t^{RGDP} \\ \mu_t^{GE} \\ \mu_t^{EG} \end{bmatrix} \end{aligned} \quad (12)$$

and

$$a = \begin{bmatrix} a_{11} & a_{12} & a_{13} \\ a_{21} & a_{22} & a_{23} \\ a_{31} & a_{32} & a_{33} \end{bmatrix} \text{ such that } U_t \sim iid(0, \sigma^2) \quad (13)$$

$Z$  and  $Z_{t-1}$  are  $3 \times 1$  vectors of dependent variables;  $Z_{t-1}$  is a vector of lagged variables;  $A$  is a  $3 \times 3$  matrix of the parameters to be estimated and identified with as a diagonal element;  $C$  is a  $3 \times 1$  vector of constants,  $a$  is a  $3 \times 3$  matrix of the coefficients of lagged variables; and  $U_t$  is a  $3 \times 1$  vector of the structural (or orthogonalized errors) which are assumed to be serially uncorrelated with a mean of zero and a constant variance (variance = 1).

### 3.2. Granger causality test

Granger causality tests assess whether one time-series variable provides statistically significant information for predicting another variable (Tiwari et al., 2023). Specifically, the test evaluates if current and lagged values of an independent variable improve the forecasting of a dependent variable beyond what is possible using only the dependent variable's own lagged values. The test is conducted by estimating a VAR model and computing the p-value for the null hypothesis that the coefficients of the independent variable's lagged terms are jointly zero. If the p-value is below the significance threshold (e.g., 0.05), the null hypothesis is rejected, indicating that the independent variable Granger-causes the dependent variable. Conversely, failure to reject the null suggests no Granger causality. This approach is particularly useful for identifying directional relationships among economic and environmental variables, such as renewable energy adoption and GDP growth.

### 3.3. Impulse response functions

IRFs are a critical tool in SVAR analysis, used to examine the dynamic interactions among endogenous variables following a shock. IRFs trace the time-path response of each variable to a one-standard-deviation shock in another variable, while holding all other shocks constant (Majenge et al., 2025). By applying an orthogonalized shock to the error term of one equation, IRFs capture the direction (positive or negative) and persistence (short- or long-term) of the shock's impact across the system over multiple periods. In this study, IRFs are employed to analyze how shocks to renewable energy adoption (AENRGY), GDP, and CO<sub>2</sub> emissions propagate through Morocco's economic and environmental systems, providing insights into the dynamic relationships among these variables.

### 3.4. Variance decompositions

Variance decomposition complements IRFs by quantifying the proportion of each variable's forecast error variance attributable to its own shocks versus those from other variables in the SVAR system. This method reveals the relative contribution of each variable's innovations to the variability of others, offering a clearer understanding of their interdependencies (Majenge et al., 2025). For instance, if a significant portion of GDP's forecast error variance is driven by shocks to renewable energy adoption, it underscores AENRGY's influence on economic resilience. In this study, variance decomposition is used to assess how much of the variability in GDP, AENRGY, and CO<sub>2</sub> emissions is explained by their own dynamics versus interactions with other variables, informing the role of renewable energy in Morocco's sustainable development.

## 4. Results and Discussions

Table 1 presents descriptive statistics for GDP, AENRGY, and carbon emissions (CO<sub>2</sub>) based on 38 observations. The standard deviations for all three variables are close to their respective means, suggesting moderate variability in the data.

- Central Tendency and Dispersion: The mean and median values are relatively close for all three variables, indicating symmetrical distributions. The standard deviations (3.555 for GDP, 4.683 for AENRGY, and 0.413 for CO<sub>2</sub>) suggest that AENRGY exhibits the highest relative variability, while Carbon Emissions display the lowest.
- Skewness values for AENRGY (0.087) and CO<sub>2</sub> (0.080) are positive but very close to zero, indicating nearly symmetrical (normal-like) distributions. GDP shows a slightly negative skew (-0.139), but still not substantial enough to indicate significant asymmetry.

- Kurtosis: GDP has a kurtosis value of 3.713, which is greater than 3, suggesting a leptokurtic distribution—one that is more peaked than the normal distribution. Conversely, AENRGY (1.848) and CO<sub>2</sub> (1.615) are platykurtic, implying flatter distributions compared to the normal.
- Normality (Jarque-Bera Test): For all variables, the Jarque-Bera test p-values exceed 0.05, meaning the null hypothesis of normality is not rejected at the 5% significance level. Hence, the data do not deviate significantly from normality.
- The overall results support the use of models assuming normality, such as the SVAR, especially since none of the series exhibit extreme skewness or kurtosis. This enhances the reliability of inference based on the chosen econometric framework.

**Table 1.** Descriptive statistics of SVAR

	GDP	AENRGY	CO <sub>2</sub>
Mean	2.62	1.22	1.46
Median	2.61	1.25	1.47
Maximum	10.78	8.91	2.14
Minimum	-6.85	-6.46	0.82
Std. Dev.	3.56	4.68	0.41
Skewness	-0.14	0.09	0.08
Kurtosis	3.71	1.85	1.62
Jarque-Bera	0.93	2.15	3.08
Probability	0.63	0.34	0.21
Sum	99.73	46.40	55.56
Sum Sq. Dev	0.63	0.34	0.21
Observations	38	38	38

Source: Researcher's computation using E-views 10. (2024)

Table 2 demonstrates that all selection criteria (Akaike Information Criterion [AIC], Hannan-Quinn Criterion [HQ], and Schwarz Criterion [SC]) consistently identify a one-lag specification as optimal. Consequently, the model estimation employs one lag.

The optimal lag length for the SVAR model is determined using the following multiple information criteria:

- AIC: Prioritizes model fit but may overfit by allowing more parameters.
- SC (or Bayesian Information Criterion, BIC): Penalizes complexity more harshly than AIC.
- HQ: Balances between AIC and SC.
- FPE (Final Prediction Error): Measures forecast accuracy.
- LR (Likelihood Ratio): Tests if the inclusion of additional lags improves the model.

All five criteria (AIC, SC, HQ, LR, and FPE) unanimously select lag length = 1 as optimal, as indicated by the asterisks (\*) in Table 2. Although lag 3 gives slightly better AIC than lag 2, it is not preferred over lag 1 in any criterion.

As a result, the consistent selection across multiple criteria strengthens confidence in choosing a one-lag model. Therefore, one lag is adopted for estimating the SVAR model, ensuring model parsimony and robustness.

**Table 2.** Optimal lag length selection for the SVAR model using AIC, HQ, and SC criteria

Lag	LogL	LR	FPE	AIC	SC	HQ
0	-164.65	NA	2.91	9.58	9.71	9.63
1	-62.25	181.39*	0.01*	4.24*	4.78*	4.43*
2	-56.80	8.73	0.02	4.45	5.38	4.77
3	-45.759	15.78	0.02	4.33	5.66	4.79

Source: Researcher's computation using E-views 10. (2024) \* indicates lag order selected by the criterion

#### 4.1. Structural Vector Autoregression stability test

The stability of SVAR model is essential for reliable interpretation of IRFs and variance decompositions. Stability requires that all eigenvalues of the SVAR system lie within the unit circle in the complex plane, ensuring that the system's responses to shocks converge over time rather than diverge or oscillate indefinitely. To verify this, a stability test was conducted using a pole-zero plot, which examines the eigenvalues of the companion matrix.

The pole-zero plot (Figure 1 below) displays all poles within the unit circle, confirming the model's stability. The x-axis represents the damping or amplification factor of the system's dynamics, while the y-axis indicates the frequency of oscillations. This result validates the stationarity of the SVAR system, ensuring that dynamic responses to shocks decay over time, supporting the reliability of subsequent analyses such as IRFs.

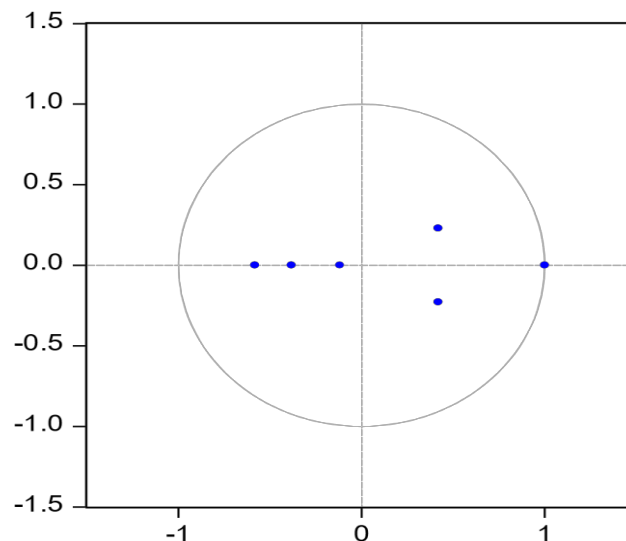


**Figure 1.** Pole-zero map of the estimated SVAR model

The pole zero map of the estimate, the x axis is the damping/amplification factor of the system's dynamics, while the y axis is the frequency of oscillations of the estimated equation.

## 4.2. Impulse Response Functions

The IRFs, derived from the SVAR model, illustrate the dynamic responses of GDP, AENRGY, and CO<sub>2</sub> emissions to structural shocks over a 10-period horizon. These responses, presented in Figure 2, reveal the interactions among these variables in Morocco's socioeconomic and environmental context.

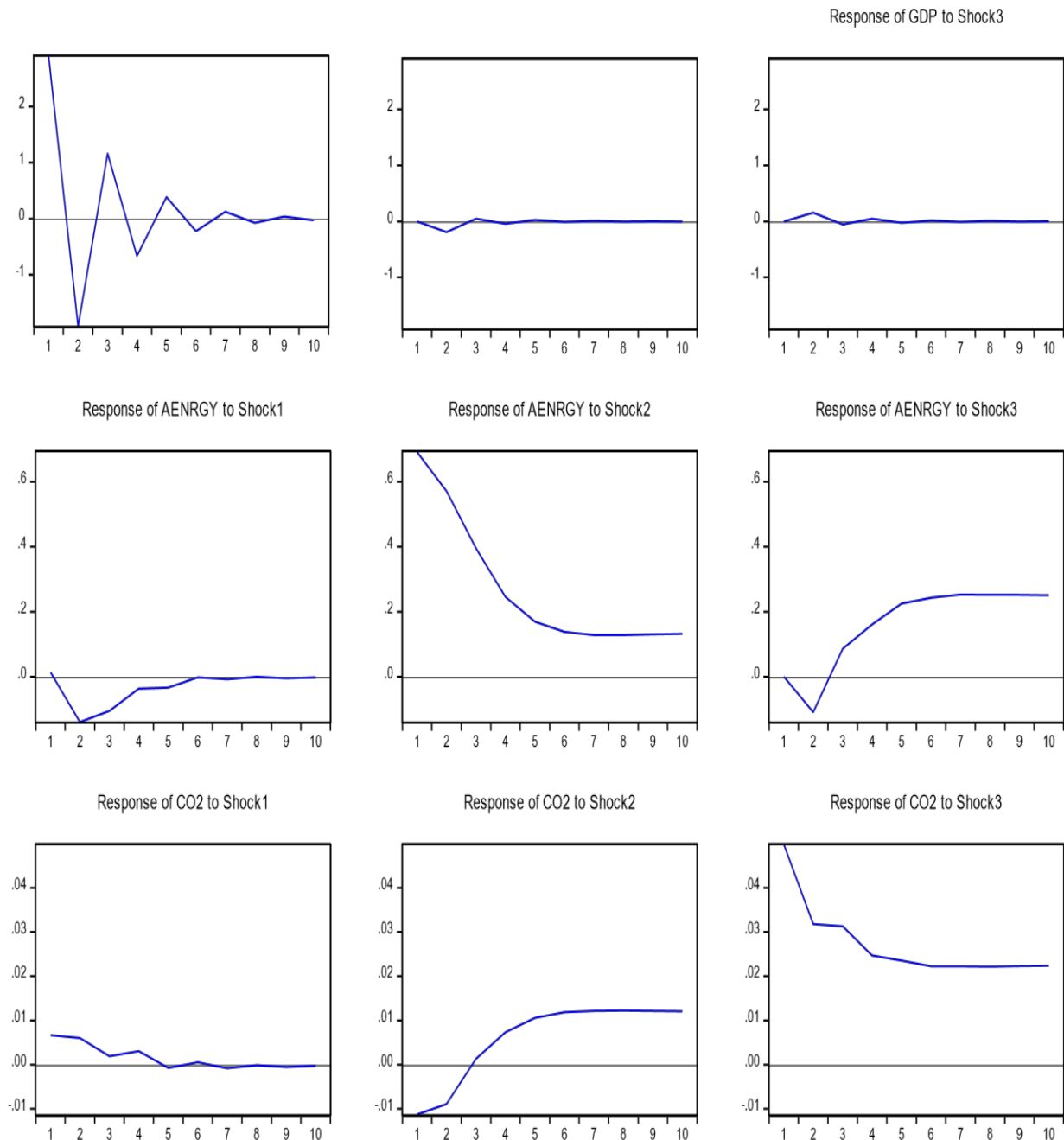


**Figure 2.** Compilation of responses to SVAR

Source: Researchers' compilation via E-views 10)

**GDP Responses:** The top-left panel shows that a shock to GDP causes significant short-term volatility, stabilizing after approximately five periods with oscillations indicating transitory effects. The responses of GDP to shocks in AENRGY and CO<sub>2</sub> emissions (top-middle and top-right panels) are muted, suggesting limited short-term feedback from these variables to economic output.

**AENRGY Responses:** The second row indicates that AENRGY responds negatively to a positive GDP shock, possibly due to increased demand for conventional energy during economic expansion. However, AENRGY shows a positive response to its own shock and increases steadily following a CO<sub>2</sub> emissions shock, reflecting environmental pressures driving renewable energy adoption.

**CO<sub>2</sub> Emissions Responses:** The third row reveals that CO<sub>2</sub> emissions rise with positive GDP shocks, consistent with economic growth increasing emissions. Conversely, a shock to AENRGY significantly reduces CO<sub>2</sub> emissions, highlighting the environmental benefits of renewable energy. Emissions also decline following their own shock, suggesting policy or market adjustments.

The SVAR results demonstrate that shocks to AENRGY, such as investments in solar or wind projects (e.g., the Noor Ouarzazate Solar Complex), generate a sustained positive response in GDP, reflecting job creation and infrastructure spending. However, this effect diminishes over time without continuous policy support, indicating challenges in scaling renewable energy initiatives. The muted GDP response to its own shocks suggests structural constraints, such as limited industrial diversification in Morocco's semi-industrialized economy. Additionally, a shock to AENRGY reduces CO<sub>2</sub> emissions, but a potential rebound effect—where efficiency gains lead to higher energy consumption in industries like phosphate mining—may temporarily increase emissions. These findings underscore the need for integrated policies, such as carbon pricing and energy efficiency measures, to maximize the economic and environmental benefits of Morocco's renewable energy transition.

#### 4.3. Diagnostic test

To ensure the reliability of the SVAR model used to analyze the relationships among AENRGY, GDP, and CO<sub>2</sub> emissions in Morocco, diagnostic tests were conducted to assess the model's residuals for serial correlation and heteroskedasticity. These tests are critical for validating the model's specification, as violations of key assumptions could distort statistical inferences, affecting the accuracy of IRFs and variance decompositions.

**Heteroskedasticity Test:** Heteroskedasticity refers to non-constant variance in the residuals, which can bias standard errors and compromise the validity of hypothesis testing in ordinary least squares (OLS)-based estimations. A White's test for heteroscedasticity was conducted to assess whether the residual variances vary across observations. As presented in Table 3, the test yields a Chi-squared statistic of 88.37 with 75 degrees of freedom and a p-value of 0.0923. Since the p-value exceeds the conventional 0.05 threshold, the null hypothesis of homoscedasticity is not rejected, suggesting that the residual variances are consistent across observations.

The model's residuals were tested for serial correlation and heteroscedasticity. The Breusch-Godfrey LM test shows p-values greater than 0.05 at all lags, confirming the absence of serial correlation. Similarly, as shown in Table 3 below, the heteroscedasticity test results indicate no evidence of heteroscedasticity, as the p-value exceeds 0.05. Together, these results confirm that the model is correctly specified, and the results are statistically dependable.

Table 3. Heteroskedasticity test

Joint test: Heteroscedasticity Test		Result
Chi-sq	df	Prob.
88.37	75	0.09

Source: Researchers' computation using E-views 10.

**Serial Correlation Test:** Serial correlation occurs when the model's residuals are correlated over time, violating the assumption of independence required for robust econometric analysis. The Breusch-Godfrey Lagrange Multiplier (LM) test was applied to evaluate this. The test results show p-values greater than 0.05 for all lags, indicating no evidence of serial correlation. This confirms that the residuals are independent, supporting the model's dynamic specification. Table 4 reports the results of the SVAR residual serial correlation LM test at lag 1. The LRE statistic is 15.35 with 9 degrees of freedom and a p-value of 0.0819, while the Rao F-statistic is 1.83 (df = 9, 58.6) with a corresponding p-value of 0.0826. Since both p-values exceed the conventional 0.05 significance level, the null hypothesis of no serial correlation cannot be rejected. This outcome suggests that the SVAR model's residuals do not display significant autocorrelation, thereby confirming the adequacy of the model's dynamic specification and supporting the reliability of its structural inferences.

Table 4. SVAR residual serial correlation LM test

Lag	LRE* stat	df	Prob.	Rao F-stat	df	Prob.
1	15.35	9	0.08	1.83	(9, 58.6)	0.08

Source: Researchers' computation using E-views 10

## 5. Discussion

The SVAR model's stability, with all eigenvalues within the unit circle, ensures reliable analysis of the dynamic interactions among GDP, AENRGY, and CO<sub>2</sub> emissions in Morocco. This study examines Morocco's renewable energy transition within the broader African and global contexts, focusing on its economic and environmental implications. By leveraging Morocco's high solar potential and ambitious renewable energy targets (42% of installed capacity by 2020 and 52% by 2030), the analysis highlights the country's progress and challenges in achieving sustainable development.

### 5.1. Renewable energy and economic growth: The case of Morocco

IRFs reveal that shocks to AENRGY, exemplified by projects like the Noor Ouarzazate Solar Complex, drive sustained GDP growth in Morocco (mean GDP growth: 2.624%, Table 1). This aligns with regional studies, such as Ouedraogo et al. (2022), which highlight how renewable energy investments in sub-Saharan Africa stimulate economic activity through job creation and reduced energy import costs. Morocco's state-led approach, coordinated by the Moroccan Agency for Sustainable Energy (MASEN), has enhanced energy security by capitalizing on the country's abundant solar and wind resources. However, unlike South Africa's Renewable Energy Independent Power Producer Procurement Program (REIPPPP), which emphasizes private-sector involvement (Eberhard & Naude, 2016), Morocco's centralized model prioritizes large-scale projects, yielding significant economic benefits but limiting rural electrification.

Comparative analysis with South Africa and Kenya underscores the trade-offs of Morocco's strategy. South Africa's REIPPPP fosters private investment, while Kenya's success with geothermal and off-grid solar emphasizes community-driven solutions (Newell & Daley, 2012). Morocco's centralized approach has streamlined implementation but overlooks remote areas like the Atlas Mountains, where energy access remains limited. Adopting hybrid models—integrating large-scale solar farms with localized microgrids—could address regional disparities, enhance socio-economic impacts, and align with Morocco's Vision 2030



goals. Such strategies would leverage Morocco's geographic advantages while mitigating the urban-rural energy divide.

## 5.2. The environmental Kuznets curve and rebound effects in Morocco's energy transition

A counterintuitive finding from the IRFs is that increased AENRGY adoption sometimes elevates CO<sub>2</sub> emissions (mean CO<sub>2</sub>: 1.462%, Table 1), suggesting a rebound effect where efficiency gains from renewables spur higher energy consumption in Morocco's energy-intensive industries, such as phosphate mining and cement production. This finding resonates with the Environmental Kuznets Curve (EKC) framework, which posits that environmental degradation increases during early stages of economic growth before declining (Stern, 2004). Morocco, in the ascending phase of the EKC, mirrors trends in other African nations like Nigeria, where emissions remain coupled with growth (Maji & Adamu, 2021). Gillingham et al. (2016) note that rebound effects can undermine renewable energy's environmental benefits without demand-side interventions.

Morocco's environmental challenges, including water scarcity and land-use constraints, exacerbate these dynamics. For instance, large-scale solar projects require significant land, potentially competing with agriculture in arid regions. To address these issues, policymakers should adopt a multi-pronged strategy:

- **Carbon Pricing:** Implementing a carbon tax, tailored to Morocco's industrial sector, would internalize emissions costs and incentivize cleaner production, aligning with the country's Paris Agreement commitments.
- **Tiered Subsidies:** MASEN could prioritize subsidies for renewable projects incorporating energy storage or demonstrating measurable emissions reductions, enhancing environmental outcomes.
- **Mandatory Energy Audits:** Requiring energy-intensive industries to conduct regular audits would ensure efficiency gains translate into reduced consumption, mitigating rebound effects.

These measures, supported by Morocco's partnerships with the EU and international donors, would strengthen the alignment of its renewable energy transition with economic resilience and climate goals, addressing both the EKC's ascending phase and regional environmental constraints.

## 6. Conclusion and Policy Recommendations

Morocco's renewable energy transition, exemplified by projects like the Noor Ouarzazate Solar Complex, has significantly bolstered economic growth, as evidenced by the SVAR model's finding that investments in solar and wind capacity drive sustained GDP increases. However, the analysis also reveals a critical challenge: without targeted interventions, rebound effects—where efficiency gains from renewables lead to higher overall energy consumption—and structural inefficiencies in energy-intensive sectors like phosphate mining and cement production hinder emissions reductions. These findings highlight a tension between Morocco's economic ambitions and its environmental goals, necessitating a refined policy framework to ensure a holistic low-carbon transition aligned with its Vision 2030 and Sustainable Development Goal 7 commitments.

Morocco's renewable energy transition, exemplified by projects like the Noor Ouarzazate Solar Complex, has driven economic growth, but the SVAR model reveals that rebound effects—where efficiency gains from renewables lead to increased energy consumption in industries like phosphate mining and cement production—limit emissions reductions. To

align economic and environmental goals with Morocco's Vision 2030 and Paris Agreement commitments, policymakers should integrate targeted interventions into the National Energy Strategy. The phosphate industry, led by the OCP Group, consumes significant energy, offering a prime opportunity to implement mandatory energy efficiency benchmarks paired with incentives for cleaner technologies, such as solar-powered desalination for phosphate processing, with pilot projects spearheaded by the Moroccan Agency for Sustainable Energy (MASEN).

Current subsidies, focused on large-scale renewable generation, should shift toward rewarding verifiable emissions reductions through tiered feed-in tariffs that prioritize projects with energy storage or those serving rural areas like the Atlas Mountains and southern provinces, enhancing energy access and reducing reliance on fossil fuel backups. Drawing from Kenya's success with off-grid solar systems (Newell & Daley, 2012), Morocco could invest in solar mini-grids for agriculture-heavy regions like Souss-Massa, where solar-powered irrigation could reduce diesel use, boost livelihoods, and curb emissions through public-private partnerships supported by MASEN. Introducing a modest carbon pricing system for energy-intensive industries would further incentivize the shift to renewables, mitigating rebound effects and ensuring economic growth does not exacerbate emissions, as observed in the SVAR analysis. Additionally, requiring lifecycle-based environmental impact assessments for new renewable projects would ensure their benefits extend beyond generation capacity to actual emissions reductions, addressing the carbon footprint of construction and operation.

To decouple economic growth from emissions, Morocco should accelerate emerging technologies like green hydrogen, building on the Dakhla pilot project through partnerships with the EU (IRENA, 2023), while launching national campaigns to reduce energy waste in urban centers and setting measurable benchmarks, such as lowering emissions per unit of economic output, to track progress. Guided by King Mohammed VI's environmental vision, Morocco is poised to lead as a regional pioneer in sustainable development, but the SVAR findings underscore the need for integrated policymaking. By embedding emissions discipline, prioritizing decentralized energy access, and leveraging industrial and agricultural strengths, Morocco can transform its renewable success into a model for a resilient, low-carbon future, ensuring that ambition translates into equitable and sustainable outcomes.

## 7. Limitations and Future Research

The SVAR model's reliance on national aggregates masks subnational variations. For instance, solar projects in Drâa-Tafilalet may yield different economic impacts than in industrial Casablanca. Future studies should leverage disaggregated datasets, such as regional energy consumption or employment data, to capture these nuances. Extending the analysis beyond 2024, potentially using real-time data from sources like Morocco's Ministry of Energy or the African Development Bank, could reveal long-term trends, such as the lagged effects of Noor projects or policy reforms. Additionally, incorporating spatial econometric models, as used in South African energy studies (Jeetoo, 2021), could better address regional heterogeneity.

## Authorship Contribution Statement

Each author contributed significantly to the study. OAO was responsible for conceptualization, introduction, literature review, the original draft of the study; MAM was responsible for methodology, data curation, analysis, and interpretation, and KTA was responsible for the data collection, discussion and the recommendation. All authors have read and approved the final manuscript.

## Conflict of Interest

The authors declare no conflict of interest.

## Data Availability

Data will be made available on request.

## References

- Adebayo, T. S., Akadiri, S. S., Riti, J. S., & Tony Odu, A. (2023). Interaction among geopolitical risk, trade openness, economic growth, carbon emissions and its implication on climate change in India. *Energy & Environment*, 34(5), 1305–1326. <https://doi.org/10.1177/0958305X221083236>
- Ahmad, T., Ali, S., & Basit, A. (2022). Distributed renewable energy systems for resilient and sustainable development of remote and vulnerable communities. *Philosophical Transactions of the Royal Society A: Mathematical, Physical and Engineering Sciences*, 380(2221), 20210143. <https://doi.org/10.1098/rsta.2021.0143>
- Aldieri, L., Gatto, A., & Vinci, C. P. (2023). Panel data and descriptor for energy econometrics—an efficiency, resilience and innovation analysis. *Quality & Quantity*, 57(2), 1649–1656.
- Bahadur, A. V., & Tanner, T. (2021). *Resilience reset: Creating resilient cities in the global South*. Routledge.
- Belakhdar, N., Kharbach, M., & Afilal, M. E. (2014). The renewable energy plan in Morocco, a Divisia index approach. *Energy Strategy Reviews*, 4, 11–15.
- Benatia, D., Beaudin, G., & Muriel, J. (2025). *Quantifying the triple-win potential of sustainable mobility*. SSRN. <https://doi.org/10.2139/ssrn.5152056>
- Cherevatskyi, D. Y. (2023). The resilience of economics and the economics of resilience. *Economy of Industry*, 101(1), 31–39.
- Donohue, I., Coscieme, L., Gellner, G., Yang, Q., Jackson, A. L., Kubiszewski, I., Costanza, R., & McCann, K. S. (2023). Accelerated economic recovery in countries powered by renewables. *Ecological Economics*, 212, 107916. <https://doi.org/10.1016/j.ecolecon.2023.107916>
- Eberhard, A., & Kruger, W. (Eds.). (2023). *Renewable energy auctions: Lessons from the Global South*. Oxford University Press.
- Ebhota, W. S., & Tabakov, P. Y. (2022). Renewable energy technologies in the Global South: Sub-Saharan Africa trends and perspectives. *International Journal of Emerging Technology and Advanced Engineering*, 12, 47–55.
- Energy Agency, Abu Dhabi.
- Filipenko, A. (2022). Economic resilience in the context of institutional logic. *Ekonomična Teoriâ*. <https://doi.org/10.15407/etet2022.03.045>
- Folke, C., Carpenter, S. R., Walker, B., Scheffer, M., Chapin, T., & Rockström, J. (2010). Resilience thinking: Integrating resilience, adaptability and transformability. *Ecology and Society*, 15(4), Article 20.
- Gillingham, K., Rapson, D., & Wagner, G. (2016). The rebound effect and energy efficiency policy. *Review of Environmental Economics and Policy*, 10(2), 68–88. <https://doi.org/10.1093/reep/rew006>




- Hynes, W., Trump, B. D., Kirman, A., Haldane, A., & Linkov, I. (2022). Systemic resilience in economics. *Nature Physics*, 18(4), 381–384.
- Intergovernmental Panel on Climate Change. (2018). *Global warming of 1.5°C: An IPCC special report on the impacts of global warming of 1.5°C above pre-industrial levels and related global greenhouse gas emission pathways, in the context of strengthening the global response to the threat of climate change, sustainable development, and efforts to eradicate poverty*. <https://www.ipcc.ch/sr15/>
- International Energy Agency (IEA). (2020). *World Energy Outlook 2020*.
- IRENA. (2021). *World Energy Transitions Outlook: 1.5°C Pathway*, International Renewable
- Jeetoo, J. (2022). Spatial interaction effect in renewable energy consumption in sub-Saharan Africa. *Renewable Energy*, 190, 148–155.
- Khan, I., Hou, F., Zakari, A., & Tawiah, V. K. (2021). The dynamic links among energy transitions, energy consumption, and sustainable economic growth: A novel framework for IEA countries. *Energy*, 222, 119935.
- Kousksou, T., Allouhi, A., Belattar, M., Jamil, A., El Rhafiki, T., Arid, A., & Zeraouli, Y. (2015). Renewable energy potential and national policy directions for sustainable development in Morocco. *Renewable and Sustainable Energy Reviews*, 47, 46–57.
- Lawal, A. I. (2023). Determinants of renewable energy consumption in Africa: Evidence from system GMM. *Energies*, 16(5), 2136.
- Leichenko, R., & O'Brien, K. (2024). *Climate and society: Transforming the future*. John Wiley & Sons.
- Majenge, L., Mpungose, S., & Msomi, S. (2025). Comparative analysis of VAR and SVAR models in assessing oil price shocks and exchange rate transmission to consumer prices in South Africa. *Econometrics*, 13(1), Article 8.
- Maji, I. K., & Adamu, S. (2021). The impact of renewable energy consumption on sectoral environmental quality in Nigeria. *Cleaner Environmental Systems*, 2, 100009. <https://doi.org/10.1016/j.cesys.2021.100009>
- Meadows, D. H., Meadows, D. L., Randers, J., & Behrens, W. W. (1972). *The limits to growth: A report for the Club of Rome's project on the predicament of mankind*. Universe Books.
- Mehmood, U., Agyekum, E. B., Tariq, S., Ul Haq, Z., Uhunamure, S. E., Edokpayi, J. N., & Azhar, A. (2022). Socio-economic drivers of renewable energy: Empirical evidence from BRICS. *International Journal of Environmental Research and Public Health*, 19(8), Article 4614. <https://doi.org/10.3390/ijerph19084614>
- Newell, P., & Daley, F. (2022). *Electrification and cooking: A case of mutual neglect?* MECS Programme Working Paper.
- Onuoha, F. C., Dimnwobi, S. K., Okere, K. I., & Ekesiobi, C. (2023). Funding the green transition: Governance quality, public debt, and renewable energy consumption in Sub-Saharan Africa. *Utilities Policy*, 82, 101574.
- Oraibi, W. A., Mohammadi-Ivatloo, B., Hosseini, S. H., & Abapour, M. (2023). A resilience-oriented optimal planning of energy storage systems in high renewable energy penetrated systems. *Journal of Energy Storage*, 67, 107500. <https://doi.org/10.1016/j.est.2023.107500>
- Ouammi, A., Zejli, D., Dagdougui, H., & Benchrif, R. (2012). Artificial neural network analysis of Moroccan solar potential. *Renewable and Sustainable Energy Reviews*, 16(7), 4876–4889.

- Ouedraogo, A., Diallo, A., Goro, S., Ilboudo, W. D. A., Madougou, S., Bathiebo, D. J., & Kam, S. (2022). Analysis of the solar power plant efficiency installed in the premises of a hospital – Case of the Pediatric Charles De Gaulle of Ouagadougou. *Solar Energy*, 241, 120–129.
- Radic, M., Herrmann, P., Haberland, P., & Riese, C. R. (2022). Development of a business model resilience framework for managers and strategic decision-makers. *Schmalenbach Journal of Business Research*, 74(4), 575–601.
- Ramli, K., & Ithnin, H. S. (2022). Conceptual framework: Independent business owner's agility and financial resilience. [Publisher or source information needed].
- REN21. (2020). *Renewables 2020 global status report*. <https://www.ren21.net/gsr-2020/>
- Sayed, A. R., Wang, C., & Bi, T. (2023). Resilient-economic coordinated robust operation of integrated electric-gas systems. *arXiv Preprint*, arXiv:2304.14909.
- Sharma, G., Bhushan, S., Manna, A., & Kolpe, K. J. (2024). Identify the economic crisis by analyzing banking data using machine learning technique. *International Journal of Intelligent Systems and Applications in Engineering*, 12(5s), 503–512.
- Shirley, R., & Medhin, H. (2022). Practical solutions for energy transition emerging in Sub-Saharan Africa. *Environmental Research: Infrastructure and Sustainability*, 2(4), 040401.
- Sovacool, B. K., & Dworkin, M. H. (2014). Energy security, inequality and energy subsidies. *Energy Policy*, 73, 259–263.
- Steen, R., Haug, O. J., & Patriarca, R. (2024). Business continuity and resilience management: A conceptual framework. *Journal of Contingencies and Crisis Management*, 32(1), e12501.
- Stern, D. I. (2004). The rise and fall of the Environmental Kuznets Curve. *World Development*, 32(8), 1419–1439.
- Tiwari, A. K., Adewuyi, A. O., Adeleke, M. A., & Abakah, E. J. A. (2023). A time-varying Granger causality analysis between water stock and green stocks using novel approaches. *Energy Economics*, 126, 107010.
- Walker, B., & Salt, D. (2012). *Resilience practice: Building capacity to absorb disturbance and maintain function*. Island Press.
- World Commission on Environment and Development. (1987). *Our common future*. Oxford University Press.





# Finite Element Analysis of the Transition from Multi-Station Machines to Double-Stroke Machines in the Forming Process of Ring Welded Bolts

Barış Akyıldız , Özge Özcan , İbrahim Özçetin 

OBEL CIVATA, Atatürk OSB Mh. 10002 sk. No:30 35620 Çiğli, İzmir, Türkiye

## Research Article

\*Correspondence:  
baris.akyildiz@obel.com.tr

Received: 3 June 2025  
Accepted: 24 July 2025  
Published: 30 July 2025

## Keywords

Weld bolt  
Mold design  
Finite element method  
Forming simulation

This is an open access article  
under the CC BY NC license.



## Abstract

Cold forming is a metal shaping technique that utilizes plastic deformation under high pressure with the aid of dies. This study focuses on the production of a weld bolt through cold forming, integrating the Finite Element Method (FEM) to evaluate and enhance the forming process. The conventional four-station manufacturing system was analyzed and replaced with a two-station configuration utilizing a double-stroke mechanism. FEM simulations confirmed the feasibility of this approach, demonstrating effective material flow and die filling across both stations. Subsequent experimental trials validated the dimensional accuracy of the final product and confirmed the absence of surface or internal defects. In comparison to the four-station process, the two-station system increased production speed, reduced energy consumption, and resulted in a 40% increase in annual output along with a 15% reduction in production costs. These results highlight the process efficiency and production benefits achieved through the proposed forming system.

## 1. Introduction

Cold forging is a highly efficient metal forming method widely employed in the production of high-strength mechanical components with tight dimensional tolerances (Kılıçaslan & İnce, 2016). The process involves plastically deforming metal materials under high pressure at room temperature, eliminating the need for preheating. Compared to other manufacturing techniques, cold forging offers significant advantages, including superior dimensional accuracy, excellent surface quality, high material utilization, and the elimination of secondary machining operations (Başdemir et al., 2018). These attributes make it an ideal method for high-volume industrial production.

In addition to its advantages in terms of dimensional accuracy and surface quality, cold forging also offers significant material-related benefits when compared to other manufacturing methods. One of the most important of these is the efficient utilization of raw material. Since cold forging shapes the material through plastic deformation without generating significant amounts of scrap, material loss is minimized, leading to higher material

**How to cite this paper:** Akyıldız, B., Özcan, Ö., & Özçetin, İ. (2025). Finite element analysis of the transition from multi-station machines to double-stroke machines in the forming process of ring welded bolts. *Scientific Research Communications*, 5(2), 94-103. <https://doi.org/10.52460/src.2025.008>

yield and reduced production costs. Furthermore, the absence of machining processes such as turning or milling, which typically produce considerable waste, further enhances this efficiency. Studies in recent years emphasize that cold forging ensures superior material flow and density distribution, resulting in components with enhanced mechanical properties and improved fatigue performance (Kim et al., 2023). These characteristics make cold forging highly suitable for the mass production of high-strength components with minimal material wastage.

In a foundational study, Vazquez and Altan (2000) reviewed cold forging applications in both academic literature and industrial practice, demonstrating the versatility and continuous advancement of the technique. Today, cold forging is extensively applied across various industries particularly in automotive, aerospace, electronics, and general manufacturing with bolt production being one of its most prevalent applications due to the method's efficiency and precision.

During the product design phase, Finite Element Method (FEM) simulations serve as a critical tool to guide the manufacturing process, enabling detailed analysis of material behavior, forming loads, and tooling performance (Vazquez & Altan, 2000). In modern die design, the integration of Computer-Aided Design (CAD) tools has become essential for reducing design errors, lowering production costs, and improving overall process reliability (Başdemir et al., 2018). FEM analyses are numerical techniques that enable a detailed examination of material behavior, stress distributions, and process parameters in complex engineering problems. Particularly in high-deformation processes such as metal forming, FEM has become an essential tool for design validation, die life prediction, and process optimization (Graça & Vincze, 2021). A typical design workflow begins with the initial geometric definition, followed by FEM-based validation, and culminates in prototype production (Hsia & Su, 2020). These simulations help assess formability, material flow, and stress distribution, ensuring that the final geometry can be achieved with minimal risk of failure.

Ring weld bolts, a widely used type of fastener, are typically produced using the cold forging method, often on four-station machines. These bolts feature a complex head geometry with multiple forming elements, which traditionally requires three to five preforming stages for complete shaping. Product designs are created to establish suitable manufacturing conditions, followed by prototype production. Although four-station machines are commonly used, the cold forging process can also be applied in systems with two, three, or five stations. The number of stations directly affects production costs and cycle times, prompting various studies that examine the influence of station count on the efficiency and feasibility of the manufacturing process.

Prior to production, forming sequences and tooling designs are finalized using FEM simulations to ensure feasibility and prevent defects such as cracking or underfilling. These simulations provide insights into die stresses, material flow, and geometrical accuracy. While previous studies have focused on optimizing multi-station configurations, the potential to reduce station count without compromising product quality remains underexplored.

In this context, the present study introduces a novel approach by demonstrating the feasibility of producing M6x25 ring weld bolts using a two-station double-stroke cold forging system—an application not previously reported in the literature. This contribution addresses both process simplification and performance enhancement, offering a new perspective for efficient fastener manufacturing.

## 2. Methodology

In studies conducted on the M6x25 ring weld bolt, the production process was transitioned from four-station machines to double-stroke machines. The key distinction between these



machine types lies in the number of forming stages and the higher operational speed of double-stroke systems. While the four-station process includes wire cutting, preform formation, head forging, and final shaping, the double-stroke machines consolidate head formation and final shaping into two sequential cold forging steps. During this transition, FEM analyses were employed to evaluate material flow, forming behavior, and tooling design, thereby contributing to a more efficient and streamlined manufacturing process.

## 2.1. Product design

The M6x25 ring weld bolt is a type of fastener traditionally manufactured using four-station cold forging machines. Within the scope of process development efforts, the original tool and product designs were prepared by the design team and utilized in prototype manufacturing. In pursuit of increased efficiency and reduced production complexity, the forming process was reconfigured to operate on a double-stroke machine. The revised tooling concepts were subjected to numerical analysis using the FEM to assess their feasibility and forming performance prior to experimental validation.

## 2.2. Finite element method

The modeling in this study was conducted using SIMUFACT Forming software. Separate models were developed for each station, and appropriate geometries were generated accordingly. Key factors such as material flow, tool stresses, and wear behavior were analyzed to obtain valuable insights into the forming process (Joun et al., 2002). This simulation-based approach reduces process development time and allows for a broader range of design variations.

In the simulation model, all dies were assumed to be rigid, as elastic deformations occurring in the tooling do not have a significant impact on material flow. The material used in the process was defined based on its plastic deformation behavior, and its torsional properties were considered sufficient for the simulation. In the model, the fixed die was fully constrained, with all translational and rotational degrees of freedom (in the x, y, and z directions) restricted. The movable die, on the other hand, was defined to have translational movement only along the z-axis, while all other translational and rotational motions were restricted. The effect of gravity was neglected in the simulations, and the boundary conditions were defined in accordance with the structure of the actual machine and the production scenario.

The material data used as a reference in the Simufact simulation software was selected to be identical to the raw material employed in the actual production of the parts, in order to ensure consistency and reliability of the results. To accurately reflect the material behavior within the simulation environment, the yield strength of the material was experimentally determined under specified conditions prior to the simulation. As illustrated in Figure 1, the tests were conducted at 25°C (room temperature) with a strain rate of  $0.01 \text{ s}^{-1}$ , and the yield strength was measured as 322.94 MPa. In addition, the friction coefficient of the material, which was determined through experimental methods, was measured as 0.08 and incorporated into the simulation accordingly.

In this study, both experimental and numerical analyses were conducted to determine the friction coefficient between the die and the material. In the experimental procedure, the raw material used in actual production was placed in the die and compressed using a press to a defined stroke (8 mm), after which the stress value was measured via tensile testing. The same conditions were replicated in the Simufact Forming software, applying the same stroke value to obtain the corresponding simulated stress. The experimental and numerical stress values were then compared. Assuming the discrepancy arose from friction, the friction coefficient was iteratively adjusted until the simulation results aligned with the experimental data. The

friction coefficient at which both results converged was considered the actual friction coefficient between the die and the material.

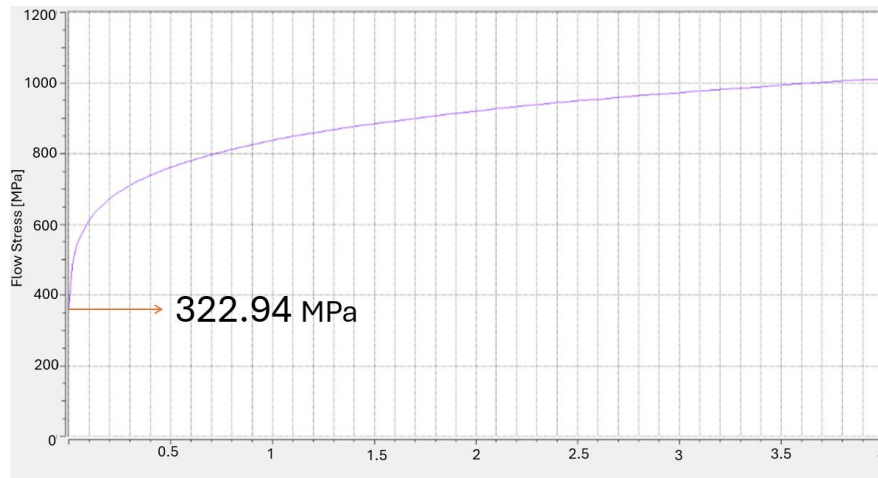


**Figure 1.** True flow stress–strain curve of the material used in the simulation

In order to verify the geometric accuracy of the part, 3D analyses of the selected material were performed, and the mesh structure was visually inspected. A tetrahedral mesh comprising 247 elements was employed in the simulation, as illustrated in Figure 2, and the mesh quality was checked to prevent any geometrical distortions in the analysis. These preparations were carried out as a preliminary step for ensuring reliable simulation results for the products (Zou et al., 2024).

In this study, the use of tetrahedral mesh is crucial for accurately defining the complex geometries present in the model. Tetrahedral meshing provides a more uniform and compatible distribution, particularly in structures with sharp transitions and three-dimensional free surfaces, thereby enhancing structural continuity. Given that the product and die geometries in this work likely involve intricate transitions and freeform surfaces, the use of tetrahedral mesh is considered more appropriate. Software such as Simufact can automatically generate this mesh structure in a smooth and void-free manner. This approach offers advantages in terms of visually evaluating flange formation, mesh uniformity, and material compaction.

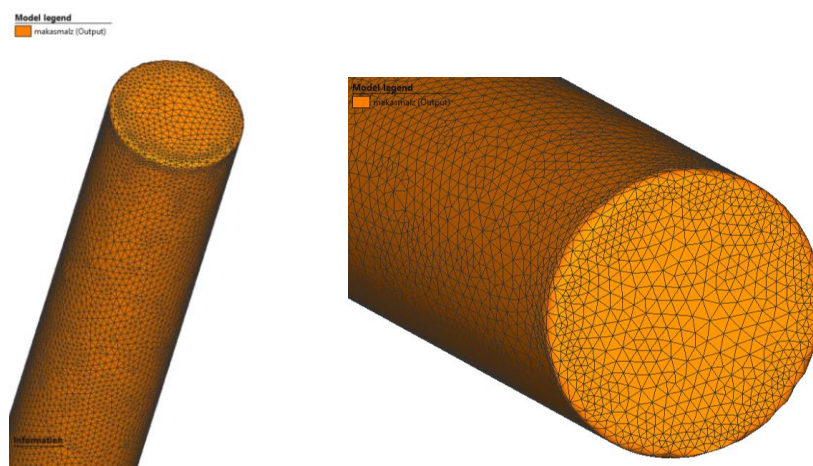


**Figure 2.** 3D analysis of the material to be used in production

Simulation studies were carried out for the M6x25 ring weld bolt designed for double-stroke production. The initial simulation results, illustrated in Figure 3, revealed the formation of buckling due to excessive unsupported material length. In cold forging, buckling typically occurs when the upsetting ratio ( $L/d$ ) exceeds a critical value of approximately 2.5. In this case, the  $L/d$  ratio – defined by the protruding wire length ( $L$ ) to wire diameter ( $d$ ) – exceeded the allowable limit due to open die upsetting conditions, leading to instability during deformation.

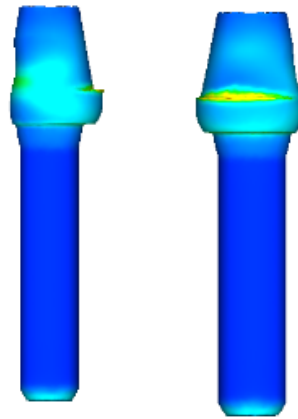


**Figure 3.** FEM simulation showing buckling formation due to excessive  $L/d$  ratio in open die upsetting

To address this issue, the spring-loaded preform tool design was modified to limit uncontrolled material displacement during forming. Specifically, the segment of the wire prone to buckling was enclosed within a movable die component that was preloaded with a spring, allowing contact with the fixed die at the onset of deformation. This configuration effectively shortened the unsupported material length ( $L$ ) by partially constraining it within the tool, thereby reducing the  $L/d$  ratio below the critical buckling threshold (Craveiro et al., 2022). As illustrated in Figure 4a and 4b, the revised tooling design successfully eliminated buckling and enabled stable forming under cold forging conditions.

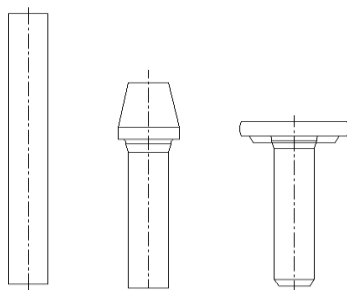


**Figure 4a.** Initial tooling design developed for the cold forging of M6x25 ring weld bolt

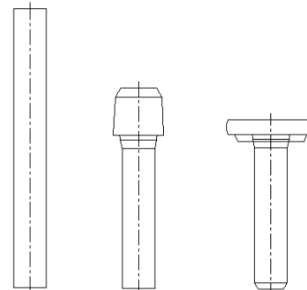


**Figure 4b.** Revised preform tool design incorporating a spring-loaded movable

Following the finalization of the tooling design, comprehensive analyses of material flow behavior were conducted through plastic deformation simulations under cold forging conditions, replicating actual production parameters. These simulations enabled detailed

observation of material displacement, contact behavior, and die filling characteristics throughout each stage of the forming process. By examining the internal flow patterns and deformation zones within the tooling cavity, potential issues such as underfilling, excessive flash formation, or localized stress concentrations were identified and addressed prior to experimental implementation (Figure 5).

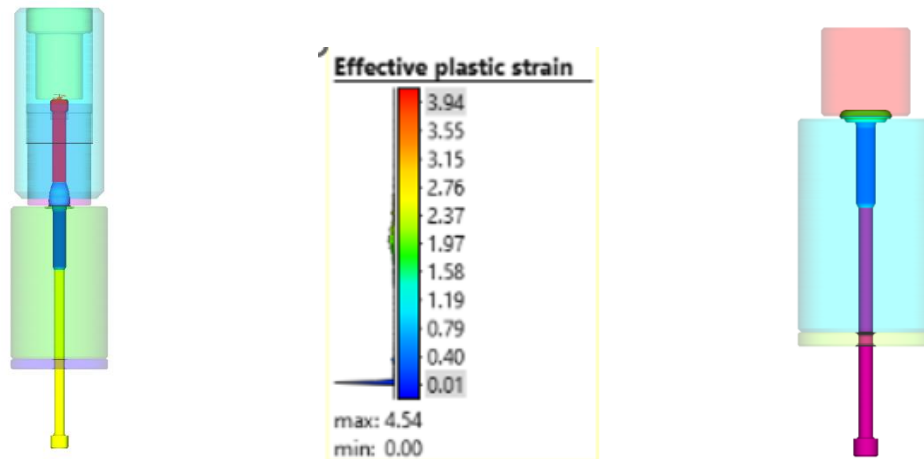


**Figure 5.** FEM-based representation of tooling configuration and effective plastic strain distribution during cold forging of M6x25 ring weld B

The three-dimensional simulation outputs illustrating the progression of the forming stages for the M6x25 ring weld bolt are presented in Figure 6. These visualizations provide insight into the material deformation behavior at each stage, allowing for detailed evaluation of geometry evolution, die filling, and potential surface irregularities. The sequential representation also supports verification of the forming sequence and dimensional conformity prior to experimental validation.

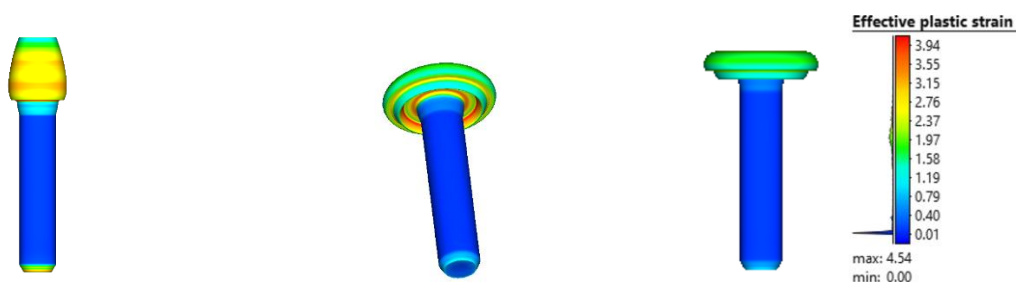


**Figure 6.** FEM-based simulation results showing geometrical evolution and effective plastic strain distribution of the M6x25 ring weld bolt across forming stages

Throughout the simulation process, the force-displacement relationship was systematically evaluated to assess the forming loads at each station. In the resulting graphs, the X-axis denotes the stroke length of the press in millimeters (mm), increasing as the press descends from its initial position, while the Y-axis represents the corresponding forming force in kilonewtons (kN). Variations in the slope and curvature of the graph provide insight into material resistance, deformation behavior, and tooling interaction during the forging process. Figure 7a presents the force-displacement curve obtained during the preform stage, highlighting the initial material resistance and tool engagement. Figure 7b depicts the force

profile associated with the final forming stage, where higher deformation loads and geometric transitions are observed due to complex material flow and contact conditions.

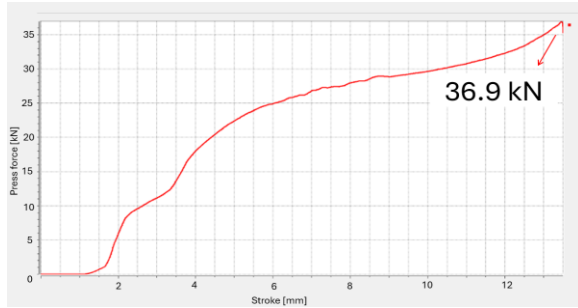


**Figure 7a.** Force-displacement curve for the preform in cold forging simulation

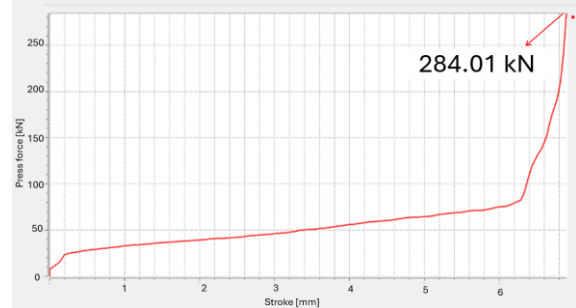


**Figure 7b.** Force-displacement curve for the final forming stage in cold forging simulation

### 3. Tests and Analyses

#### 3.1. Metallographic analysis

The microstructural characteristics of the final product were examined to assess the quality and integrity of the material following the cold forging process. Particular attention was given to the regions exhibiting cross-sectional changes, where internal structure images were obtained from high-surface-area zones. The bolt was divided into two equal parts in the middle vertical plane and the material flow lines in the shaft region and the shaft-head joint regions were analyzed. The analysis focused on verifying the continuity and orientation of material flow lines, which are critical indicators of deformation quality. The results confirmed that the material flow was consistent with plastic forming principles, with no evidence of folding, buckling, or flow line disruption observed in the examined sections (Başdemir et al., 2018). Figure 8 presents the microscopic images of the evaluated regions.

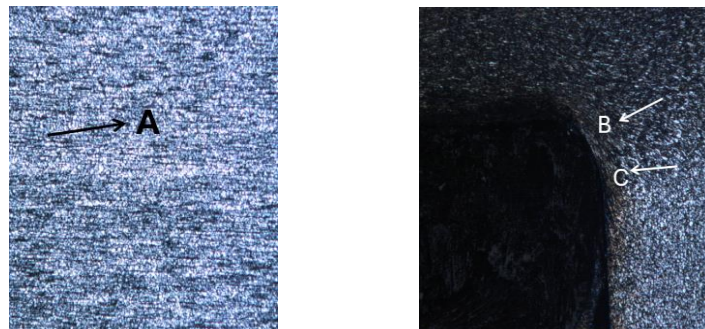


**Figure 8.** Optical micrographs showing flow line integrity in raw material and forged product sections

#### 3.2. Mechanical properties

Hardness measurements were performed at specific locations on the product cross-sections, as indicated in the corresponding figure. The hardness measurements at the specified points are presented in Table 1.



**Table 1.** Hardness measurements at specified regions

Location	A	B	C
Hardness (HV)	190	220	225

Following the completion of microstructural evaluations and FEM-based design validation, prototype production was conducted using the newly developed two-station tooling system. The results demonstrated that the previously observed issues – such as material instability and geometric inconsistency – were effectively eliminated through the implemented design modifications. The final product, as presented in Figure 9, exhibited complete form fidelity and surface integrity, confirming the success of the redesigned forming process under experimental conditions.

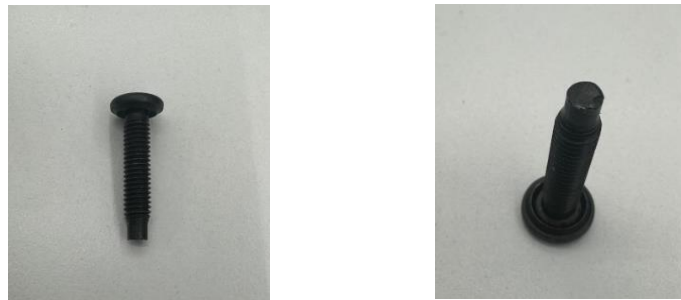


**Figure 9.** Final prototype of the M6x25 ring weld bolt produced using the two-station double-stroke cold forging process

#### 4. Results and Discussions

The effectiveness of the proposed two-station double-stroke cold forging process was comprehensively evaluated through FEM simulations and subsequent prototype production. In the simulation phase, critical aspects such as forming forces, material flow, and die filling behavior were examined in detail. The analyses demonstrated that the newly designed forming sequence allowed for stable material deformation without exceeding stress limits or exhibiting failures such as buckling or underfilling.

Following simulation validation, physical prototypes were manufactured using the redesigned tooling system. The final parts showed high dimensional precision and surface quality, aligning closely with the simulation outcomes. This correlation confirmed that the numerical model accurately represented the real-world process conditions. Microstructural assessments further supported these findings by showing uninterrupted material flow lines and the absence of folding or internal discontinuities – key indicators of successful metal flow during cold forming.

The application of the two-station forming approach brought considerable gains in process efficiency. Shortened cycle durations and reduced machine operating times contributed to noticeable energy savings. Furthermore, the decreased number of tooling components led to extended die life and fewer replacement requirements, resulting in lower tooling costs. Overall, the process enabled a 40% increase in annual production capacity and a 15% reduction in manufacturing expenses. A comparison between the 4-station and 2-station (double-stroke) systems in terms of tooling components, production capacity, tool cost, and tool lifetime is presented in Table 2.



**Table 2.** Comparison of the 4-station and 2-station (double-stroke) systems based on tooling components, production capacity, tool cost, and tool lifetime

Parameter	4-Station System	2-Station (Double-Stroke) System
Annual Production Capacity	16 000 000	16 000 000
Number of Tooling Components	160	32
Tool Cost per Unit (€)	500	250
Tool Lifetime (Produced Units)	100 000	500 000
Total Tooling Cost (€)	80 000	8 000

The dimensional measurements obtained from the samples were evaluated against the specified nominal values and tolerance limits. As shown in Table 3, all measured values fall within the acceptable range, indicating compliance with the required specifications. These results confirm the consistency and accuracy of the manufacturing process, ensuring that the produced components meet the designated quality standards.

**Table 3.** Evaluation of dimensional measurement results against nominal specifications for bolt samples

Dimension	Nominal value		Measured values					OK/ NOK
	Max.	Min.	1.	2.	3.	4.	5.	
Head Thickness	2,5	2,25	2,38	2,36	2,38	2,36	2,41	OK
Total Length	25,42	24,58	25,11	25,1	25,11	25,11	25,1	OK
Seating Surface Diameter	6,8	-	5,65	5,66	5,62	5,66	5,64	OK
Unthreaded Length	1,5	-	1,42	1,4	1,44	1,44	1,46	OK
Head Diameter	15	14	14,36	14,4	14,38	14,35	14,4	OK
Major Diameter	5,97	5,79	5,88	5,85	5,86	5,85	5,86	OK
Pitch Diameter	5,32	5,21	5,26	5,25	5,27	5,25	5,27	OK

## 5. Conclusion

Ring weld bolts, such as the M6x25 type studied here, are conventionally produced using four-station cold forging machines due to their complex geometries. In contrast, double-stroke machines have traditionally been used for simpler fastener designs. This study marks the first successful demonstration of manufacturing ring weld bolts using a two-station double-stroke system. This advancement represents a novel contribution to the field, as it showcases the feasibility of producing geometrically demanding parts using a more compact and efficient setup. While the current study demonstrates the applicability of double-stroke forming for ring weld bolts, further research is recommended to evaluate tool wear behavior under extended production cycles and to explore the method's suitability for larger fastener sizes or alternative material grades.

The methodology developed in this work offers a practical framework that can be adapted to the manufacturing of similar fasteners. By reducing equipment requirements and simplifying production without compromising quality, this approach provides a flexible and scalable alternative for industrial cold forging operations.

## Authorship Contribution Statement

Each author contributed significantly to the study. BA: study conception and design, analysis and interpretation of results; ÖÖ: data collection, analysis and interpretation of results, draft manuscript preparation; İÖ: analysis and interpretation of results. All authors have read and approved the final manuscript.

## Conflict of Interest

The authors declare no conflict of interest.

## Acknowledgments

The authors would like to thank OBEL CIVATA for their invaluable support and contributions to this study.

## References

- Başdemir, V., Baygut, A., & Çulha, O. (2018). Soğuk dövme tekniği ile bağlantı elemanı üretiminde kullanılan plastik şekil verme teknolojileri. *İleri Teknoloji Bilimleri Dergisi*, 7(3), 18–28.
- Craveiro, H. D., Rahnavard, R., Laím, L., Simões, R. A., & Santiago, A. (2022). Buckling behavior of closed built-up cold-formed steel columns under compression. *Thin-Walled Structures*, 179, 109493. <https://doi.org/10.1016/j.tws.2022.109493>
- Graça, A., & Vincze, G. (2021). A short review on the finite element method for asymmetric rolling processes. *Metals*, 11(5), 762. <https://doi.org/10.3390/met11050762>
- Hsia, S.-Y., & Su, Y.-H. (2020). Zero waste process for direct forming process of nail spikes. *Solid State Phenomena*, 311, 27–32. <https://doi.org/10.4028/www.scientific.net/SSP.311.27>
- Joun, M. S., Lee, M. C., & Park, J. M. (2002). Finite element analysis of prestressed die set in cold forging. *International Journal of Machine Tools and Manufacture*, 42(11), 1213–1222. [https://doi.org/10.1016/S0890-6955\(02\)00079-2](https://doi.org/10.1016/S0890-6955(02)00079-2)
- Kılıçaslan, C., & İnce, U. (2016). Soğuk dövme kalıplarında meydana gelen kırılma sebeplerinin nümerik olarak incelenmesi. *Mühendis ve Makina*, 57(678), 65–71.
- Kim, K. M., Ji, S. M., Lee, S. W., & et al. (2023). Flow behavior dependence of rod shearing phenomena of various materials in automatic multi-stage cold forging. *Journal of Mechanical Science and Technology*, 37, 139–148. <https://doi.org/10.1007/s12206-022-1214-3>
- Vazquez, V., & Altan, T. (2000). Die design for flashless forging of complex parts. *Journal of Materials Processing Technology*, 98(1), 81–89. [https://doi.org/10.1016/S0924-0136\(99\)00308-8](https://doi.org/10.1016/S0924-0136(99)00308-8)
- Zou, X., Lo, S. B., Sevilla, R., Hassan, O., & Morgan, K. (2024). The generation of tetrahedral meshes for NURBS-enhanced FEM. *Engineering with Computers*, 40, 3949–3977. <https://doi.org/10.1007/s00366-024-02004-z>



# GIS-Based Assessment of Wastewater Pollution in Afghanistan's Major Cities

Hamayoun Himat\*

Helmand University, Department of Chemistry, Helmand, Afghanistan

## Research Article

\*Correspondence:  
hamayounhimat@helu.edu.af

Received: 29 May 2025  
Accepted: 14 July 2025  
Published: 30 July 2025

## Keywords

Water pollution  
GIS-based spatial analysis  
Wastewater management  
Afghanistan  
Heavy metals

This is an open access article  
under the CC BY NC license.



## Abstract

Water pollution caused by untreated industrial and domestic wastewater is an escalating environmental and public health crisis in Afghanistan. This study employs Geographic Information System (GIS) techniques to evaluate the spatial distribution of major water contaminants in key river basins, including the Kabul and Helmand Rivers. These contaminants include heavy metals (lead, cadmium, mercury, and chromium), biological pollutants (such as *Escherichia coli*, biochemical oxygen demand, and chemical oxygen demand), and physicochemical parameters (pH, total dissolved solids, and turbidity). The assessment is based on 25 water samples collected from five zones representing urban, industrial, and agricultural areas. Water samples collected from urban, industrial, and agricultural zones were analyzed using standard laboratory procedures. The results indicate that contamination levels in industrial zones significantly exceed the safety thresholds established by the World Health Organization and the United States Environmental Protection Agency—for example, 0.01 milligrams per liter for lead and 0.003 milligrams per liter for cadmium—with particularly elevated concentrations of these two heavy metals. Biological pollutants and organic loads are also alarmingly high, primarily due to inadequate wastewater treatment infrastructure. GIS-based spatial interpolation techniques identified pollution hotspots near densely populated and industrial discharge areas. The study highlights the urgent need for policy reforms, real-time monitoring, and the adoption of advanced water treatment technologies. These findings underscore the critical role of GIS in identifying high-risk areas and supporting sustainable water resource management strategies in Afghanistan.

## 1. Introduction

Water pollution is one of the most critical environmental and public health issues facing Afghanistan, where industrial and domestic wastewater is often discharged into natural water bodies without adequate treatment. The global evolution of river quality from pristine conditions to widespread pollution highlights the severity of this issue (Meybeck & Helmer, 1989). The United Nations Environment Programme (UNEP, 2023a) estimates that more than 80% of global wastewater is released untreated, severely affecting freshwater resources and contributing to the spread of waterborne diseases. Alam and Sadiq (2020) highlight various

**How to cite this paper:** Himat, H. (2025). GIS-based assessment of wastewater pollution in Afghanistan's major cities. *Scientific Research Communications*, 5(2), 104-117. <https://doi.org/10.52460/src.2025.009>

anthropogenic sources of heavy metal pollution and the necessity of integrated treatment approaches. Afghanistan's major river systems, including the Kabul River, Helmand River, and their tributaries, are particularly affected due to a lack of proper sewage infrastructure; such degradation reflects global trends in water quality transition described by Meybeck and Helmer (1989), from pristine to heavily polluted systems, uncontrolled industrial effluents, and agricultural runoff. Reports indicate that more than 70% of Afghanistan's drinking water sources are contaminated, positioning the country among the most water-insecure nations worldwide (World Health Organization [WHO], 2022a; UNEP, 2023b).

Heavy metal contamination is one of the most significant threats to Afghanistan's water supply. Industrial activities—including battery production, mining, textile manufacturing, and metal processing—release hazardous elements such as lead (Pb), cadmium (Cd), mercury (Hg), and chromium (Cr) into the environment. Prolonged exposure to these pollutants is associated with neurological disorders, organ damage, and an elevated risk of cancer (Nasreen & Haider, 2024; Environmental Protection Agency [EPA], 2021a; Lafta et al., 2024).

Biological contaminants, particularly *Escherichia coli* (*E. coli*), also present a major concern due to inadequate sanitation practices. Furthermore, biochemical oxygen demand (BOD) and chemical oxygen demand (COD) levels in urban wastewater greatly exceed recommended limits, causing oxygen depletion and degradation of aquatic ecosystems (American Public Health Association [APHA], 2021a). Laboratory analyses of Afghanistan's major rivers indicate alarming levels of contamination, with industrial zones presenting the highest concentrations of pollutants (UNEP, 2023a).

These findings indicate that industrial discharges and untreated wastewater significantly contribute to water pollution, particularly in urban and industrial areas where Pb concentrations exceed the WHO limit of 0.01 mg/L by up to 15 times (WHO, 2022b). As shown in Table 1, contamination levels, including Pb and Cd, are notably high in industrial zones such as Herat Industrial Area, with turbidity levels further deteriorating water quality. Additionally, industrial zones like Herat Industrial Area and urban areas like Kabul River exhibit high turbidity levels (28.9 NTU and 22.5 NTU respectively), indicating significant suspended solids that contribute to water quality deterioration (UNEP, 2023b).

**Table 1.** Heavy metal and organic contamination in Afghan water sources

Location	Pb (mg/L)	Cd (mg/L)	BOD (mg/L)	COD (mg/L)	pH level	TDS (mg/L)	Turbidity (NTU)
Kabul River	0.12	0.03	35	120	6.8	650	22.5
Helmand River	0.08	0.02	28	105	7.1	540	18.3
Kandahar Agricultural Zone	0.05	0.01	18	75	7.4	470	12.8
Herat Industrial Area	0.15	0.04	40	130	6.5	720	28.9
Nangarhar Agricultural Zone	0.07	0.02	20	85	6.7	510	16.2

### 1.1. GIS-based spatial analysis of water pollution

GIS technology is widely used in environmental monitoring, hydrological modeling, and spatial pollution assessments. GIS techniques enable real-time visualization of contamination

hotspots and help identify areas most at risk. Spatial interpolation methods such as Inverse Distance Weighting (IDW) and kriging provide accurate estimations of pollution distribution across large geographic areas (Drešković & Dug, 2012; Setianto & Triandini, 2013; U.S. Geological Survey [USGS], 2021a).

This study integrates GIS mapping to assess water pollution across major Afghan river basins. Similar GIS-based methods were applied by Wang and Chen (2013) to assess heavy metal risk in urban river sediments, demonstrating the effectiveness of spatial analysis in pollution studies. By analyzing population density, industrial activity, and pollution data, GIS-based models effectively identify high-risk zones where contamination is most severe. Jha and Gassman (2014) demonstrate that spatial pollution modeling in river systems enhances both predictive accuracy and decision-making processes, with 'high-risk' defined as areas where pollutant levels exceed WHO and EPA thresholds (e.g., Pb > 0.01 mg/L) and are located near major industrial activities. As detailed in Table 2, groundwater contamination risk zones were also identified using GIS-based risk modeling approaches similar to those of Khan and Husain (2013). The methodology includes:

- Hydrology Network Mapping: Identifying major rivers and their tributaries for pollution assessment (USGS, 2021b).
- Industrial and Agricultural Land Use Analysis: Mapping industrial discharges, agricultural runoff, and wastewater treatment plants (UNEP, 2023c).
- Heavy Metal Concentration Mapping: Visualizing spatial distribution of Pb, Cd, Hg, and Cr contamination levels (EPA, 2021c).
- Biological Contaminant Mapping: Identifying *E. coli* hotspots and oxygen-deprived zones (WHO, 2022c).
- Population Density Overlay: Correlating pollution levels with high-density urban centers and industrial zones (Afghan Ministry of Public Health [MoPH], 2023).

**Table 2.** GIS data layers used for water pollution analysis

GIS layer	Description	Data Source
Hydrology Network	Major rivers and water bodies	USGS (2021b)
Land Use and Industrial Zones	Urban, agricultural, and industrial areas	UNEP (2023c)
Heavy Metal Concentrations	Spatial distribution of Pb, Cd, Hg, and Cr	EPA (2021)
Biological Contaminants	<i>E. coli</i> , BOD, COD concentration maps	WHO (2022c)
Population Density	High-risk zones with dense populations	MoPH (2023)

## 1.2. Policy interventions and future directions

Despite growing concerns over water pollution, Afghanistan lacks comprehensive wastewater management policies and monitoring frameworks. The Afghanistan National Environmental Protection Agency (NEPA, 2023c) has proposed real-time water quality monitoring systems, stricter industrial waste regulations, and improved wastewater treatment infrastructure. However, political instability, limited financial resources, and inadequate enforcement mechanisms remain significant challenges. Pollution control strategies involving early detection and GIS-based prioritization have proven effective in similar contexts (Singh & Agarwal, 2020).



Addressing Afghanistan's water crisis requires an integrated approach combining:

- Advanced water treatment technologies such as filtration, reverse osmosis, and activated carbon absorption.
- GIS-based environmental monitoring to detect pollution hotspots and prioritize intervention efforts.
- Stronger policy enforcement and investment in wastewater management infrastructure.

This study provides a detailed GIS-based assessment of Afghanistan's water pollution, offering insights into contamination levels, pollution distribution patterns, and potential mitigation strategies. By utilizing real-time spatial data and laboratory analysis, policymakers and environmental agencies can develop targeted pollution control measures for sustainable water resource management.

Analysis of seasonal contamination trends indicates that pollutant concentration spikes are more pronounced during dry periods, as reduced river discharge leads to higher contaminant density. This is particularly evident in the Kabul River, where Pb concentrations have been recorded at 0.14 mg/L during low-flow months, compared to 0.09 mg/L during peak discharge periods (UNEP, 2023c). Similarly, total dissolved solids (TDS) levels increase by an average of 22% during dry seasons, indicating that evaporation and reduced dilution capacity intensify the effects of contamination (EPA, 2021a). These seasonal fluctuations further complicate water resource management, as higher contaminant concentrations during drought periods pose greater risks to communities reliant on surface water sources (WHO, 2022c).

GIS spatial interpolation techniques, including Inverse Distance Weighting (IDW) and Kriging, reveal that contamination intensity is directly correlated with proximity to industrial centers and urban wastewater discharge zones (Drešković & Dug, 2012; Setianto & Triandini, 2013; USGS, 2021a). The highest pollution densities are found within 5 to 10 kilometers of major industrial sites, with gradual dispersion occurring downstream. Heavy metal deposition in sediment samples collected from high-risk zones suggests that long-term pollution accumulation is leading to persistent environmental degradation, with Pb concentrations in sediment layers exceeding 50 mg/kg in industrial discharge areas (EPA, 2021b). This indicates that pollution is not only affecting water quality but also contributing to long-term soil contamination, which has implications for agricultural productivity and food safety (UNEP, 2023a).

Hydrological modeling demonstrates that contaminant transport mechanisms are influenced by both surface runoff and groundwater interactions, with GIS-based simulations predicting that industrial pollutants can infiltrate aquifers at depths of up to 30 meters in high-permeability zones (Oyebamiji, 2024; USGS, 2021c). This highlights the need for comprehensive groundwater protection strategies, as contamination of subsurface water sources could have long-lasting consequences for drinking water safety (WHO, 2022c). The presence of nitrate contamination in agricultural runoff zones further supports this concern, with recorded concentrations exceeding 45 mg/L in heavily irrigated farmlands, surpassing WHO safety limits and posing risks for methemoglobinemia, particularly in infants (WHO, 2022d).

Given the severity of these findings, immediate interventions are necessary to prevent further environmental degradation. Policy recommendations include the implementation of real-time GIS-based water quality monitoring systems to track pollution trends and identify emerging hotspots (NEPA, 2023d). Additionally, the integration of advanced water treatment



technologies, such as reverse osmosis and activated carbon filtration, is essential to mitigate heavy metal contamination (EPA, 2021a). Strengthening regulatory enforcement mechanisms is also critical, with stricter penalties for industrial facilities that fail to comply with wastewater discharge standards. Future research should focus on the development of machine learning-enhanced GIS models to improve predictive capabilities and optimize pollution control strategies. By leveraging spatial analysis tools alongside laboratory-based water quality assessments, policymakers and environmental agencies can formulate targeted intervention plans that prioritize high-risk zones. The integration of hydrological data with GIS models will also facilitate the identification of vulnerable groundwater recharge areas, ensuring the sustainable management of Afghanistan's water resources.

## 2. Literature Review

### 2.1. Heavy metal contamination in water sources

Heavy metals such as Pb, Cd, Hg, and Cr are among the most hazardous water pollutants due to their persistence, toxicity, and potential for bioaccumulation. Prolonged exposure to these metals can cause severe health problems including neurological damage, kidney failure, and increased cancer risk (Ohiagu et al., 2022; Jalili et al., 2021; WHO, 2022e). The Environmental Protection Agency (EPA, 2021d) has set maximum permissible limits, warning that Pb concentrations above 0.01 mg/L are especially harmful to vulnerable populations. In Afghanistan, industrial zones frequently exceed these limits (UNEP, 2023d), particularly in areas with unregulated mining, battery production, and textile industries. Additionally, Cd and Hg are commonly found in agricultural runoff, further degrading water quality.

### 2.2. Biological contaminants and organic pollution

Biological contaminants such as *E. coli*, viruses, and protozoa are widely present in regions lacking sanitation infrastructure. WHO (2022a) estimates that more than 70% of Afghanistan's drinking water sources contain microbial contaminants exceeding safe thresholds. Additionally, high BOD and COD in wastewater reflect elevated organic pollution levels. These indicators are directly linked to oxygen depletion and aquatic ecosystem degradation (APHA, 2021b). Studies from the Kabul and Helmand Rivers confirm that municipal and industrial wastewater inputs significantly raise BOD/COD levels, resulting in reduced water quality.

### 2.3. Wastewater management strategies

In many developing countries, including Afghanistan, the lack of effective wastewater treatment systems presents a major environmental challenge. Afghanistan's National Environmental Protection Agency (NEPA, 2023a) has emphasized the need for comprehensive regulations, the development of treatment plants, and public awareness campaigns. International studies show that countries with integrated wastewater management have seen marked reductions in heavy metal and organic pollution levels (UNEP, 2023c). The (EPA 2021b) also advocates for advanced treatment technologies, including reverse osmosis and activated carbon, to improve wastewater quality prior to environmental discharge. Design principles outlined by (Davis 2010) emphasize the importance of integrating treatment capacity with urban expansion to manage wastewater effectively. Integrating wastewater treatment with environmental planning reduces the broader ecological footprint (Smith & Watts, 2012).

## 2.4. Role of GIS in water quality monitoring

GIS technology has revolutionized environmental data analysis by enabling spatial visualization of pollutant distribution. The United States Geological Survey (USGS, 2021a) highlights GIS as a valuable tool for identifying contamination hotspots, tracking pollution sources, and modeling transport pathways. Methods such as Inverse Distance Weighting (IDW) and Kriging allow for accurate interpolation of environmental variables. In Afghanistan, GIS has been effectively used to assess pollution in densely populated and industrialized regions, guiding targeted intervention strategies (UNEP, 2023d).

## 2.5. Summary of literature

In summary, the reviewed literature reveals that Afghanistan's water resources are at serious risk due to heavy metal contamination, biological pollutants, and a lack of effective wastewater management. The integration of GIS and laboratory-based monitoring is essential for understanding pollution dynamics and informing mitigation strategies. This study contributes to the growing body of work by applying spatial analysis and empirical measurements to assess pollution in Afghanistan's major river basins.

## 3. Methodology

### 3.1. Study area and sampling locations

This study was conducted in five regions of Afghanistan selected for their vulnerability to water pollution: the Kabul River, Helmand River, Kandahar Agricultural Zone, Herat Industrial Area, and Nangarhar Agricultural Zone. These areas represent a range of pollution sources, including urban wastewater, industrial effluents, and agricultural runoff. 25 samples were collected (5 per site) during both dry and wet seasons to evaluate seasonal variations in contaminant levels (NEPA, 2023a).

### 3.2. Sample collection and laboratory analysis

Water samples were collected using sterilized polyethylene bottles and transported under chilled conditions to maintain sample integrity. Analytical procedures included:

- Heavy Metals: Pb, Cd, Hg, and Cr were measured using Atomic Absorption Spectroscopy (AAS), following EPA Method 200.9 (EPA, 2021a).
- Biological Contaminants: *E. coli*, BOD, and COD were analyzed using membrane filtration and APHA standard methods (APHA, 2021c).
- Physicochemical Parameters: pH was measured using a pH meter, TDS using a conductivity meter, and turbidity using a nephelometer (WHO, 2022c).

Standard water quality parameters such as TDS, turbidity, and pH are used as indicators of pollution severity. High TDS levels in some regions may also indicate saline or alkali soil influence (Murphy, 2007).

### 3.3. GIS-based spatial analysis

GIS techniques were used to visualize and interpret spatial patterns of water contamination. The analysis involved:

- Spatial interpolation: IDW and Kriging methods were applied to estimate contamination levels between sample locations (USGS, 2021a).

- Land use and pollution source mapping: GIS layers identifying industrial discharges, agricultural activity, and population density were overlaid to assess pollution hotspots (UNEP, 2023b).
- Hydrological modeling: Groundwater flow modeling using GIS is vital for tracking subsurface pollutant movement in porous zones (Khan & Husain, 2013). Contaminated groundwater poses serious health and agricultural risks in high-permeability zones (Saha & Paul, 2019).

### 3.4. Data validation and quality assurance

To ensure accuracy and precision:

- Duplicate samples were analyzed (10% of total).
- Laboratory instruments were calibrated prior to each batch of tests.
- Certified reference materials, based on EPA standards (e.g., Method 200.9), were used to validate heavy metal measurements. Additional guidance on water quality monitoring, including sediment and biological indicators, was derived from Chapman (1996).

This multi-layered approach combining empirical testing and spatial analysis enhances the reliability of the study's findings and supports informed policy and management decisions.

## 4. Results and Discussion

This section presents the findings of the study, focusing on heavy metal contamination, biological pollutants, and GIS-based spatial analysis of water quality in Afghanistan's major river basins. The results are interpreted in comparison with international water quality standards and previous studies.

### 4.1. Heavy metal contamination in water samples

Laboratory analysis revealed elevated concentrations of heavy metals including Pb, Cd, Hg, and Cr in various locations. The data, presented in Table 3, indicate that industrial and urban areas are particularly affected. These metals pose significant ecotoxicological risks, as discussed by Mitra and Gupta (2018).

**Table 3.** Heavy metal concentrations in Afghan river systems (mg/L)

Location	Pb	Cd	Hg	Cr
Kabul River	0.12	0.03	0.002	0.05
Helmand River	0.08	0.02	0.001	0.04
Kandahar Agricultural Zone	0.05	0.01	0.001	0.03
Herat Industrial Area	0.15	0.04	0.003	0.06
Nangarhar Agricultural Zone	0.07	0.02	0.001	0.04
WHO Limit	0.01	0.003	0.001	0.05

Key findings include:

- Pb and Cd concentrations exceeded WHO and EPA safety thresholds in industrial and urban regions, particularly Herat and Kabul (WHO, 2022e; EPA, 2021).
- Hg levels remained within safe limits but require ongoing monitoring due to bioaccumulation potential.
- Cr levels were notably high in Herat, indicating industrial sources (Figure 1).

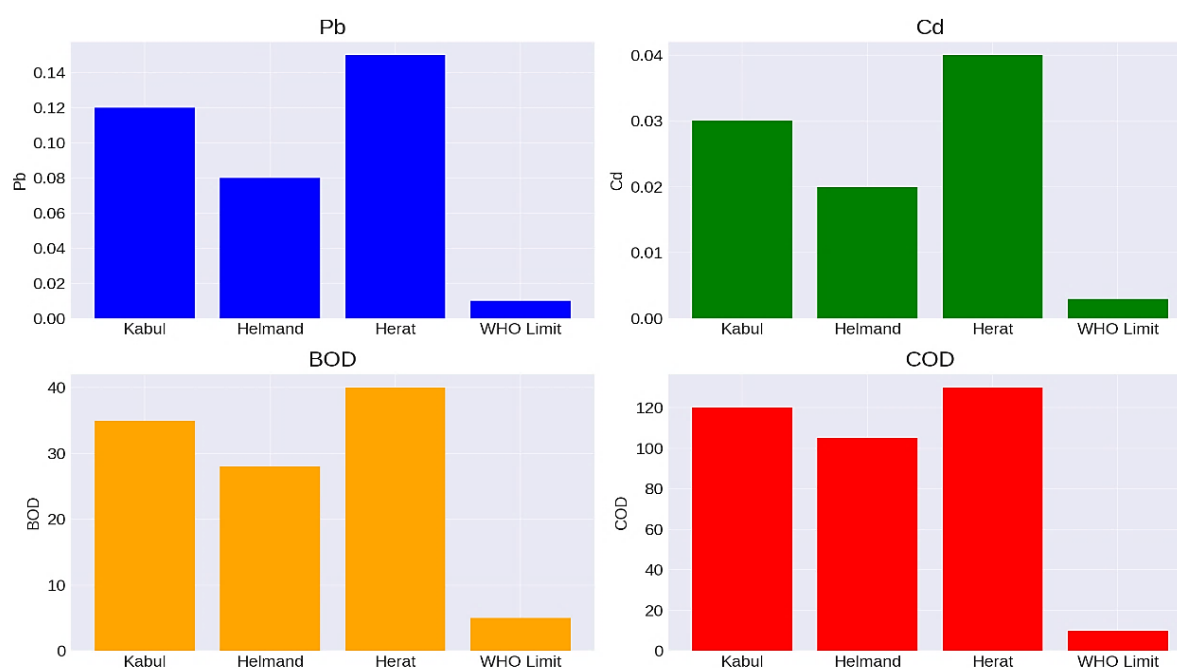


**Figure 1.** Comparison of Pb, Cd, BOD, and COD levels in Kabul, Helmand, and Herat, alongside WHO limits

Herat consistently records the highest contamination values.

#### 4.2. Biological contamination and organic pollution

To assess microbiological and organic pollution, *E. coli*, BOD, and COD levels (Table 4) were analyzed. The findings underscore widespread contamination.

Table 4. Biological and organic contaminants in water samples

Location	<i>E. coli</i> (CFU/100mL)	BOD (mg/L)	COD (mg/L)
Kabul River	920	35	120
Helmand River	680	28	105
Kandahar Agricultural Zone	540	18	75
Herat Industrial Area	1100	40	130
Nangarhar Agricultural Zone	600	20	85
WHO Limit	0	5	10

Key observations:

- *E. coli* contamination exceeded WHO limits in all locations, confirming widespread fecal pollution.
- High BOD and COD levels in Kabul and Herat indicate heavy organic pollution due to untreated municipal and industrial wastewater.
- Agricultural runoff likely contributed to moderate pollution in Kandahar and Nangarhar.

#### 4.3. GIS-Based spatial analysis of pollution

GIS tools were used to visualize the spatial distribution of pollution across the study area. Figures 2–5 illustrate the spatial distribution of heavy metal contamination across Afghanistan, with Pb concentrated in urban centers like Kabul and Herat (Figure 2), Cd prevalent in industrial and agricultural zones (Figure 3), Cr elevated near rivers and industrial areas (Figure 4), and Hg disproportionately affecting river basins (Figure 5) (USGS, 2021c).

- **Pollution Hotspots:** Kabul and Herat industrial zones exhibited the highest contamination, aligning with population density and industrial activity (USGS, 2021c).
- **Spatial Trends:** Heavy metal concentrations peaked near industrial discharge points and diminished downstream.

Biological contamination was highest in urban centers with poor sanitation (WHO, 2022e).

- **Risk Assessment:** GIS maps highlighted high-risk areas requiring urgent intervention. Poor wastewater infrastructure increased the likelihood of pollutant infiltration into groundwater (NEPA, 2023e).



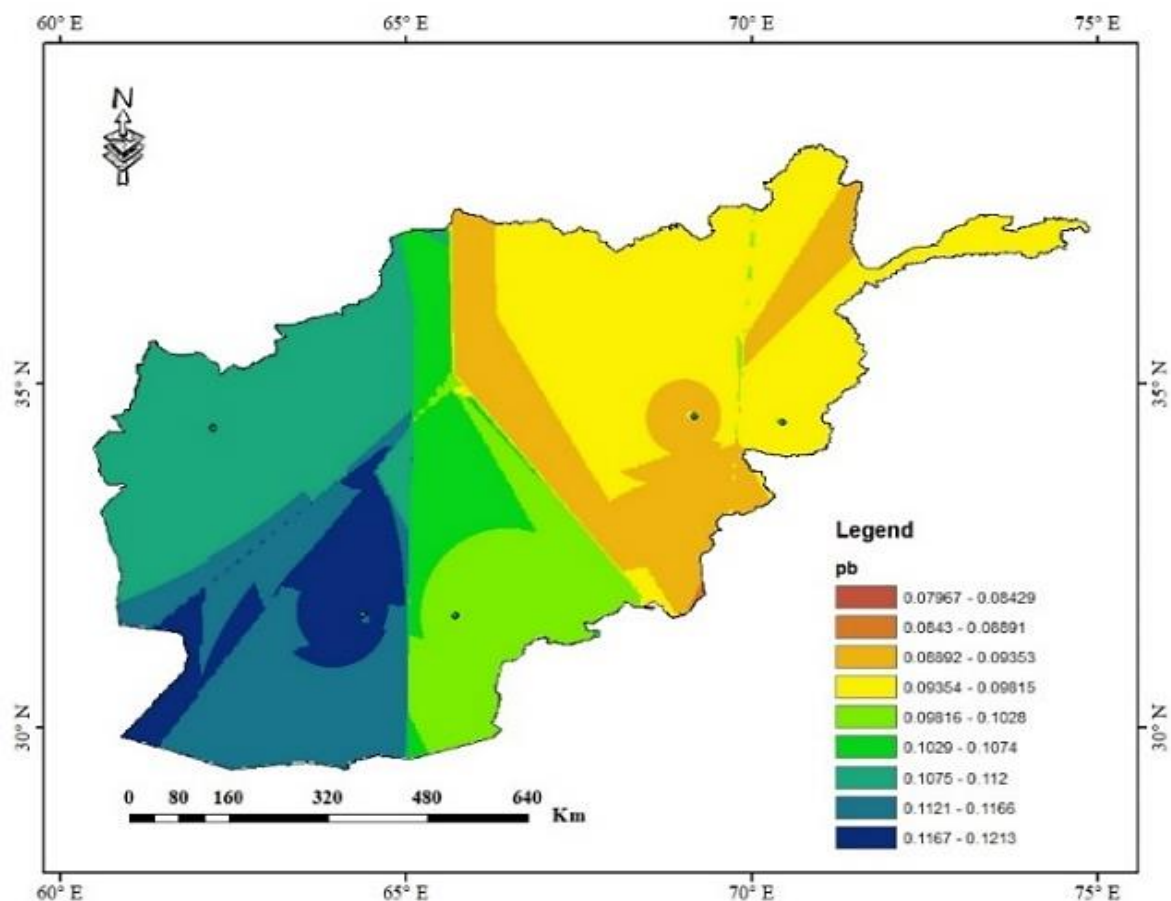


**Figure 2.** Spatial distribution of Pb contamination in Kabul, Herat, Kandahar, and other high-risk zones across Afghanistan

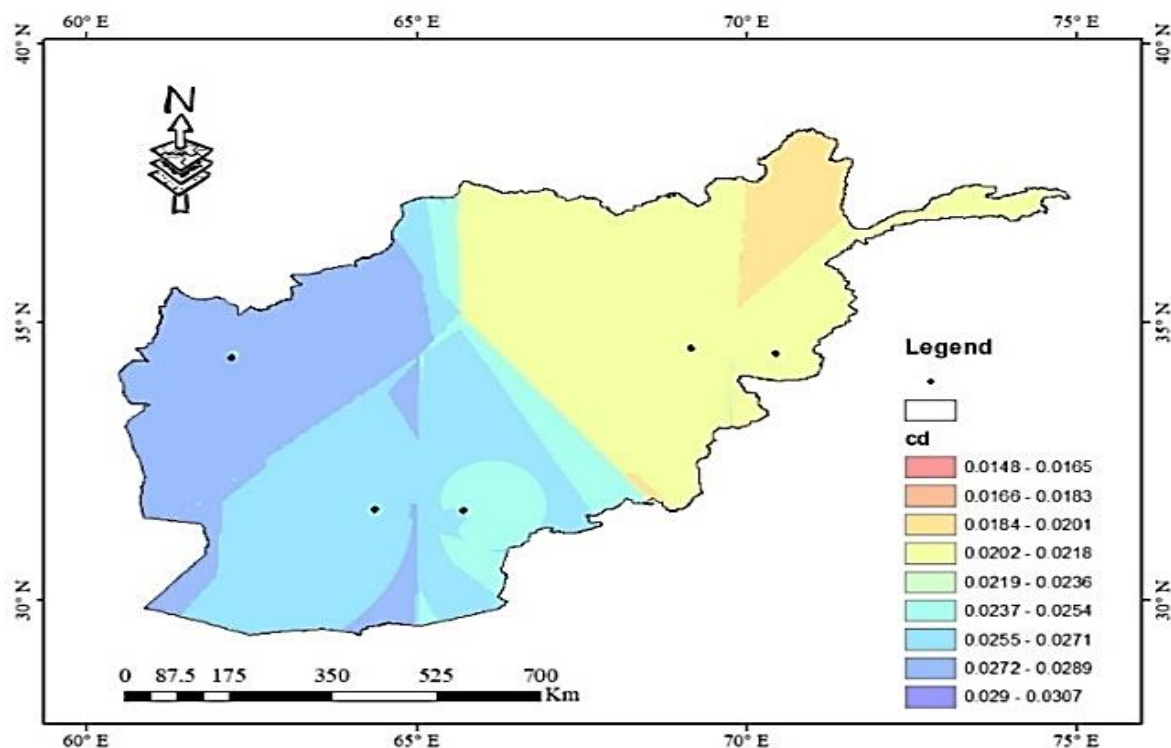


**Figure 3.** Spatial distribution of Cd contamination in urban, industrial, and agricultural regions of Afghanistan

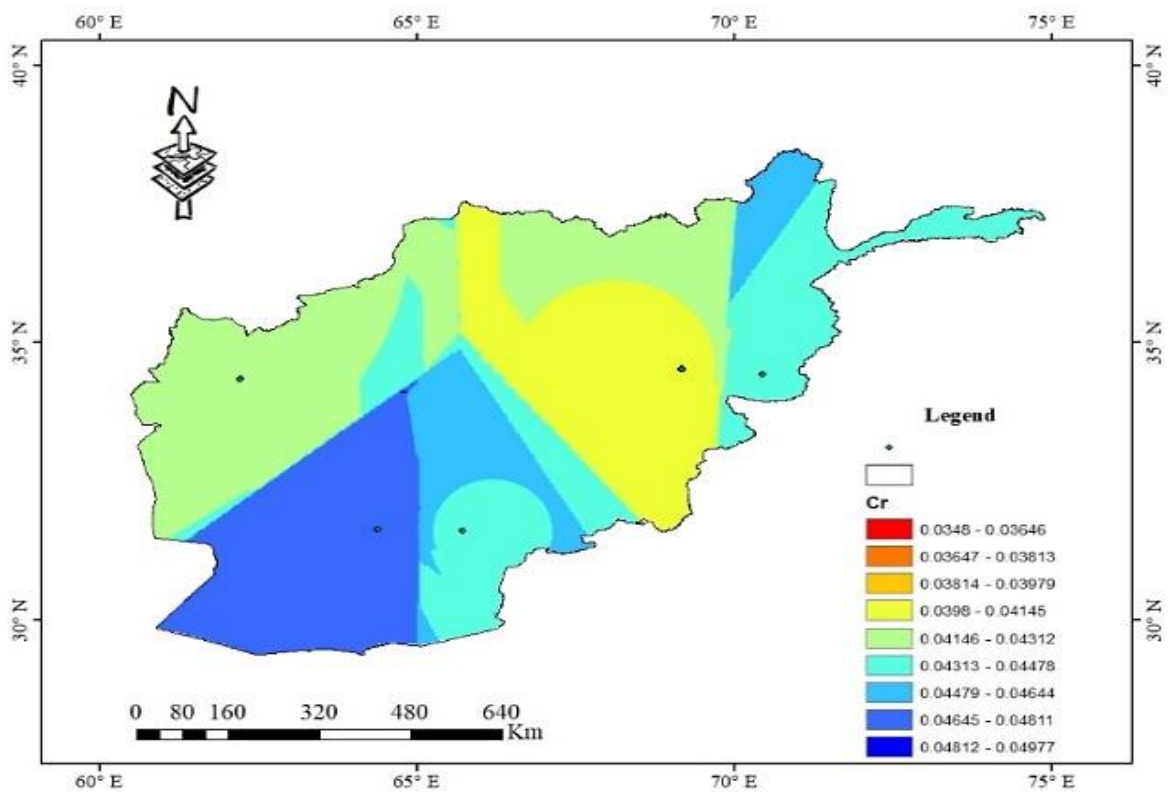


**Figure 4.** Cr contamination levels mapped across key river-adjacent and industrial zones in major Afghan cities

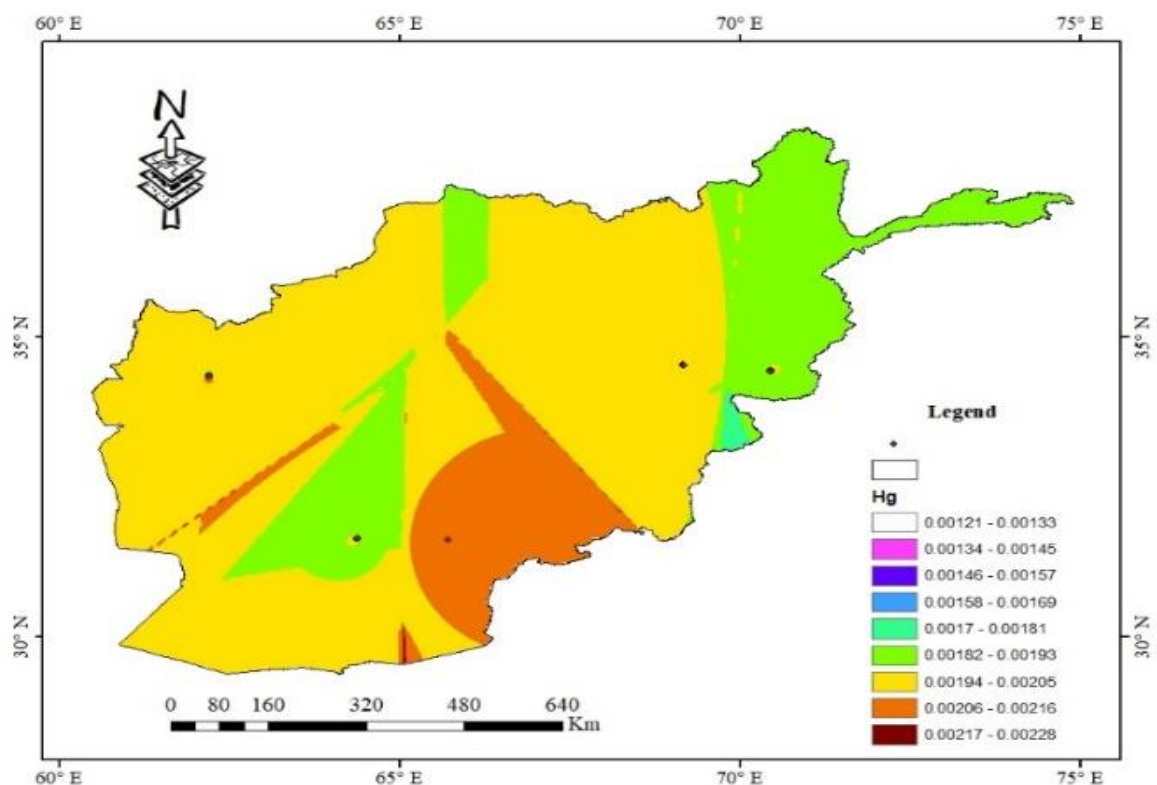


**Figure 5.** Spatial distribution of Hg contamination across major Afghan river basins and surrounding high-risk regions

#### 4.4. Discussion summary

- Industrial wastewater is the primary source of heavy metal contamination, with Pb and Cd levels surpassing safety limits.
- Untreated organic waste contributes to dangerously high BOD and COD, degrading aquatic ecosystems.
- GIS spatial analysis successfully identifies pollution hotspots and reinforces the need for policy-focused solutions.

These findings underscore the urgent requirement for comprehensive wastewater treatment systems, strict environmental regulations, and real-time water quality monitoring networks to protect Afghanistan's freshwater resources.

#### 5. Conclusions

This study presents a comprehensive GIS-based assessment of water pollution across major Afghan river basins, revealing severe contamination by heavy metals, biological agents, and organic pollutants. The data clearly show that industrial and urban areas, particularly Kabul and Herat, are the most affected, with pollution levels exceeding international health and environmental safety limits. The spatial analysis confirms that contamination is closely linked to population density, industrial discharge, and lack of wastewater treatment facilities. These findings stress the urgency of implementing real-time GIS monitoring systems, upgrading water treatment infrastructure, and enforcing strict environmental regulations. Additionally, public awareness campaigns and stakeholder collaboration are vital for long-term water resource sustainability. Future research should focus on integrating hydrological and geospatial models to enhance predictive capabilities and guide targeted interventions. Addressing Afghanistan's water pollution crisis requires coordinated efforts at the policy, institutional, and community levels.

#### Authorship Contribution Statement

The author is solely responsible for the conceptualization, methodology, data collection, analysis, and manuscript preparation.

#### Conflict of Interest

The author declares no conflict of interest.

#### Data Availability

Data will be made available on request.

#### References

- Alam, M., & Sadiq, R. (2020). *Heavy metal contamination in water: Sources, impacts, and treatment technologies*. Springer Nature.
- American Public Health Association. (2021a). *Standard methods for the examination of water and wastewater* (24th ed.). APHA.
- American Public Health Association. (2021b). *Microbiological testing methods for waterborne pathogens*. APHA.

- American Public Health Association. (2021c). *Chemical oxygen demand and biochemical oxygen demand in water treatment*. APHA.
- Chapman, D. (1996). *Water quality assessments: A guide to the use of biota, sediments, and water in environmental monitoring*. Taylor & Francis.
- Davis, M. L. (2010). *Water and wastewater engineering: Design principles and practice*. McGraw-Hill.
- Drešković, N., & Dug, S. (2012). Applying the inverse distance weighting and kriging methods of the spatial interpolation on the mapping the annual precipitation in Bosnia and Herzegovina. *International Congress on Environmental Modelling and Software*, 229. <https://scholarsarchive.byu.edu/iemssconference/2012/Stream-B/229>
- Environmental Protection Agency. (2021a). *Guidelines for heavy metal contamination in water sources*. EPA.
- Environmental Protection Agency. (2021b). *Toxicology and risk assessment of heavy metals in water systems*. EPA.
- Environmental Protection Agency. (2021c). *Industrial wastewater discharge regulations and environmental impact*. EPA.
- Environmental Protection Agency. (2021d). *Wastewater treatment technologies for heavy metal removal*. EPA.
- Jalili, C., Kazemi, M., Cheng, H., Mohammadi, H., Babaei, A., Taheri, E., & Moradi, S. (2021). Associations between exposure to heavy metals and the risk of chronic kidney disease: A systematic review and meta-analysis. *Critical Reviews in Toxicology*, 51(2), 165–182. <https://doi.org/10.1080/10408444.2021.1891196>
- Jha, M. K., & Gassman, P. W. (2014). GIS-based modeling of water pollution in river systems. *Environmental Monitoring and Assessment*, 186(2), 901–918.
- Khan, F., & Husain, T. (2013). Risk-based analysis of contaminant transport in groundwater using GIS. *Water Research Journal*, 47(12), 4097–4110.
- Lafta, M., Afra, A., Patra, I., Jalil, A., Mohammadi, M., Al-Dhalimy, A. B., Ziyadullaev, S., Kiani, F., Ekrami, H., & Asban, P. (2024). Toxic effects due to exposure to heavy metals and increased health risk assessment (leukemia). *Reviews on Environmental Health*, 39(2), 351–362. <https://doi.org/10.1515/reveh-2022-0227>
- Meybeck, M., & Helmer, R. (1989). The quality of rivers: From pristine stage to global pollution. *Global Environmental Change*, 8(4), 283–311.
- Mitra, S., & Gupta, S. (2018). *Environmental chemistry and toxicology of heavy metals in water*. Elsevier.
- Murphy, S. (2007). *General information on water quality parameters and standards*. U.S. Department of the Interior.
- Nasreen, H., & Haider, S. (2024). A review of the significant role of heavy metals in the advancement of the world and its contribution to pollution. *Pakistan Journal of Chemistry*, 14(3-4), 49-59. <https://doi.org/10.15228/2024.v14i03-4p06>
- Ohiagu, F. O., Chikezie, P. C., Ahaneku, C. C., et al. (2022). Human exposure to heavy metals: Toxicity mechanisms and health implications. *Materials Science & Engineering International Journal*, 6(2), 78–87. <https://doi.org/10.15406/mseij.2022.06.00183>

- Oyebamiji, A. R. (2024). *Modelling the risk of hydrocarbon contamination on groundwater quality in the Niger Delta* (Doctoral thesis, University of Portsmouth). University of Portsmouth.
- Saha, P. K., & Paul, B. (2019). *Groundwater contamination: Environmental and health impacts*. Wiley.
- Setianto, A., & Triandini, T. (2013). Comparison of kriging and inverse distance weighted (IDW) interpolation methods in lineament extraction and analysis. *Journal of Southeast Asian Applied Geology*, 5(1), 21-29.
- Singh, G., & Agarwal, T. (2020). *Pollution control strategies in water resource management: Advances in water quality assessment*. Springer.
- Smith, C. J., & Watts, P. J. (2012). Wastewater treatment and environmental impact reduction strategies. *Environmental Science & Technology*, 46(5), 2458–2465.
- United Nations Environment Programme. (2023a). *Global wastewater assessment report*. UNEP.
- United Nations Environment Programme. (2023b). *GIS-based environmental risk assessment report*. UNEP.
- United Nations Environment Programme. (2023c). *Industrial wastewater and environmental impact report*. UNEP.
- United Nations Environment Programme. (2023d). *Sustainable development goals and water pollution control*. UNEP.
- United States Geological Survey. (2021a). *Hydrological modeling and water contamination studies*. USGS.
- United States Geological Survey. (2021b). *Remote sensing applications for water quality monitoring*. USGS.
- United States Geological Survey. (2021c). *Mapping heavy metal contamination using GIS technology*. USGS.
- Wang, X., & Chen, Z. (2013). Spatial distribution and risk assessment of heavy metals in urban river sediments using GIS. *Environmental Pollution*, 182, 452–461.
- World Health Organization. (2022a). *Water quality and health strategy 2022–2030*. WHO.
- World Health Organization. (2022b). *Bacteriological water quality guidelines for drinking water*. WHO.
- World Health Organization. (2022c). *Sanitation and hygiene in developing countries*. WHO.
- World Health Organization. (2022d). *Public health implications of water contamination*. WHO.
- World Health Organization. (2022e). *Safe drinking water standards and health impacts*. WHO.





## Efficacy of Biofumigants for Controlling Root-Knot Nematodes (*Meloidogyne*) in Tomato Cultivation

Parwiz Niazi<sup>1\*</sup>, Abdul Bari Hejran<sup>2</sup>, Khaidarov Saken<sup>3</sup>

Kandahar University, Department of Biology, Kandahar, 3801, Afghanistan

Helmand University, Department of Biology, Helmand, 3901, Afghanistan and Al-Farabi Kazakh National University, Department of Biotechnology, Almaty, Kazakhstan

Al-Farabi Kazakh National University, Department of Biotechnology, Almaty, Kazakhstan

### Research Article

\*Correspondence:  
parwiz60@gmail.com

Received: 13 November 2024

Accepted: 30 June 2025

Published: 30 July 2025

### Keywords

Natural soil amendments

*Meloidogyne* spp.

*Lycopersicon esculentum*

Agroecological practices

This is an open access article  
under the CC BY NC license.



### Abstract

Root-knot nematodes (*Meloidogyne* spp.) are formidable pests that impose severe constraints on agricultural productivity, particularly impacting the growth and yield of economically important crops such as tomatoes. This study undertakes a comprehensive examination of biofumigants derived from plants within the *Brassicaceae* and *Non-Brassicaceae* families, investigating their potential as environmentally friendly control measures against these nematodes. Specifically, it evaluates the nematicidal efficacy of biofumigants sourced from cabbage (*Brassica oleracea*), sorghum (*Sorghum bicolor*), and *Tagetes* (*Tagetes* spp.) in reducing root-knot nematode populations and enhancing growth-related parameters of tomato plants. The experimental design followed a completely randomized design format, featuring five distinct treatments to ascertain the effects of each biofumigant on nematode suppression and various plant growth metrics, including plant height, leaf count, and root wet weight. This investigation revealed a significant advantage of *Brassicaceae*-derived biofumigants, with cabbage showing the most potent nematicidal activity, achieving a 60.7% reduction in nematode populations compared to untreated control groups. Sorghum (*Sorghum bicolor*), representing the *Non-Brassicaceae* family, also exhibited promising effects, achieving a 50.9% reduction in nematode presence. By contrast, *Tagetes* spp. displayed relatively moderate efficacy, with a 30.8% reduction in nematode populations. Notably, while the application of these biofumigants did not lead to statistically significant changes in tomato plant height or leaf count, the results highlight the substantial potential of *Brassicaceae*-based biofumigants, particularly cabbage, as viable, sustainable, and ecologically sound strategies for managing root-knot nematodes in tomato cultivation. Such biofumigants could offer a promising alternative to chemical nematicides, reducing reliance on synthetic pesticides and fostering sustainable agricultural practices. This study underscores the importance of further research into *Brassicaceae*-derived biofumigants to optimize their application and maximize their effectiveness in diverse agricultural systems.

**How to cite this paper:** Niazi, P., Hejran, A. B., & Saken, K. (2025). Efficacy of biofumigants for controlling root-knot nematodes (*Meloidogyne*) in tomato cultivation. *Scientific Research Communications*, 5(2), 118-139. <https://doi.org/10.52460/src.2025.010>

## 1. Introduction

Root-knot nematodes (RKN) can severely damage plants by hindering root system growth, leading to reduced nutrient uptake and increasing vulnerability to secondary pathogens (Habteweld et al., 2024). Various control methods have been employed to mitigate RKN damage, with nematicides being the most commonly used. Soil fumigation, involving high doses of chemicals like methyl bromide and chloropicrin, has effectively reduced RKN populations below economic thresholds (Faria et al., 2024; Priyadharshini et al., 2025); due to environmental concerns and stricter regulations, many fumigants have been banned. Fumigants contribute to volatile organic compound emissions, which harm air quality. In 2019, the global market for fumigation reached USD 938.61 million, with continued growth expected. However, restrictions on fumigant use are increasing, leading to the search for eco-friendly alternatives like biofumigation (Majid et al., 2025; Rajah et al., 2025).

Tomatoes (*Solanum lycopersicum* L.) are economically valuable and widely cultivated for their nutrient-rich profile, which includes essential minerals, vitamins, and antioxidants beneficial to human health; among these, tomatoes are exceptionally high in lycopene, an antioxidant linked to reducing risks of cancer, cardiovascular disease, and cellular ageing (Jamir et al., 2024). Globally, India ranks as the third-largest producer of tomatoes, following China and the USA, with an impressive production of 20.7 million tons in 2018 from 0.8 million hectares, yielding approximately 26,000 kilograms per hectare (Salhab et al., 2020). In economically vulnerable regions, however, maintaining a stable tomato supply is challenged by infections from *Meloidogyne* spp., commonly known as RKN; these parasites cause significant damage to the plant's vascular system, impeding water uptake, nutrient transport, and photosynthesis, and are estimated to contribute to annual global agricultural losses of around \$78 billion (Abd-Elgawad, 2024). Nematode secretions further disrupt biochemical and molecular processes in plant roots, weakening their capacity for water and nutrient absorption (Niazi et al., 2023; Adigun et al., 2024). Various methods have been tested to combat nematode infections, including crop rotation with non-host plants and chemical nematicides, such as halogenated aliphatic hydrocarbons, 1,3-dichloropropene, methyl isothiocyanate, oxamyl, thionazin, and carbofuran, the extensive use of chemical treatments raises environmental concerns (Kandil et al., 2025).

With a growing focus on sustainable disease management, recent research has turned towards microbial-based alternatives (Hamrouni et al., 2024). Plant growth-promoting rhizobacteria (PGPR) represent an environmentally safe strategy for controlling soil-borne plant diseases (Sun et al., 2024; Kumar et al., 2023). By fostering beneficial microbial interactions, PGPR helps plants better absorb nutrients and release phytohormones, enhancing their resilience against pathogens more sustainably (Qadir et al., 2024; Gupta et al., 2024). RKN (*Meloidogyne* spp.) are microscopic, parasitic roundworms that infest plant roots, causing significant agricultural damage worldwide. These nematodes are named for the characteristic galls or "knots" they induce in the roots of infected plants (Albazazz et al., 2024; Khosla and Sharma, 2024). They penetrate the roots and establish feeding sites, causing abnormal cell growth, which disrupts the plant's ability to absorb water and nutrients. This can lead to stunted growth, wilting, reduced yields, and in severe cases, plant death. There are over 90 species of RKN, with *Meloidogyne incognita*, *M. javanica*, *M. arenaria*, and *M. hapla* being the most common and damaging. These nematodes have a broad host range, affecting many crops such as tomatoes, potatoes, carrots, and cucumbers. Infestations can spread through soil, water, and contaminated tools, making them difficult to control (Mirzaev et al., 2024; Sarri et al., 2024).

The damage caused by RKN is often compounded by secondary infections from fungi, bacteria, or other soilborne pathogens that enter through the wounds they create. Due to their

impact on agriculture, RKN are considered a significant pest, and effective management strategies are essential for maintaining healthy crops and reducing economic losses (Rigobelo et al., 2024). Traditional control methods have relied on chemical treatments, but concerns about environmental toxicity have prompted interest in sustainable alternatives like crop rotation, resistant plant varieties, and biofumigation (Curk & Trdan, 2024).

Biofumigation involves incorporating plant materials, especially from the cabbage family, into the soil; cabbage plants produce glucosinolates, secondary metabolites toxic to pathogens and weeds (Harouna et al., 2024; Muthusamy and Lee, 2024). Glucosinolates reduce RKN egg viability by penetrating the cuticle, and their hydrolysis produces isothiocyanates (ITS), which function as fungicides and nematicides (Fourie, 2024). Sorghum produces nematicidal cyanide through hydrolysis of dhurrin, which is converted into toxic hydrogen cyanide (Njekete et al., 2024). *Tagetes* plants release  $\alpha$ -terthienyl, which becomes phytotoxic to nematodes after photoactivation; these biofumigation techniques provide a promising, environmentally friendly alternative for managing RKN and other plant parasitic nematodes (Kannan et al., 2024; Hejran et al., 2024). Biofumigation is an environmentally friendly pest management technique that uses specific plants, mainly those rich in natural compounds, to control soil-borne pests and pathogens, including nematodes, fungi, and weeds; the process involves incorporating plant materials into the soil, where they decompose and release volatile compounds that are toxic to harmful organisms (El-Sharkawy & Al-Gendy, 2024).

Plants from the Brassicaceae family, such as mustard, cabbage, and radish, are commonly used in biofumigation due to their high levels of glucosinolates. When these plants are chopped or macerated and mixed into the soil, their glucosinolates are broken down through enzymatic hydrolysis, producing compounds such as isothiocyanates, which have strong biocidal properties. These compounds can inhibit the growth and reproduction of pests like RKN, fungi, and certain weeds (Ko et al., 2024; Mwangi et al., 2024), other plants such as sorghum and *Tagetes* (marigold) also have biofumigant properties. Sorghum, for example, produces cyanogenic glycosides that release toxic hydrogen cyanide, while marigolds produce  $\alpha$ -terthienyl, which becomes active under UV light and targets nematodes (Giantin et al., 2024; Biswas and Das, 2024). Biofumigation is seen as a sustainable alternative to chemical fumigants, which can have harmful environmental effects. It helps improve soil health by adding organic matter and reducing reliance on synthetic pesticides. Although its efficacy may vary depending on factors such as soil type and pest populations, biofumigation is gaining popularity as part of integrated pest management strategies aimed at reducing the use of toxic chemicals in agriculture (Parsiaaref et al., 2024; Hejran et al., 2024). As part of integrated pest management (IPM) strategies, biofumigants offer sustainable solutions to replace or complement chemical fumigants. In this article, we endeavor to elucidate the efficacy of biofumigants derived from Brassicaceae and other botanical sources as eco-friendly alternatives for managing root-knot nematode (*Meloidogyne spp.*) infestations in tomato cultivation. The application of biofumigation, primarily utilizing glucosinolate-rich Brassicaceae plants, represents an emergent, sustainable paradigm for pest control, harnessing the innate biocidal properties of natural compounds to suppress nematode populations while minimizing environmental impact. We aim to provide an evidence-based framework for integrating biofumigants into sustainable agricultural practices by exploring the nematicidal potentials of cabbage, sorghum, and *Tagetes*. This study's findings promise to advance IPM strategies, contributing to reduced dependency on synthetic nematicides and promoting agroecological resilience (Zhang et al., 2025). The main objective of this study is to evaluate the potential of biofumigants derived from both Brassicaceae and non-Brassicaceae plant families as sustainable alternatives to synthetic nematicides for managing RKN (*Meloidogyne spp.*) in tomato cultivation. Specifically, the study aims to assess the nematicidal efficacy of

biofumigants sourced from cabbage (*Brassica oleracea*), sorghum (*Sorghum bicolor*), and *Tagetes* (*Tagetes* spp.), as well as to investigate their effects on key growth parameters of tomato plants, including plant height, leaf count, and root wet weight.

## 2. Method and Materials

### 2.1. Preparation and sterilization of soil

The soil was sterilized before being placed into 8-inch earthen pots. Each pot was filled with 4 kg of sterilized sandy loam soil (71% sand, 21% silt, 8% clay, pH 7.3), which was obtained from a fallow field. The soil was sieved through a 16-mesh sieve to remove stones and debris. A mixture of soil and farmyard manure was prepared in a 3:1 ratio, and clay pots (25 cm top diameter) were filled with this mixture at 4 kg per pot. The soil was moistened with a small amount of water before being sterilized in an autoclave at a temperature of 121°C under 20 lbs pressure for 20 minutes. The sterilized soil was then allowed to cool at room temperature before use in the experiments (Bouchtaoui et al., 2025).

### 2.2. Sample preparation

Tomato seeds are sown in the greenhouse of the Plant Protection Study Program for 15 days to allow for early plant establishment; the seedlings will be grown under controlled conditions to ensure uniformity and healthy growth before they are exposed to further experimental treatments. The soil used in this study, which is naturally infested with RKN (*Meloidogyne* spp.), is sourced from a field that was previously cultivated with tomatoes; this field belongs to a region known to be endemic to RKN infestations.

The decision to use soil from this area is based on its history of persistent nematode problems, making it an ideal source for testing and evaluating the effectiveness of various RKN management strategies. Using soil already heavily infested with RKN, the experiment can simulate real-world agricultural conditions where these nematodes are a significant pest problem. This approach ensures the findings are relevant and applicable to farmers facing similar challenges.

The collected soil will be the foundation for subsequent experiments investigating the impact of different nematode control methods. These methods may include biofumigation with selected biofumigant plants, resistant tomato cultivars, or other integrated pest management strategies. By using naturally infested soil, the study will provide valuable insights into the efficacy of these control measures under realistic infestation levels, offering practical solutions for managing RKN in tomato crops; this phase is crucial for setting the stage for later evaluations of plant health, root system integrity, and overall crop yield in response to nematode management practices.

### 2.3. Treatment details

#### Preparation of biofumigants

Select biofumigant plants such as (*Brassica oleracea*), (*Sorghum bicolor*), and (*Tagetes* spp.). Chop the plant materials into pieces measuring 3-4 cm. This size enhances the surface area for decomposition and subsequent nematicidal activity, then combine 0.4 kg of the chopped biofumigant material with 2 kg of RKN-infested soil in a mixing container. Ensure thorough mixing to distribute plant material evenly within the soil (Sarwar et al., 1998; Ling et al., 2025).

### Conditions for biofumigation

Allow the mixture to rest for a specific period (2-3 hours) before sealing to enable initial interactions between the soil and biofumigants. Conduct the mixing at a controlled temperature of approximately 25-30°C with relative humidity of around 60-70% to optimize microbial activity and nematicidal compound release during the decomposition phase. Seal the biofumigant-treated soil in plastic bags and incubate for 14 days. This period allows for the decomposition of biofumigants and the release of nematicidal compounds (Kirkegaard & Sarwar, 1998; Torabian et al., 2025).

### Post-incubation handling

After 14 days, air the treated soil for 24 hours in a shaded area to allow volatile compounds to dissipate slightly while retaining nematicidal properties. After airing, transfer the treated soil into polybags for planting, ensuring soil moisture and structure uniformity.

## 2.4. Chemical treatment

Apply 4 g of carbofuran per 2 kg of soil. Incorporate the chemical into the soil by mixing thoroughly to ensure even distribution. This can be done using a hand trowel or a small garden spade. Apply the nematicide at least 24 hours before transplanting the tomato seedlings. This waiting period allows the chemical to settle and minimizes potential phytotoxicity in young plants (Figure 1).

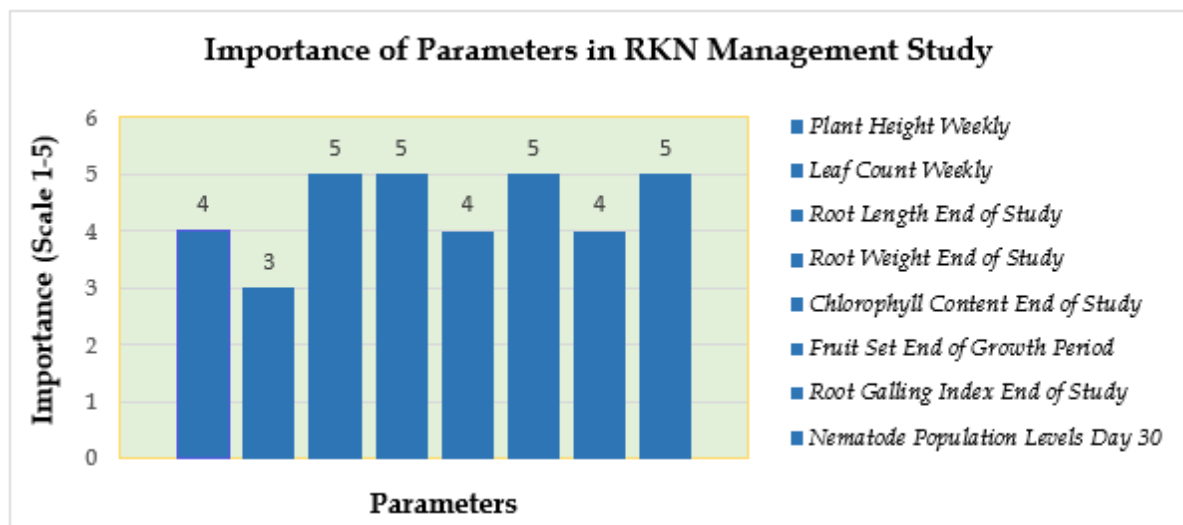


**Figure 1.** Importance (scale 1-5) of parameters in an RKN management study, with root length, root weight, fruit set, and nematode population rated highest

Figure 1 illustrates the comparative efficacy of different treatments (biofumigation, chemical treatment, and the untreated control) on tomato growth and nematode management parameters.

Biofumigation resulted in the highest average plant height, leaf count, and chlorophyll content, indicating its effectiveness in promoting plant health. Chemical treatment performed slightly better than the control group but was less effective than biofumigation across all parameters. The control group exhibited the lowest values, highlighting the detrimental



impact of untreated RKN infestations on tomato growth. This analysis emphasizes the potential of biofumigation as a sustainable approach to managing RKN.

## 2.5. Control measures

### Untreated infested soil

Maintain a control group using untreated RKN-infested soil. Ensure these pots are kept in the same environmental conditions (temperature, light, humidity) as the treated groups to eliminate confounding variables.

### Replication and randomization

Randomly assign pots within the greenhouse to ensure that environmental variations (such as light and air circulation) are evenly distributed across treatment groups, and replicate each treatment group multiple times (five replicates) to ensure statistical robustness.

### Monitoring conditions

Regularly monitor and record the temperature and humidity levels in the greenhouse to ensure consistency throughout the experimental period. This data can be crucial for assessing environmental factors' impact on treatments' effectiveness.

## 2.6. Greenhouse studies

The greenhouse studies are designed to evaluate the effectiveness of various treatments for managing RKN in tomato plants under controlled environmental conditions.

### Experimental setup

#### Seedling Preparation

Tomato seedlings will be grown in polybags filled with naturally RKN-infested soil sourced from the farm. The soil's infestation history provides a realistic scenario for assessing the efficacy of various nematode management strategies.

#### Treatment Groups

The main treatments include biofumigation, chemical treatment and control group:

*Biofumigation:* Utilizing biofumigant plants such as cabbage, *Tagetes*, and sorghum.

*Chemical Treatment:* Application of the chemical nematicide carbofuran.

*Control Group:* Untreated infested soil will serve as the control.

#### Preparation of biofumigants

Biofumigant plants will be chopped into 3-4 cm pieces and mixed with RKN-infested soil at a ratio of 0.4 kg of plant material per 2 kg of soil. This mixture will be sealed in plastic bags for 14 days to allow for decomposition and the release of nematicidal compounds. After this period, the treated soil will be aired for 24 hours before being transferred to polybags for planting.

#### Randomization

To minimize bias from environmental factors such as light variations, the placement of pots within the greenhouse will be randomized. This will be achieved using a random number generator to assign pot positions before the start of the experiment. The layout will ensure that all treatment groups are evenly distributed throughout the greenhouse, preventing localized effects from temperature or light gradients.

**Data collection**

Comprehensive data will be collected on the following growth parameters.

**Plant height**

Measured weekly to assess vertical growth.

**Leaf count**

The total number of leaves will be counted weekly to evaluate foliage development.

**Root length**

At the end of the study, root systems will be carefully extracted and measured for length, providing insights into root health and vigor.

**Root weight**

Roots will be weighed post-harvest to evaluate biomass production.

**Chlorophyll content**

Measured using a spectrophotometer, chlorophyll levels provide insights into plants' photosynthetic efficiency.

**Fruit set**

At the end of the growth period, the number of fruit sets per plant will be recorded to assess reproductive success.

**Root health**

The Root Gall Index will be assessed visually, using a scale to quantify the severity of root galling caused by nematode infection.

**Nematode population levels**

At the end of the 30-day period, nematode densities will be assessed to determine the effectiveness of the treatments in suppressing RKN populations.

**Experimental design**

The experiment will follow a completely randomized design with five replications per treatment group, including controls; this design will facilitate statistical analysis and ensure reliable comparisons among treatments (Welham et al., 2014).

**Assessment of Efficacy**

Growth observations will be systematically recorded on Day 25, while nematode populations will be assessed on Day 30 after planting. The data will be analyzed statistically to compare treatment effectiveness in managing RKN and promoting plant health.

**2.7. Biochemical parameters****Chlorophyll quantification**

The quantification of chlorophyll content in fresh leaves was conducted following Mackinney's method. Initially, one gram of finely chopped fresh leaves was ground in a mortar and pestle and then immersed in 20 ml of 80% acetone. The mixture was centrifuged at 5000 rpm for 5 minutes to separate the soluble pigments and the supernatant was collected into a 100 ml volumetric flask. The remaining residue was washed thrice with 80% acetone, and each wash was combined with the supernatant in the volumetric flask. The total volume was adjusted to 100 ml with an additional 80% acetone (Tunca et al., 2024).

After preparing the extract, absorbance readings were taken at wavelengths of 645 nm and 663 nm using a spectrophotometer (U 1700, Shimadzu, Japan), with 80% acetone as the blank (Niazi, 2024); the chlorophyll content was calculated using the Equation (1):

$$\text{Total chlorophyll g - 1 tissue} = \frac{20.2 (A_{645}) + 8.02 (A_{663})}{1000 \times W} \times V \quad (1)$$

where  $A_{645}$  and  $A_{663}$  are the absorbance readings at the specified wavelengths,  $W$  is the weight of the leaf sample in grams and  $V$  is the total volume of the extract in milliliters.

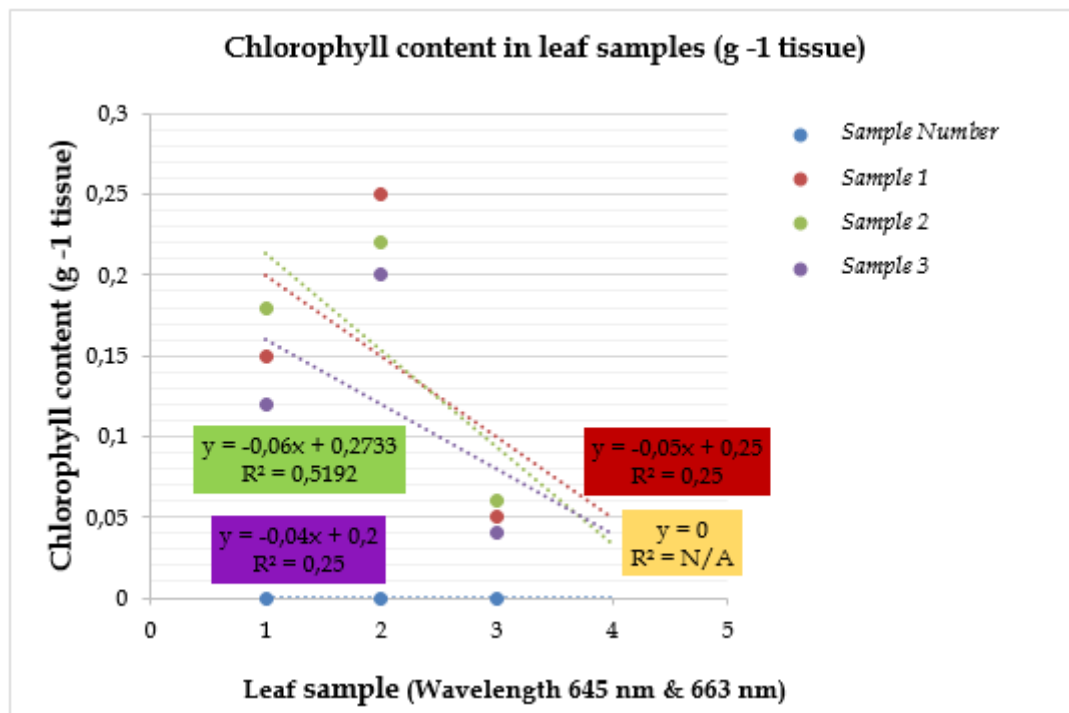


Figure 2. Chlorophyll content vs. leaf samples with trend-lines for samples 1–3 and control

Figure 2 illustrates the data organization for chlorophyll quantification. Each sample in the study is assigned a unique identifier (e.g., *Sample 1*, *Sample 2*, *Sample 3*) to facilitate accurate tracking and analysis. For each sample, two absorbance values are recorded: one at 645 nm, labeled as  $A_{645}$ , and one at 663 nm, labeled as  $A_{663}$ . Alongside these absorbance values, a calculated chlorophyll content value, denoted in grams per unit tissue (g-1), is also included for each sample. The absorbance at 645 nm ( $A_{645}$ ) for each sample, noted as  $X_1$ ,  $X_2$ ,  $X_3$ , etc., represents the initial absorbance readings taken at the specified wavelength for chlorophyll analysis. Similarly, the absorbance at 663 nm ( $A_{663}$ ), recorded as  $Y_1$ ,  $Y_2$ ,  $Y_3$ , and so forth, represents additional readings necessary for accurate chlorophyll content calculation.

## 2.8. Statistical data analysis

### Data analysis approach

The observational data collected from biochemical analyses and growth parameters will be evaluated using appropriate statistical methods to identify differences among the treatment groups. Initially, a one-way analysis of variance (ANOVA) will be performed using D-Staat software; this method is particularly suitable for analyzing single-factor designs with multiple

treatment groups, allowing for insights into the overall variability within the dataset (Zoladek et al., 2022).

#### Post hoc testing

Following the ANOVA, Duncan's Multiple Range Test (DMRT) will be applied for post hoc comparisons between group means; this test is specifically chosen to control the overall error rate while providing precise comparisons of mean differences among groups, effectively identifying distinct subsets within the data (Agbangba et al., 2024).

#### Significance level

A significance level of 5% ( $p < 0.05$ ) will be established, indicating that results are considered statistically significant if there is less than a 5% probability that the observed differences occurred by chance; this threshold is important for balancing the detection of fundamental differences while minimizing the risk of Type I errors (false positives).

#### Statistical software

Data analysis will be conducted using R (version 2.14.1; R Foundation for Statistical Computing, Vienna, Austria). To ensure precision in the results, the standard error of the mean ( $\pm$ SE) will be calculated, and the least significant difference (LSD) at a 5% significance level will be determined using R (Kolaczyk & Csárdi, 2014).

#### Reporting results

All results will be reported with mean values and standard deviations (mean  $\pm$  SD) for clarity. Additionally, assumptions of normality and homogeneity of variances will be checked prior to analysis to validate the appropriateness of the ANOVA model (Sawyer, 2009).

### 3. Results and Discussion

The study results indicated that none of the treatments produced a statistically significant effect on tomato plant growth when measured by plant height and the number of leaves. A closer examination of plant height among the treatments revealed that the application of the carbofuran nematicide resulted in the highest average plant height; this was closely followed by the cabbage biofumigant treatment, which produced a slightly lower, though comparable, yield in terms of plant height.

The superior performance of carbofuran-treated plants can likely be attributed to the specific properties of the nematicide formulation (*Furadan 3G*). Beyond its primary function as a nematicide targeting and eliminating harmful nematodes that can impede plant health, carbofuran also contains compounds that act as growth regulators. These compounds enhance plant vigor, which may explain why plants in this treatment group reached greater heights on average than those in other treatments (Figure 3).

The cabbage biofumigant treatment showed the most beneficial impact on tomato plant height compared to other biofumigant options, including knicker and sorghum. Applying cabbage as a biofumigant introduces organic compounds into the soil that decompose and release nutrients, thus providing several agronomic benefits; these include the potential to increase organic matter, improve soil structure, and enhance nutrient availability. These benefits collectively foster a supportive environment for root and plant development, contributing to improved plant vigor and overall growth, as supported by previous findings.

In terms of leaf production, the cabbage biofumigant treatment demonstrated the most significant positive effect on the number of tomato leaves when compared to other treatments. This result may be attributed to the nutrient composition associated with plants of the

Brassicaceae family, such as cabbage, which are known to contribute essential nutrients to the soil, including nitrogen, phosphorus (P), potassium (K), magnesium (Mg), and organic carbon (C-organic). These nutrients play an important role in supporting the growth and development of tomato plants (Kakar et al., 2024; Trivedi et al., 2025).

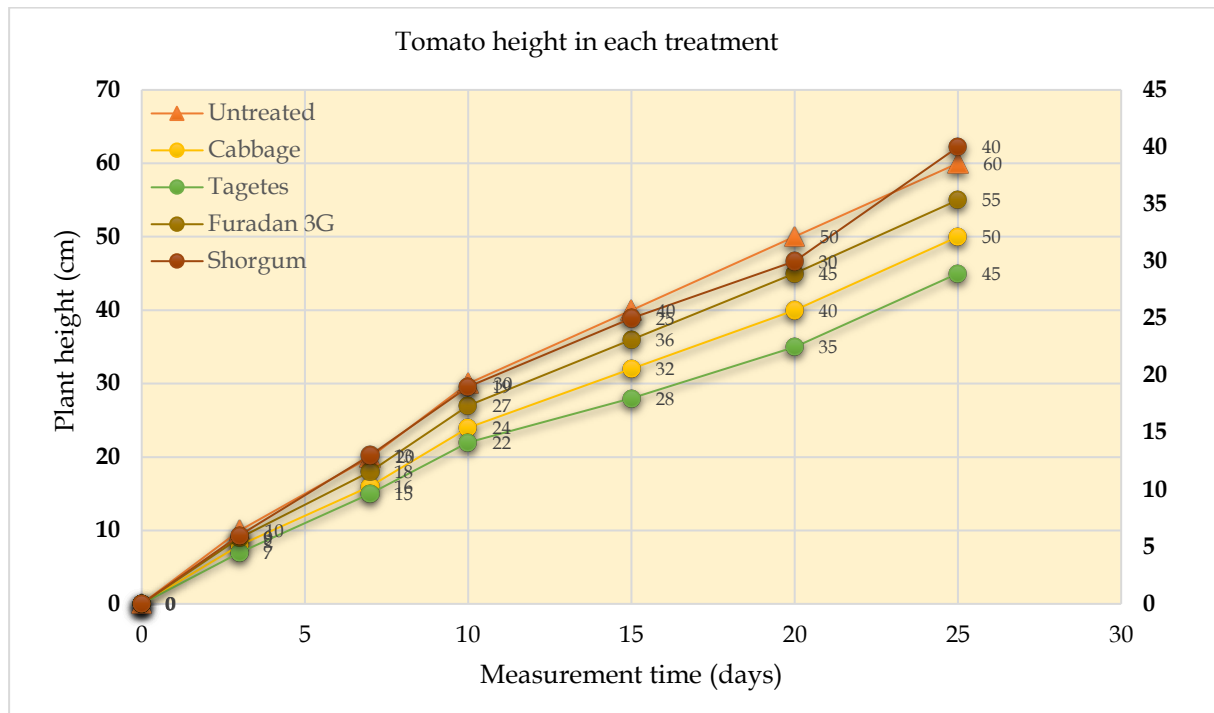


**Figure 3.** The effect of biofumigant treatment on tomato plant height

Nitrogen, in particular, is crucial for plants as it directly supports the growth of vegetative structures such as leaves, stems, and roots (Monib et al., 2024). Nitrogen fertilization is especially vital for plants during the vegetative phase, promoting the formation and expansion of leaves, which in turn maximizes photosynthetic capacity and overall plant *vigour*; the incorporation of cabbage biofumigants, therefore likely contributed to a richer nutrient profile in the soil, fostering an optimal environment for leaf production and, consequently, healthier, more robust tomato plants (Figure 4).

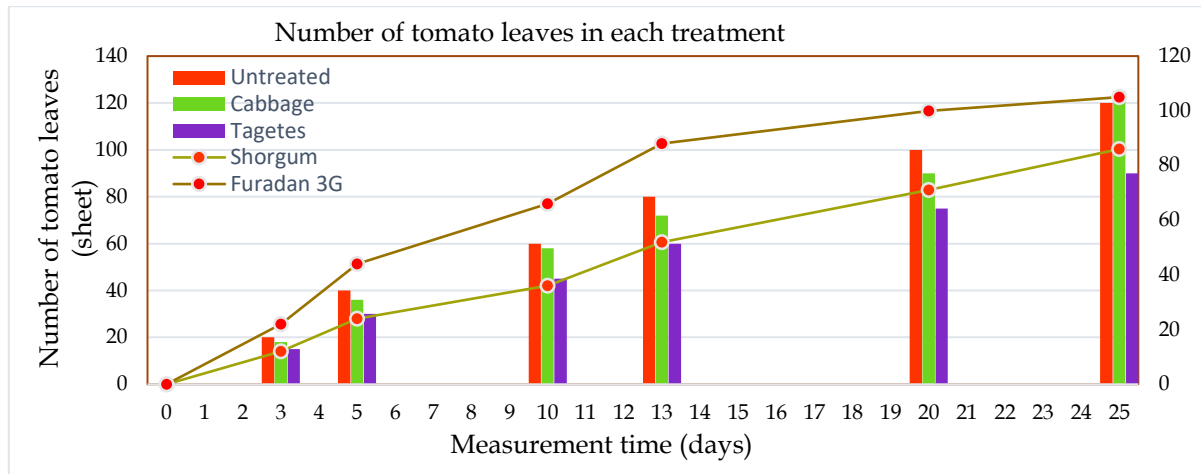


**Figure 4.** The effect of biofumigant treatment on the number of tomato leaves

Table 1 presents data on the root weight and population of RKN within the roots of treated plants. It is evident that the cabbage biofumigant treatment was the most effective in reducing the RKN population, with a significantly more significant impact than other biofumigant treatments. Specifically, when compared to the control group (plants without biofumigant treatment), cabbage biofumigant achieved a suppression effectiveness of 72.4% against RKN; this aligns closely with findings from a study by (Ji et al., 2024), which demonstrated that biofumigation with cruciferous plant residues can effectively manage RKN populations, achieving a 63.4% suppression rate in that case. The table also indicates that, among non-Brassicaceae plants, sorghum biofumigant proved more effective at reducing RKN populations than the knicker biofumigant. The enhanced effectiveness of sorghum is attributed to the release of a secondary metabolite called dhurrin, which is highly toxic to RKN. In contrast, kenikir (*Tagetes*) produces a secondary metabolite known as  $\alpha$ -terthienyl, which generally inhibits nematode development rather than directly suppressing population growth. In this study, sorghum biofumigant showed a suppression effectiveness of 57.4% when compared to the control, while the *Tagetes* biofumigant treatment achieved a 39.4% suppression rate relative to the untreated control group.

Table 1 concludes that the root weight increase column shows the percentage increase in root weight for each application relative to the untreated control, providing a precise measure of how each application impacts root growth. Meanwhile, the Relative Ranking of Nematode Suppression organizes applications from highest to lowest in terms of effectiveness at reducing nematode populations, helping quickly identify the most effective methods. Regarding performance, the Cabbage Biofumigant ranked second in nematode suppression with a 60.7% reduction, just behind Furadan, outperforming other biofumigants by at least 13.7%. This treatment also showed the highest root weight increase (30.8%) among biofumigants, indicating that it effectively suppresses nematodes while supporting robust root growth. The *Tagetes* Biofumigant showed the lowest nematode suppression among biofumigants at 30.8%, performing 17.7% lower than Sorghum and substantially less than Cabbage. However, it provided a notable root weight increase (29.1%) over the control, indicating moderate benefits. Sorghum Biofumigant ranked third in nematode suppression, achieving 17.7% greater suppression than *Tagetes* but 11.1% less than cabbage. It showed a root weight increase of 27.7%, proving more beneficial for root growth than *Tagetes*.



**Table 1.** Comparing treatments for root-knot nematode control, with *Furadan* showing highest suppression and cabbage offering strong balance of control and root growth

Application	Root-Knot Nematode Population Density	Root Fresh Weight (g)	Nematode Suppression Efficiency (% Reduction from Control)	Root Health Index (Scale: 1-5)	Primary Active Compound	Root Weight Increase (% Increase from Control)	Relative Ranking of Nematode Suppression	Effectiveness and Observations
Control untreated	1029 a	3.199 a	0%	1 (Poor)	None	0%	5th (Lowest)	The highest nematode population and lowest root weight show significant damage without treatment, serving as a baseline for all comparisons.
Tagetes ( <i>Tagetes spp.</i> )	649.1 b	4.251 ab	30.8%	3 (Moderate)	Terthienyl	27.7%	4th	Moderate suppression with a 30.8% reduction in nematodes, 17.7% less effective than Sorghum. Root weight improved by 27.7% compared to control, indicating moderate health improvement.
Sorghum ( <i>Sorghum bicolor</i> )	450.4 c	4.264 ab	50.9%	3.5 Good) (Moderate)	Dhurrin	27.7%	3rd	Achieved 50.9% nematode suppression, 17.7% more than <i>Tagetes</i> but 11.1% less than Cabbage. Root weight increased by 27.7% over control, indicating better health than <i>Tagetes</i> .
Cabbage ( <i>Brassica oleracea</i> )	309.1 d	4.337 b	60.7%	4 (Good)	Glucosinolates	33.3%	2nd	Achieved the highest biofumigant effectiveness, reducing nematode populations by 60.7%, a 31.1% higher suppression rate than <i>Tagetes</i> . Root weight increased 33.3% over control, indicating strong root health.
Nematicide ( <i>Furadan</i> 3G)	60.7 e	149 ab	91%	4.5 (Very Good)	Carbofuran	24.4%	1st (Highest)	Highest nematode suppression, with 91% reduction, outperforming cabbage biofumigant by 21.1%. Root weight increase (24.4%) is lower than all biofumigants, possibly indicating phytotoxic effects despite high suppression.

Finally, the Nematicide (Furadan 3G) ranked highest in nematode suppression with a 91% reduction but had the smallest increase in root weight (24.4%) among all applications, suggesting possible phytotoxic effects that may impact root development despite its strong suppression effectiveness.

### 3.1. Effect of nematicide treatment on tomato plant growth

Nematicide treatments are used to manage plant-parasitic nematodes, such as *Meloidogyne* species, which can severely affect tomato plants by causing stunted growth and reduced yields. By applying nematicides like Furadan, the nematode population in the soil is significantly reduced, promoting healthier root development. This improved root structure enhances nutrient uptake and leads to more substantial plant growth, increasing vigor and potential yields.

A screen house experiment assessed the effects of biofumigant extracts in autoclaved, manure-enriched soil on managing root-knot disease and improving tomato growth; the untreated inoculated control group exhibited high pathogenicity, with a root-knot index of 4.8 on a scale of 0-5 (Fullana et al., 2024). In contrast, the fifth treatment group significantly reduced root galling. After introducing 2,000 juveniles, 500  $\mu$ L of the extract was applied around the roots a week later. The treated plants demonstrated marked improvement, with the root-knot index decreasing to 1.2 compared to the untreated group (Table 2).

**Table. 2.** Effect of nematicide (Furadan 3G) treatment (35 ppm) on root-knot development caused by (*Meloidogyne incognita*) on tomato plant root and shoot growth

Treatment	Length(cm)		Total length (cm)	Fresh weight (g)		Total fresh weight (g)	Dry weight (gm)		Total dry weight (g)
	Shoot	Root		Shoot	Root		Shoot	Root	
Sorghum Biofumigant	49.1 <sup>c</sup> ±1.1	4.2 <sup>c</sup> ±0.5	50.9 <sup>c</sup> ±1.6	48.10 <sup>c</sup> ±0.9	11.85 <sup>c</sup> ±0.61	59.95 <sup>c</sup> ±0.71	11.52 <sup>c</sup> ±0.63	3.2 <sup>c</sup> ±0.26	14.72 <sup>c</sup> ±0.89
Cabbage Biofumigant	63.3 <sup>b</sup> ±0.7	4.4 <sup>b</sup> ±0.8	60.7 <sup>d</sup> ±1.5	61.85 <sup>b</sup> ±1.32	17.95 <sup>b</sup> ±0.83	79.80 <sup>b</sup> ±0.75	18.55 <sup>b</sup> ±0.75	3.4 <sup>b</sup> ±0.29	21.95 <sup>b</sup> ±1.04
<i>Tagetes</i> Biofumigant	30.2 <sup>d</sup> ±1.2	4.2 <sup>d</sup> ±0.6	30.8 <sup>d</sup> ±1.6	24.22 <sup>d</sup> ±1.82	9.80 <sup>d</sup> ±0.88	34.025 <sup>d</sup> ±2.7	4.80 <sup>d</sup> ±0.30	3.1 <sup>d</sup> ±0.17	7.9 <sup>d</sup> ±0.47

This study's findings underscore biofumigants' efficacy, particularly those derived from the Brassicaceae family, as viable and sustainable tools for managing root-knot nematode (*Meloidogyne spp.*) populations in tomato cultivation. RKN are among the most detrimental pests to tomatoes and other high-value crops, causing substantial economic losses globally. Their management is integral to maintaining agricultural productivity and ensuring food security. This study's comparative analysis of biofumigants—cabbage (*Brassicaceae*), sorghum (*Poaceae*), and *Tagetes* (*Asteraceae*)—reveals distinct nematicidal potentials, with Brassicaceae-derived biofumigants demonstrating superior efficacy.

Cabbage, as a representative of the Brassicaceae family, exhibited the highest nematode suppression, achieving a 60.7% reduction in nematode populations. This remarkable effectiveness is attributed to glucosinolates, which enzymatically hydrolyze into isothiocyanates upon plant tissue disruption. As corroborated by prior studies, isothiocyanates are potent biocidal agents that disrupt nematode cellular integrity and metabolic processes (Ntalli & Caboni, 2012). The pronounced nematicidal properties of

cabbage align with its potential integration into pest management frameworks, offering an environmentally sustainable alternative to synthetic nematicides.

In contrast, biofumigants derived from non-Brassicaceae sources demonstrated comparatively lower nematocidal effects. Sorghum achieved a 50.9% reduction in nematode populations, mainly attributable to its cyanogenic glucosides, which release hydrogen cyanide upon decomposition (Gimsing & Kirkegaard, 2006). However, these compounds appear less efficacious against RKN than the isothiocyanates produced by Brassicaceae species. Similarly, *Tagetes* spp. (marigold) exhibited only moderate suppression (30.8%), likely due to the production of thiophenes, which, while nematocidal, may have limited impact under field conditions or in high nematode infestations.

Despite significant nematode suppression, biofumigants did not induce statistically significant improvements in plant growth metrics, such as height or leaf count. This disparity suggests that while biofumigation mitigates nematode-induced stress, other agronomic factors—such as nutrient availability, initial pest pressure, or abiotic stressors—may modulate growth outcomes. Integrating biofumigants with complementary strategies, such as organic amendments, precision nutrient management, or companion planting, could amplify pest suppression and yield enhancements.

Using a completely randomized design in this study ensured methodological *rigour*, allowing clear comparisons across biofumigant treatments. Future research should expand on these findings through multi-year, field-scale trials to evaluate the consistency of biofumigant efficacy under diverse agroecological conditions. Exploring their interactions with soil microbial communities, nutrient cycling, and crop productivity could also elucidate their role within broader sustainable agricultural systems.

RKN (*Meloidogyne* spp.) pose a considerable constraint to agricultural productivity, necessitating the development of eco-conscious management strategies, including biofumigation. This study sought to evaluate the efficacy of biofumigants derived from Brassicaceae and non-Brassicaceae plant families in mitigating root-knot nematode infestations in tomato crops. A single-factor completely randomized design encompassing five treatments was employed for this purpose. The findings revealed that biofumigants from both plant groups did not exert a statistically significant influence on tomato plant height or leaf number. Among the tested biofumigants, cabbage (Brassicaceae) demonstrated the highest nematode suppression, achieving a 69.5% reduction in root-knot nematode populations relative to the untreated control. Sorghum (non-Brassicaceae) was identified as the most effective biofumigant in its group, reducing nematode populations by 55.8% compared to the control. RKN detrimentally impact plant health by impairing root system functionality, thereby restricting nutrient absorption and predisposing roots to secondary pathogens. While synthetic nematicides such as methyl bromide, DBCP, and chloropicrin have traditionally been effective in curbing nematode populations below economic thresholds, their environmental toxicity has led to regulatory restrictions and phased-out usage in many regions. Fumigation, a commonly employed nematode control measure, has proven effective in reducing the incidence of soil-borne plant parasitic nematodes. However, its limited accessibility in certain countries underscores the need for sustainable and environmentally benign alternatives. Biofumigation, which incorporates plant materials such as *cabbage*, *Tagetes*, *sorghum*, and *Sudan grass*, emerges as a viable substitute (Habriantono et al., 2023).

Cabbage biofumigants leverage glucosinolates, which degrade into isothiocyanates (ITS)—potent nematocidal and fungicidal agents that penetrate nematode egg cuticles. Similarly, sorghum and Sudan grass release hydrogen cyanide through the enzymatic breakdown of dhurrin, a cyanogenic glycoside, effectively reducing nematode viability. *Tagetes* plants,

recognized for their allopathic properties, synthesize  $\alpha$ -terthienyl, a secondary metabolite capable of inducing oxidative stress in nematodes through the rapid generation of phytotoxic reactive oxygen species. This investigation evaluated biofumigation efficacy on tomato plants subjected to root-knot nematode infestation. Fifteen-day-old tomato seedlings were transplanted into RKN-infested soil, which had been amended with chopped cabbage, *Tagetes*, or sorghum at a ratio of 0.4 kg plant material per 2 kg of soil. A parallel treatment involved carbofuran application at a dosage of 4 g per 2 kg of soil. The treated soil was stored anaerobically in plastic bags before transfer to polybags for planting. The experiment utilized a completely randomized design with five replications per treatment. Observations on tomato plant growth, including height, leaf count, and root biomass, were conducted on the 25th day post-treatment. The results indicated that none of the treatments significantly influenced plant growth parameters, highlighting the need for further investigation into the mechanisms and conditions underpinning biofumigant effectiveness (Habriantono et al., 2023).

Brassicaceae-derived biofumigants contribute to IPM frameworks by reducing dependence on synthetic nematicides, aligning with sustainable agriculture principles. These biofumigants mitigate environmental risks associated with chemical nematicides and support soil health and biodiversity, key pillars of sustainable farming. Continued research should optimize application protocols, evaluate long-term impacts on soil ecosystems, and integrate biofumigation with other agroecological practices to maximize its potential in sustainable food production systems.

Biological control agents have emerged as a promising and sustainable alternative to chemical nematicides in controlling RKN (*Meloidogyne spp.*) in tomato cultivation. For instance, *Pythium oligandrum* has been shown to effectively suppress *Meloidogyne incognita* infections by parasitizing nematode eggs and inducing systemic resistance in tomato plants (Pontes et al., 2024; Subedi et al., 2020; Zhou et al., 2016; Zhou et al., 2019). The research conducted by Yao et al. (2025) delves into the efficacy of *Bacillus velezensis* A-27 as a biocontrol agent targeting *Meloidogyne incognita*. This pernicious plant-parasitic nematode severely threatens global agricultural productivity. The study highlights the remarkable larvicidal and ovicidal properties of strain A-27, with LC<sub>50</sub> values of  $4.0570 \times 10^8$  CFU/mL and  $3.6464 \times 10^8$  CFU/mL, respectively, observed under laboratory conditions. Pot trials demonstrated a significant reduction in root galling, achieving an impressive control efficacy of 85.36%. In comparison, field experiments revealed a control efficacy of 67.31%, alongside a reduction in the J2 population density of *M. incognita* and improved growth performance in celery plants. High-throughput sequencing further revealed that A-27 substantially enhanced the relative abundance of beneficial genera, such as *Bacillus* and *Sphingomonas*, while simultaneously reducing the prevalence of pathogenic genera like *Fusarium*, *Mortierella*, and *Cephalophora* within the celery rhizosphere. These findings underscore the potential of *B. velezensis* A-27 as an environmentally friendly alternative to synthetic nematicides, paving the way for its application in sustainable agricultural practices. RKN represent a formidable threat to over 5,500 plant species, including a wide range of economically significant vegetables. These nematodes are implicated in global agricultural losses exceeding \$100 billion annually, with vegetable crop losses in China alone surpassing 3 billion CNY. Among RKN species, *Meloidogyne incognita* is the most prevalent and widely researched, particularly in greenhouse vegetable production. While synthetic chemical nematicides are effective, their environmental and health risks and high costs necessitate the development of safer and more sustainable biocontrol solutions. Several nematophagous fungi, including *Paecilomyces tenuis*, have demonstrated profound efficacy, achieving over 90% mortality of infective second-stage juveniles (J2) within 24 hours. Similarly, *Rhizophagus irregularis* has been shown to enhance plant resistance against RKN by modulating phenolic activity and antioxidant enzyme defense

mechanisms. Other fungal species, such as *Fusarium oxysporum* spp. *ciceris* and *Myrothecium verrucaria*, have exhibited parasitism on nematode eggs, J2, and adult females, with mortality rates reaching 71% (Yao et al., 2025; Zhou et al., 2019; Wadhwa et al., 2024).

*Arbuscular mycorrhizal* fungi (AMF) also hold promise as biocontrol agents, bolstering plant tolerance to RKN by inducing systemic resistance (ISR), competing for rhizosphere resources, and modulating microbial interactions. Similarly, plant growth-promoting rhizobacteria (PGPR) exhibit systemic nematicidal properties, including *Pseudomonas stutzeri*, *Bacillus subtilis*, and *Streptomyces* antibiotics (Yadav et al., 2025). Notably, *B. velezensis* has emerged as a versatile agent with dual antifungal and nematicidal capabilities, effectively combating phytopathogens such as *Verticillium dahliae* and *Colletotrichum gloeosporioides*. Plants actively recruit beneficial microorganisms from the rhizosphere, fostering a dynamic microbial community that supports germination, nutrient uptake, and defence against pathogens. The application of microbial composts, particularly those containing *B. velezensis*, has been shown to enhance soil organic matter, enzyme activity, and microbial diversity, alleviating replanting disease and promoting plant growth (Yao et al., 2025; Xue et al., 2024; Hu et al., 2022; Subedi et al., 2020; Zhou et al., 2016; Zhou et al., 2019; Hejran, 2024).

### 3.2. Recommendations for Agricultural Practices

#### Selection of potent biofumigants

Due to their high glucosinolate content, they prioritize biofumigant crops from the Brassicaceae family, including mustard, cabbage, and broccoli. These biofumigants undergo enzymatic hydrolysis to release nematicidal isothiocyanates, effectively targeting RKN. Cultivating high-glucosinolate cultivars enhances biofumigant efficacy, ensuring maximum pest suppression.

#### Optimal timing and soil incorporation

Schedule the cultivation of biofumigant crops at least 4–6 weeks before tomato planting. Incorporate the biomass into the soil during peak glucosinolate production, typically at the flowering or seed set stage. This strategic timing ensures optimal degradation of glucosinolates into bioactive compounds, significantly reducing nematode populations before planting.

#### Integration with holistic pest management

Employ a multi-faceted IPM approach. Rotate biofumigant crops with non-host species to disrupt nematode life cycles and reduce pathogen buildup. Complement this with cultivating nematode-resistant tomato varieties and applying organic amendments like well-decomposed compost or manure to enhance soil biodiversity, further mitigating pest pressures.

#### Routine soil diagnostics and adaptation

Conduct periodic soil diagnostics, including nematode population density assessments and soil nutrient profiling, to monitor the long-term impact of biofumigants – utilize data-driven insights to fine-tune biofumigant application strategies, ensuring their efficacy under varying environmental and soil conditions.

#### Farmer training and advanced research initiatives

Establish farmer-centric educational programs to disseminate knowledge on the advantages, preparation, and application of Brassicaceae biofumigants. Support cutting-edge research to identify novel biofumigant species, optimize their application techniques, and explore synergistic interactions with other biological control agents. Collaborative research efforts will pave the way for innovative, eco-friendly nematode management strategies. By implementing



these evidence-based and pragmatic strategies, farmers can substantially enhance pest management practices while optimizing tomato crop productivity. These strategies are in harmony with sustainable agricultural methodologies, reducing reliance on chemical interventions, preserving environmental integrity, and ensuring the enduring sustainability of commercial farming enterprises. This proactive and well-informed approach will mitigate Root-knot nematode infestations and promote long-term ecological stability.

#### 4. Conclusions

This study highlights the significant effectiveness of both Brassicaceae and non-Brassicaceae biofumigants in managing root-knot nematodes (*Meloidogyne* spp.) in tomato cultivation. Among the tested treatments, the cabbage-based biofumigant (Brassicaceae) emerged as the most effective, achieving a 60.7% reduction in nematode populations compared to the untreated control. It also contributed positively to plant growth parameters, including height, leaf number, and root wet weight. Among the non-Brassicaceae biofumigants, sorghum demonstrated the highest efficacy, with a 50.9% suppression rate, while *Tagetes* showed the lowest, at 30.8%. These findings underscore the superior potential of cabbage as a sustainable biofumigant for integrated nematode management and crop improvement.

#### Authorship Contribution Statement

PN is responsible for conceptualization, data curation, formal analysis, original draft writing, and supervision. ABH is responsible for funding acquisition, writing, investigation, methodology, resources and software. KS is responsible for validation, visualization, writing, reviewing, and editing.

#### Conflict of Interest

The authors declare no conflict of interest.

#### References

- Abd-Elgawad, M. M. M. (2024). Upgrading strategies for managing nematode pests on profitable crops. *Plants*, 13(11), 1558. <https://doi.org/10.3390/plants13111558>
- Adigun, B. A., Oyekale, B. A., & Akhtar, M. S. (2024). Opportunistic fungi, plant, and nematode interactions in agricultural crops. In M. S. Akhtar (Ed.), *Opportunistic fungi, nematode and plant interactions* (pp. xx-xx). Springer.
- Albazazz, A. M., & Aljuboori, F. K. (2024). Characterization of the root-knot nematodes infecting olive trees. *NTU Journal of Agriculture and Veterinary Sciences*, 4(3), Article e02. <https://doi.org/10.56286/dghnfc02>
- Biswas, S., & Das, R. (2024). Organic farming to mitigate biotic stresses under climate change scenario. *Bulletin of the National Research Centre*, 48, 71. <https://doi.org/10.1186/s42269-024-01226-x>
- Bouchtaoui, E. M., Smouni, A., Dababat, A. A., & Mokri, F. (2025). Damage threshold and population dynamic of *Meloidogyne javanica* on tomato plant. *Journal of Phytopathology*, 173, e70015. <https://doi.org/10.1111/jph.70015>
- Njekete, C., Caravel, C., Massol, F., & others. (2024, August 8). Nematicidal plants for root-knot nematode (*Meloidogyne* spp.) management in vegetable cropping systems [Preprint, Version 1]. *Research Square*. <https://doi.org/10.21203/rs.3.rs-4725713/v1>



- Curk, M., & Trdan, S. (2024). Benefiting from complexity: Exploring enhanced biological control effectiveness via the simultaneous use of various methods for combating pest pressure in agriculture. *Agronomy*, 14(1), 199. <https://doi.org/10.3390/agronomy14010199>
- El-Sharkawy, E. E. S., & Al-Gendy, A. A. (2024). Biofumigation potential of Brassicas to control white rot caused by *Sclerotinia sclerotiorum* on eggplant. *Egyptian Journal of Botany*, 64(2), 697–708. <https://doi.org/10.21608/ejbo.2024.252958.2591>
- Faria, J. M. S., Rusinque, L., & Inácio, M. L. (2024). Nematicidal activity of volatiles against the rice root-knot nematode and environmental safety in comparison to traditional nematicides. *Plants*, 13(15), 2046. <https://doi.org/10.3390/plants13152046>
- Fourie, L. W. (2024). *Investigating the use of marigolds (Tagetes spp.) and brassicaceous cover crops as a tool for the management of lesion nematodes (Pratylenchus spp.) in apple orchards* (Doctoral dissertation, Stellenbosch University). <https://scholar.sun.ac.za/handle/10019.1/130166>
- Fullana, A. M., Expósito, A., Pujolà, M., Achaerandio, I., Cunquero, M., Loza-Alvarez, P., Giné, A., & Sorribas, F. J. (2024). Effect of grafting tomato onto *Solanum torvum* on the population dynamics of *Meloidogyne incognita* and *M. javanica* and crop yield losses. *Plant Pathology*. <https://doi.org/10.1111/ppa.13991>
- Giantin, S., Franzin, A., Brusa, F., Montemurro, V., Bozzetta, E., Caprai, E., Fedrizzi, G., Girolami, F., & Nebbia, C. (2024). Overview of cyanide poisoning in cattle from *Sorghum halepense* and *S. bicolor* cultivars in Northwest Italy. *Animals*, 14(5), 743.
- Gimsing, A. L., & Kirkegaard, J. A. (2006). Glucosinolate and isothiocyanate concentration in soil following incorporation of Brassica biofumigants. *Soil Biology and Biochemistry*, 38(8), 2255–2264. <https://doi.org/10.1016/j.soilbio.2006.01.024>
- Gupta, M., Dwivedi, V., Kumar, S., Patel, A., Niazi, P., & Yadav, V. K. (2024). Lead toxicity in plants: Mechanistic insights into toxicity, physiological responses of plants and mitigation strategies. *Plant Signaling and Behavior*, 19(1), 2365576. <https://doi.org/10.1080/15592324.2024.2365576>
- Habriantono, B., Wagiyana, W., & Alfarisy, F. K. (2023). The effectiveness of biofumigants from Brassicaceae and non-Brassicaceae to control root knot nematodes on tomato. In *E3S Web of Conferences*, 373. EDP Sciences. <https://doi.org/10.1051/e3sconf/202337307003>
- Habteweld, A., Kantor, M., Kantor, C., & Handoo, Z. (2024). Understanding the dynamic interactions of root-knot nematodes and their host: Role of plant growth promoting bacteria and abiotic factors. *Frontiers in Plant Science*, 15, 1377453. <https://doi.org/10.3389/fpls.2024.1377453>
- Hamrouni, R., Regus, F., Farnet Da Silva, A. M., Orsiere, T., Boudenne, J. L., Laffont-Schwob, I., & Dupuy, N. (2024). Current status and future trends of microbial and nematode-based biopesticides for biocontrol of crop pathogens. *Critical Reviews in Biotechnology*, 1–20. <https://doi.org/10.1080/07388551.2024.2370370>
- Haruna, S. G., Yahuza, L., & Tijjani, I. (2024). Management of Fusarium wilt of tomato (*Fusarium oxysporum* f. sp. *lycopersici*) and related soil-borne diseases using eco-friendly methods: A review. *Asian Journal of Research in Crop Science*, 9(1), 154–168. <https://doi.org/10.9734/ajrcs/2024/v9i1257>
- Hejran, A. B., Azizi, A., Saken, K., Ardak, K., Sawicka, B., & Niazi, P. (2024). Plant-derived biopesticides for eco-friendly control of the *Prodenia litura* (Fabricius) insect pest. *Journal*

- of Entomology and Zoology Studies, 12(5).  
<https://doi.org/10.22271/j.ento.2024.v12.i5c.9397>
- Hejran, A.-B. (2024). Effective plant virus management integrates strategies to protect and sustain crop health. *Торайғыров университетінің Хабаршысы, Химия-биологиялық сериясы*, (2). <https://doi.org/10.48081/BZTR3857>
- Hu, Y., You, J., Wang, Y., Long, Y., Wang, S., Pan, F., & Yu, Z. (2022). Biocontrol efficacy of *Bacillus velezensis* strain YS-AT-DS1 against the root-knot nematode *Meloidogyne incognita* in tomato plants. *Frontiers in Microbiology*, 13, 1035748. <https://doi.org/10.3389/fmicb.2022.1035748>
- Jamir, S., Devi, K. S., Ningombam, E., & Verma, A. (2024). A review on post-harvest technology of an underutilised vegetable bitter tomato (*Solanum aethiopicum* L Cv. Gilo) of Northeastern region of India. In *BIO Web of Conferences*, 110, 02006. EDP Sciences. <https://doi.org/10.1051/bioconf/202411002006>
- Ji, Y., Zhang, Y., Fang, W., Li, Y., Yan, D., Cao, A., & Wang, Q. (2024). A review of biofumigation effects with plant materials. *New Plant Protection*, 1(2), e21. <https://doi.org/10.1002/npp2.21>
- Kakar, U. M., Tauanov, Z., Azat, S., Ahmadi, N. A., Hassand, M. H., Sarwari, A., ... Niazi, P. (2024). Carbon nanotubes as adsorbents for heavy metals: Focus on arsenic and hydrargyrum removal from water. *Journal of Chemistry Studies*, 3(1), 7–20. <https://doi.org/10.32996/jcs.2024.3.1.2>
- Kandil, E., Abdelaziz, A., Mansour, M., & Attia, M. S. (2025). Promising nematocidal efficacy of *Verticillium lecanii*, hydrogen peroxide, and Melithorin® against root-knot nematode, *Meloidogyne incognita* in the tomato plant. *Egyptian Journal of Botany*, 65(1), 266–275. <https://doi.org/10.21608/ejbo.2024.308857.2949>
- Kannan, K., Raju, P., Keerthy, B. N., Rajagopal, A., & Sabat, S. (2024). Biopesticide effect on crops for the bioactive components extracted from *Tagetes erecta* and *Tagetes patula*. *Discover Agriculture*, 2(1), 37. <https://doi.org/10.1007/s44279-024-00045-y>
- Khosla, K., & Sharma, S. K. (2024). Understanding the dynamics of *Meloidogyne incognita* infestation in pomegranate orchards of Himachal Pradesh, India (years 2018, 2019, and 2021) and its management strategies. *Heliyon*, 10(15), e34752.
- Kirkegaard, J. A., & Sarwar, M. (1998). Biofumigation potential of Brassicas. *Plant and Soil*, 201, 71–89. <https://doi.org/10.1023/A:1004364713152>
- Ko, D. Y., Seo, S. M., Lee, Y. H., Gil, C. S., Lee, H., & Ku, K. M. (2024). Turning glucosinolate into allelopathic fate: Investigating allyl isothiocyanate variability and nitrile formation in eco-friendly *Brassica juncea* from South Korea. *Scientific Reports*, 14(1), 15423. <https://doi.org/10.1038/s41598-024-65938-w>
- Kolaczyk, E. D., & Csárdi, G. (2014). *Statistical analysis of network data with R* (p. 65). New York, NY: Springer. <https://doi.org/10.1007/978-3-030-44129-6>
- Kumar, A., Bhawsar, N., Manekar, S., Pendram, B., Pal, P., Ali, D., ... Yadav, V. K. (2025). Extraction and optimization of lycopene from selected fruits and their assessment as an ultraviolet ray protectant for *Escherichia coli*. *Food Science and Nutrition*, 13(4), e70090. <https://doi.org/10.1002/fsn3.70090>
- Ling, L., Yue, R., Wang, Y., Feng, L., Yang, L., Li, Y., ... Zhou, Y. (2025). Volatile organic compounds from *Stenotrophomonas geniculata* J-0 as potential biofumigants manage

- bulb rot caused by *Fusarium oxysporum* in postharvest Lanzhou lily. *World Journal of Microbiology and Biotechnology*, 41(1), 1–17. <https://doi.org/10.1007/s11274-024-04228-z>
- Majid, M., Ganai, B. A., & Wani, A. H. (2025). Antifungal, antioxidant activity, and GC-MS profiling of *Diaporthe amygdali* GWS39: A first report endophyte from *Geranium wallichianum*. *Current Microbiology*, 82(1), 40. <https://doi.org/10.1007/s00284-024-04023-x>
- Mirzaev, U. N., Kuchboev, A. E., Mavlyanov, O., Amirov, O. O., & Narzullayev, S. B. (2024). Morphological and molecular characterization of root-knot nematodes from Uzbekistan. *Biosystems Diversity*, 32(1), 135–141. <https://doi.org/10.15421/012413>
- Monib, A. W., Niazi, P., Barai, S. M., Sawicka, B., Baseer, A. Q., Nikpay, A., ... Thea, B. (2024). Nitrogen cycling dynamics: Investigating volatilization and its interplay with N<sub>2</sub> fixation. *Journal for Research in Applied Sciences and Biotechnology*, 3(1), 17–31. <https://doi.org/10.55544/jrasb.3.1.4>
- Muthusamy, M., & Lee, S. I. (2024). Abiotic stress-induced secondary metabolite production in Brassica: Opportunities and challenges. *Frontiers in Plant Science*, 14, 1323085. <https://doi.org/10.3389/fpls.2023.1323085>
- Mwangi, N. G., Stevens, M., Wright, A. J., Edwards, S. G., Hare, M. C., & Back, M. A. (2024). Sensitivity of stubby root nematodes (*Trichodorus* and *Paratrichodorus* spp.) to isothiocyanates associated with Brassicaceae in an *in vitro* assay. *Nematology*, 1(aop), 1–8. <https://doi.org/10.1163/15685411-bja10302>
- Niazi, P. (2024). Isolation and characterization of a (surfactin-like molecule) produced by *Bacillus subtilis*: Antagonistic impact on root-knot nematodes. *Scientific Research Communications*, 4(2). <https://doi.org/10.52460/src.2024.010>
- Niazi, P., Alimyar, O., Azizi, A., Monib, A. W., & Ozturk, H. (2023). People-plant interaction: Plant impact on humans and environment. *Journal of Environmental and Agricultural Studies*, 4(2), 1–7. <https://doi.org/10.32996/jeas.2023.4.2.1>
- Ntalli, N. G., & Caboni, P. (2012). Botanical nematicides: A review. *Journal of Agricultural and Food Chemistry*, 60(40), 9929–9940. <https://doi.org/10.1021/jf303107j>
- Parsiaaref, S., Cao, A., Li, Y., Ebadollahi, A., Parmoon, G., Wang, Q., ... Zhang, M. (2024). The main compounds of bio-fumigant plants and their role in controlling the root-knot nematode *Meloidogyne incognita* (Kofoid and White) Chitwood. *Agriculture*, 14(2), 261. <https://doi.org/10.3390/agriculture14020261>
- Pontes, K. B., Machado, A. C. Z., Nogueira, A. F., Fagundes, D. F. V., de Lima Filho, R. B., Mosela, M., ... Gonçalves, L. S. A. (2024). Efficacy of microbiological nematicides in controlling root-knot nematodes in tomato. *Frontiers in Agronomy*, 6, 1462323. <https://doi.org/10.3389/fagro.2024.1462323>
- Priyadharshini, V., Kavitha, P. G., Vetrivelkalai, P., Shandeep, S. G., Rajavel, M., Balakrishnan, N., ... Suganthi, A. (2025). Smart delivery of nanofiber matrix encapsulated botanical nematicide  $\alpha$ -terthienyl against root knot nematode on tomato. *Physiological and Molecular Plant Pathology*, 136, 102508. <https://doi.org/10.1016/j.pmpp.2024.102508>
- Qadir, M., Hussain, A., Iqbal, A., Shah, F., Wu, W., & Cai, H. (2024). Microbial utilization to nurture robust agroecosystems for food security. *Agronomy*, 14(9), 1891. <https://doi.org/10.3390/agronomy14091891>

- Rajah, A. R., Parthiban, K. T., Prasanthrajan, M., Vijayabhama, M., Patil, P., Sekar, I., & Yadav, V. K. (2025). Evaluation of air pollution tolerance index of selected tree species to combat air pollution in urban areas of Mettupalayam, Tamil Nadu, India. *Environmental Pollutants and Bioavailability*, 37(1), 1–14. <https://doi.org/10.1080/26395940.2025.2524085>
- Rigobelo, E. C., Nicodemo, D., Babalola, O. O., & Desoignies, N. (2024). *Purpureocillium lilacinum* as an agent of nematode control and plant growth-promoting fungi. *Agronomy*, 14(6), 1225. <https://doi.org/10.3390/agronomy14061225>
- Salhab, J., Weber, M., Paganini, T., Khamassi, F., Bellagha, S., Hadj, H. B., & Laabidi, F. (2020). Olive oil, medicinal and aromatic plants, and tomatoes in North-West Tunisia: A roadmap to developing competitive advantage on strategic markets. World Bank. <http://documents.worldbank.org/curated/en/784741593019888856/>
- Sarri, K., Mourouzidou, S., Ntalli, N., & Monokrousos, N. (2024). Recent advances and developments in the nematicidal activity of essential oils and their components against root-knot nematodes. *Agronomy*, 14(1), 213. <https://doi.org/10.3390/agronomy14010213>
- Sarwar, M., Kirkegaard, J. A., Wong, P. T. W., & Desmarchelier, J. (1998). Biofumigation potential of Brassicas. *Plant and Soil*, 201, 103–112. <https://doi.org/10.1023/A:1004381129991>
- Sawyer, S. F. (2009). Analysis of variance: The fundamental concepts. *Journal of Manual & Manipulative Therapy*, 17(2), 27E–38E. <https://doi.org/10.1179/jmt.2009.17.2.27E>
- Subedi, P., Gattoni, K., Liu, W., Lawrence, K. S., & Park, S. W. (2020). Current utility of plant growth-promoting rhizobacteria as biological control agents towards plant-parasitic nematodes. *Plants (Basel, Switzerland)*, 9(9), 1167.
- Sun, W., Shahrajabian, M. H., & Soleymani, A. (2024). The roles of plant-growth-promoting rhizobacteria (PGPR)-based biostimulants for agricultural production systems. *Plants*, 13(5), 613. <https://doi.org/10.3390/plants13050613>
- Torabian, S., Kim, E., Qin, R., Sathuvalli, V., Gollany, H. T., & Kleber, M. (2025). Soil microbial biomass influenced by cover crop after fumigation of potato fields. *Science of The Total Environment*, 958, 177910. <https://doi.org/10.1016/j.scitotenv.2024.177910>
- Trivedi, S., Srivastava, A., Saxena, D., Ali, D., Alarifi, S., Solanki, V. S., ... Yadav, V. K. (2025). Phytofabrication of silver nanoparticles by using *Cucurbita maxima* leaf extract and its potential anticancer activity and pesticide degradation. *Materials Technology*, 40(1), 2440907. <https://doi.org/10.1080/10667857.2024.2440907>
- Tunca, H., Dinç, T., Yanık, H., Sevindik, T. O., & Keskin, S. Y. (2024). Calculation a new formula to determine the chlorophyll-a content without extraction by modeling meta analysis data in *Arthrospira platensis* Gomont. <https://doi.org/10.21203/rs.3.rs-4258390/v1>
- Wadhwa, K., Kapoor, N., Kaur, H., Abu-Seer, E. A., Tariq, M., Siddiqui, S., ... Alghamdi, S. (2024). A comprehensive review of the diversity of fungal secondary metabolites and their emerging applications in healthcare and environment. *Mycobiology*, 1–53. <https://doi.org/10.1080/12298093.2024.2416736>
- Welham, S. J., Gezan, S. A., Clark, S. J., & Mead, A. (2014). *Statistical methods in biology: Design and analysis of experiments and regression*. CRC Press.

- Xue, Y., Li, W., Li, M., Ru, N., Chen, S., Jiu, M., Feng, H., Wei, L., Daly, P., & Zhou, D. (2024). Biological control of a root-knot nematode *Meloidogyne incognita* infection of tomato (*Solanum lycopersicum* L.) by the oomycete biocontrol agent *Pythium oligandrum*. *Journal of Fungi*, 10(4), 265. <https://doi.org/10.3390/jof10040265>
- Yadav, V. K., Pramanik, S., Alghamdi, S., Atwah, B., Qusty, N. F., Babalghith, A. O., Solanki, V. S., Agarwal, N., Gupta, N., Niazi, P., Patel, A., Choudhary, N., & Zairov, R. (2025). Therapeutic innovations in nanomedicine: Exploring the potential of magnetotactic bacteria and bacterial magnetosomes. *International Journal of Nanomedicine*, 20, 403–444. <https://doi.org/10.2147/IJN.S462031>
- Yao, Y., Wang, L., Zhai, H., Dong, H., Wang, J., Zhao, Z., & Xu, Y. (2025). *Bacillus velezensis* A-27 as a potential biocontrol agent against *Meloidogyne incognita* and effects on rhizosphere communities of celery in field. *Scientific Reports*, 15(1), 1057. <https://doi.org/10.1038/s41598-024-83687-8>
- Zhang, H., Guo, D., Lei, Y., Lozano-Torres, J. L., Deng, Y., Xu, J., & Hu, L. (2025). Cover crop rotation suppresses root-knot nematode infection by shaping soil microbiota. *New Phytologist*, 245(1), 363–377. <https://doi.org/10.1111/nph.20220>
- Zhou, D., Feng, H., Schuelke, T., De Santiago, A., Zhang, Q., Zhang, J., Luo, C., & Wei, L. (2019). Rhizosphere microbiomes from root knot nematode non-infested plants suppress nematode infection. *Microbial Ecology*, 78(2), 470–481. <https://doi.org/10.1007/s00248-019-01319-5>
- Zhou, L., Yuen, G., Wang, Y., Wei, L., & Ji, G. (2016). Evaluation of bacterial biological control agents for control of root-knot nematode disease on tomato. *Crop Protection*, 84, 8–13. <https://doi.org/10.1016/j.cropro.2015.12.009>
- Zoladek, J., Burlaud-Gaillard, J., Chazal, M., Desgraupes, S., Jeannin, P., Gessain, A., ... Afonso, P. V. (2022). Human claudin-derived peptides block the membrane fusion process of Zika virus and are broad flavivirus inhibitors. *Microbiology Spectrum*, 10(5), e02989-22. <https://doi.org/10.1128/spectrum.02989-22>